

University of Kentucky

UKnowledge

---

Theses and Dissertations--Rehabilitation  
Sciences

College of Health Sciences

---


2020

## DETERMINING THE ROLE OF SATELLITE CELLS DURING SKELETAL MUSCLE ADAPTATION

Davis A. Englund

*University of Kentucky*, [davis.englund@uky.edu](mailto:davis.englund@uky.edu)

Author ORCID Identifier:

 <https://orcid.org/0000-0002-3375-4576>

Digital Object Identifier: <https://doi.org/10.13023/etd.2020.291>

[Right click to open a feedback form in a new tab to let us know how this document benefits you.](#)

### Recommended Citation

Englund, Davis A., "DETERMINING THE ROLE OF SATELLITE CELLS DURING SKELETAL MUSCLE ADAPTATION" (2020). *Theses and Dissertations--Rehabilitation Sciences*. 69.

[https://uknowledge.uky.edu/rehabsci\\_etds/69](https://uknowledge.uky.edu/rehabsci_etds/69)

This Doctoral Dissertation is brought to you for free and open access by the College of Health Sciences at UKnowledge. It has been accepted for inclusion in Theses and Dissertations--Rehabilitation Sciences by an authorized administrator of UKnowledge. For more information, please contact [UKnowledge@lsv.uky.edu](mailto:UKnowledge@lsv.uky.edu).

## **STUDENT AGREEMENT:**

I represent that my thesis or dissertation and abstract are my original work. Proper attribution has been given to all outside sources. I understand that I am solely responsible for obtaining any needed copyright permissions. I have obtained needed written permission statement(s) from the owner(s) of each third-party copyrighted matter to be included in my work, allowing electronic distribution (if such use is not permitted by the fair use doctrine) which will be submitted to UKnowledge as Additional File.

I hereby grant to The University of Kentucky and its agents the irrevocable, non-exclusive, and royalty-free license to archive and make accessible my work in whole or in part in all forms of media, now or hereafter known. I agree that the document mentioned above may be made available immediately for worldwide access unless an embargo applies.

I retain all other ownership rights to the copyright of my work. I also retain the right to use in future works (such as articles or books) all or part of my work. I understand that I am free to register the copyright to my work.

## **REVIEW, APPROVAL AND ACCEPTANCE**

The document mentioned above has been reviewed and accepted by the student's advisor, on behalf of the advisory committee, and by the Director of Graduate Studies (DGS), on behalf of the program; we verify that this is the final, approved version of the student's thesis including all changes required by the advisory committee. The undersigned agree to abide by the statements above.

Davis A. Englund, Student

Dr. Charlotte A. Peterson, Major Professor

Dr. Esther Dupont-Versteegden, Director of Graduate Studies

DETERMINING THE ROLE OF SATELLITE CELLS DURING SKELETAL  
MUSCLE ADAPTATION

---

DISSERTATION

---

A dissertation submitted in partial fulfillment of the  
requirements for the degree of Doctor of Philosophy in the  
College of Health Sciences  
at the University of Kentucky

By

Davis Alan Englund

Lexington, Kentucky

Co-Directors: Dr. Charlotte A. Peterson, Professor of Physical Therapy

and Dr. Esther Dupont-Versteegden, Professor of Physical Therapy

Lexington, Kentucky

2020

Copyright © Davis Alan Englund 2020  
<https://orcid.org/0000-0002-3375-4576>

## ABSTRACT OF DISSERTATION

### DETERMINING THE ROLE OF SATELLITE CELLS DURING SKELETAL MUSCLE ADAPTATION

Physical inactivity, advancing age, limb immobilization, degenerative diseases and various systemic diseases (many cancers, sepsis, HIV, COPD, kidney disease) all lead to skeletal muscle wasting. The loss of muscle mass is of major clinical importance because it leads to an increased risk for morbidity, disability, and the loss of independence; collectively contributing to a substantive increase in healthcare utilization and cost. The prevalence of cachexia (disease-induced muscle wasting) can reach as high as 80% in certain patient populations and the average cost per hospital stay is \$4,641 more than in non-cachectic patients. Direct healthcare costs attributable to sarcopenia were estimated to be \$18.5 billion in 2002. Therefore, developing effective skeletal muscle restoration therapies is critical to improve quality of life and prolong functional independence in the broad patient population afflicted by the loss of muscle mass.

There are few promising strategies emerging to treat loss of muscle mass. Currently, exercise (e.g., resistance training) is the most effective lifestyle intervention used to promote muscle growth, and testosterone is a well-known pharmacological intervention used to increase muscle mass. A greater understanding of the underlying cellular mechanisms that promote muscle growth and adaptation in response to exercise and pharmacological agents will enable the design of more targeted and effective interventions. Moreover, identifying the mechanisms that regulate muscle growth provides an opportunity to discover novel therapeutic targets for those who cannot or are unwilling to participate in exercise. In particular, a fundamental understanding of the role of muscle stem cells (satellite cells) during regeneration and recovery from volumetric muscle loss made targeting and improving satellite cell function and restorative capacity during these conditions possible. Gaining an in depth understanding for the function of satellite cells during muscle growth may likewise allow them to be targeted and increase their ability to promote muscle growth.

Our lab previously showed that while a lack of satellite cells does not limit short-term muscle growth, satellite cells are required to support sustained growth, at least in the plantaris (100% type 2 fibers). As myonuclear accretion and satellite cell abundance are tightly associated with growth in satellite cell replete muscle, the compensatory pathways activated in the absence of satellite cell fusion to enable short-term muscle growth are of

interest. In line with this, the mechanism precipitating a shift in the requirement for satellite cells during sustained muscle growth remains to be elucidated. Due to the method of mechanical overload (synergist ablation) used to induce muscle growth in previous studies, our understanding for satellite cell-mediated muscle growth in adult mice is currently restricted to the plantaris. Emerging evidence suggests that these findings may not extend to muscles with a more oxidative phenotype, like the soleus (50% type 1 and 50% type 2) or to muscles which are undergoing robust metabolic adaptations in response to exercise. Whether these findings extend to testosterone induced muscle growth is currently unknown. The mode and length of perturbation utilized to induce muscle growth, the duration of satellite cell depletion, the timing of depletion (pre, post or at some point during adaptation) all may influence requirements for satellite cells.

In order to address these gaps in our understanding of the regulation of muscle growth, I utilized the Pax7-DTA mouse strain, which allows for the inducible depletion of satellite cells and 3 distinct interventions to drive muscle growth and adaptation. I utilized testosterone to determine if testosterone-induced myonuclear accretion by satellite cells is required for skeletal muscle hypertrophy (Chapter 2), a lifelong wheel running stimulus to determine if reduced satellite cell content throughout adulthood influences the transcriptome-wide response to physical activity and diminishes the adaptive response of skeletal muscle Chapter (3) and a short (4-wk) and long (8-wk) term weighted wheel running model to induce hypertrophy in the plantaris and soleus to determine the muscle-specific requirements for satellite cells during growth and elucidate the intracellular mechanisms regulating satellite cell independent and dependent muscle growth over a time course of muscle hypertrophy (Chapter 4). My overarching hypothesis is that satellite cells are required for growth in response to exercise induced muscle growth and that these requirements are more stringent in muscles with an oxidative phenotype. The findings from these studies will enhance the ability to target satellite cells as a method to increase muscle mass and provide information necessary to evaluate the therapeutic potential of this strategy, and potentially identify compensatory mechanisms enabling growth in the absence of satellite cells that may also be potential therapeutic targets.

The findings from these studies show that while satellite cells are not *required* for skeletal muscle hypertrophy, they are critical for optimal adaptation to exercise, including maximal muscle growth. Our results show distinct differences for the reliance on satellite cells based on the stimulus used to induce muscle growth and length of the intervention. We show no differences in SC+ and SC- muscle growth in response to testosterone, but blunted growth and adaptation in response to short and long term exercise. This may be due to an inability of resident myonuclei to meet the increased transcriptional demands of metabolic adaptation to exercise in the absence of satellite cell communication and myonuclear addition. In response to lifelong wheel running we show myonuclear fusion in the soleus and increased GPCR signaling in the plantaris which are absent in SC- skeletal muscle and likely contributed to blunted adaptation. In response to 4-weeks and 8-weeks of weighted wheel running, our transcriptional data reveal an aberrant response in SC- skeletal muscle leading to a maladaptive response in the soleus, including a failure to promote ECM remodeling, attenuated capillarization and muscle growth. To what

extent these processes are related directly to fusion or more related to satellite cell related signaling to the muscle fiber and other cell types remains to be established.

KEYWORDS: Satellite Cells, Stem Cells, Skeletal Muscle, Hypertrophy, Exercise, Testosterone

---

Davis Alan Englund  
*(Name of Student)*

---

06/03/2020  
Date

DETERMINING THE ROLE OF SATELLITE CELLS DURING SKELETAL  
MUSCLE ADAPTATION

By

Davis Alan Englund

Charlotte A. Peterson

---

Co-Director of Dissertation

Esther Dupont-Versteegden

---

Co-Director of Dissertation

Esther Dupont-Versteegden

---

Director of Graduate Studies

06/03/2020

---

Date

## DEDICATION

To My father Warren David Englund PhD., a lifelong educator and knowledge-seeker.



## ACKNOWLEDGMENTS

I would like to acknowledge my Dissertation Committee: Dr. Charlotte Peterson, Dr. Esther Dupont-Versteegden, Dr. John McCarthy and Dr. Hiroshi Saito for their exceptional mentorship and continued support.

TABLE OF CONTENTS

ACKNOWLEDGMENTS ..... iii

LIST OF TABLES ..... ix

LIST OF FIGURES ..... x

CHAPTER 1. INTRODUCTION ..... 1

    1.1 Satellite cells and the Myonuclear Domain ..... 1

    1.2 Satellite cells and skeletal muscle maintenance..... 2

    1.3 Evidence for Myonuclear Domain Flexibility During Hypertrophy ..... 2

    1.4 Evidence for Prerequisite Myonuclear Accretion to Support Adult Muscle  
    Fiber Hypertrophy ..... 5

    1.5 Perspectives on the Early Satellite Cell Response to Resistance Exercise ..... 6

CHAPTER 2. RESIDENT MUSCLE STEM CELLS ARE NOT REQUIRED FOR  
TESTOSTERONE-INDUCED SKELETAL MUSCLE HYPERTROPHY ..... 8

    Abstract of Chapter 2 ..... 9

    2.1 Introduction..... 10

    2.2 Methods..... 11

    Experimental design..... 12

    Testosterone Enzyme-Linked Immunosorbent Assay (ELISA) ..... 12

    Immunohistochemistry ..... 13

    Image quantification ..... 14

Statistical analysis.....	14
2.3 Results.....	15
Testosterone pellet implantation leads to higher satellite content in SC+ mice ...	15
Testosterone administration induces higher whole-body weight, muscle weights and muscle fiber CSA, independent of satellite cell content.....	15
Myonuclear addition in response to testosterone administration is dependent on the presence of satellite cells .....	16
2.4 Discussion.....	16
CHAPTER 3. DEPLETION OF RESIDENT MUSCLE STEM CELLS NEGATIVELY IMPACTS RUNNING VOLUME, PHYSICAL FUNCTION AND MUSCLE FIBER HYPERTOPHY IN RESPONSE TO LIFELONG PHYISCAL ACTIVITY .....	24
Abstract of Chapter 3 .....	25
3.1 Introduction.....	26
3.2 Methods.....	27
Animals.....	27
Experimental design.....	28
Immunohistochemistry .....	28
Image quantification .....	30
RNA isolation .....	30
RT-qPCR.....	30
Microarray analysis.....	31

Gene expression analysis .....	31
Functional testing.....	31
Data Analysis .....	32
3.3 Results.....	32
Satellite cell replete mice (SC+) had higher satellite cell and myonuclear density in response to lifelong physical activity than satellite cell depleted mice (SC-)..	32
Lifelong physical activity influenced whole-body and heart weight independent of satellite cell content .....	33
Satellite cells were not required for an oxidative shift in fiber type composition in response to lifelong physical activity .....	34
Satellite cell depletion limited hypertrophic growth in response to lifelong physical activity.....	34
Satellite cell content influenced the transcriptome-wide response to lifelong physical activity.....	34
Satellite cell depletion throughout adulthood negatively influenced physical function and running volume .....	35
Satellite cell depletion led to aberrant muscle spindle characteristics .....	36
Satellite cell depletion did not lead to fibrosis in response to lifelong physical activity .....	36
3.4 Discussion.....	36
Figure .....	44

CHAPTER 4: RESIDENT MUSCLE STEM CELL DEPLETION BLUNTS MUSCLE  
FIBER HYPERTOPHY AFTER SHORT AND LONG TERM WEIGHTED WHEEL

RUNNING ..... 54

    Abstract of Chapter 4 ..... 55

    4.1 Introduction..... 57

    4.2 Methods..... 59

    Animals ..... 59

    Experimental design..... 60

    Immunohistochemistry ..... 61

    Image quantification ..... 63

    RNA isolation ..... 63

    RNA-seq analysis..... 64

    Myonuclear isolation ..... 65

    Construction of libraries and generation of cDNA on the 10x genomics platform  
    ..... 65

    Single myonuclear (smn)RNA-seq analyses ..... 65

    Pathway analysis..... 66

    Strength testing ..... 67

    Statistical Analysis..... 68

    4.3 Results..... 68

PoWeR-induced muscle growth is blunted in the absence of satellite cells .....	68
Higher satellite cell density in the soleus and plantaris of SC+ PoWeR trained mice .....	69
PoWeR led to a greater proportion of oxidative fibers in the plantaris, independent of satellite cell content.....	69
Higher myonuclear density and fiber size in the soleus and plantaris of SC+ PoWeR trained mice.....	69
Extracellular matrix accumulation did not limit muscle fiber hypertrophy in response to PoWeR .....	70
Whole-muscle and smnRNA-seq reveal dysregulated signaling during adaptation to 4-wks of PoWeR in SC- skeletal muscle .....	70
After 8-wks of PoWeR SC- skeletal muscle displayed delayed transcriptional activity .....	72
Aberrant skeletal muscle adaptation in response to PoWeR in the absence of satellite cells .....	74
4.4 Discussion.....	74
REFERENCES .....	103
VITA.....	115

## LIST OF TABLES

Table 3.1 qPCR primer list .....	40
Table 3.2 TA and EDL characteristics.....	41

## LIST OF FIGURES

Figure 2.1 Testosterone administration.....	20
Figure 2.2 Testosterone administration.....	21
Figure 2.3 Testosterone administration.....	22
Figure 2.4 Testosterone administration.....	23
Figure 3.1 Lifelong exercise .....	42
Figure 3.2 Lifelong exercise .....	43
Figure 3.3 Lifelong exercise .....	44
Figure 3.4 Lifelong exercise .....	45
Figure 3.5 Lifelong exercise .....	46
Figure 3.6 Lifelong exercise .....	47
Figure 3.7 Lifelong exercise .....	49
Figure 3.8 Lifelong exercise .....	51
Figure 3.9 Lifelong exercise .....	52
Figure 3.10 Lifelong exercise .....	53
Figure 4.1 Weighted wheel running.....	81
Figure 4.2 Weighted wheel running.....	83
Figure 4.3 Weighted wheel running.....	84
Figure 4.4 Weighted wheel running.....	86
Figure 4.5 Weighted wheel running.....	87
Figure 4.6 Weighted wheel running.....	88
Figure 4.7 Weighted wheel running.....	90
Figure 4.8 Weighted wheel running.....	92



Figure 4.9 Weighted wheel running.....	93
Figure 4.10 Weighted wheel running.....	95
Figure 4.11 Weighted wheel running.....	97
Figure 4.12 Weighted wheel running.....	99
Figure 4.13 Weighted wheel running.....	100
Figure 4.14 Weighted wheel running.....	102

## CHAPTER 1. INTRODUCTION

### 1.1 Satellite cells and the Myonuclear Domain

Skeletal muscle is a unique tissue for many reasons, the most striking of which is that its cells are multi-nucleated (i.e. syncytial). Further, as skeletal muscle nuclei are post-mitotic, there is a reliance on the dedicated myogenic stem cell population, called satellite cells, to fuse into the syncytium for the purposes of myonuclear addition or possibly replacement. These properties make satellite cells essential for post-natal muscle growth and muscle fiber regeneration after injury<sup>1-5</sup>. Following the discovery of satellite cells<sup>6-8</sup>, scientists postulated that a given myonucleus can only transcriptionally govern a fixed volume of cytoplasm, or “myonuclear domain”<sup>9-11</sup>. This hypothesis was reinforced by early experiments in rodents that indicated load-induced hypertrophy was accompanied by myonuclear accretion<sup>12</sup>.

The myonuclear domain theory in skeletal muscle can be traced back to the work of Dr. Charles Epstein, who reported that cell size was directly proportional to gene dosage in polyploidy liver cells<sup>13</sup>. Incidentally, hepatocytes have a marked capacity for hypertrophy without DNA synthesis<sup>14,15</sup>, and resident hepatocyte nuclei can transcriptionally support at least a doubling in cell size<sup>16</sup>. The idea of a rigid nuclear domain is nevertheless ascribed to highly plastic, multi-nucleated skeletal muscle fibers and is pervasive and engrained within the context of skeletal muscle fiber hypertrophy. The controversy surrounding this idea is evidenced by a recent debate regarding the necessity of satellite cell-mediated myonuclear accretion for loading-induced hypertrophy<sup>17,18</sup>, as well as recent studies supporting the existence of a rigid myonuclear domain during hypertrophy<sup>19-24</sup>.

## **1.2 Satellite cells and skeletal muscle maintenance**

In the absence of injury, satellite cells are thought to maintain quiescence. However, a few studies indicate myonuclear addition via satellite cell fusion in uninjured muscle fibers<sup>25-29</sup>. While this is not a consistent findings, it suggests myonuclear turnover may occur and that satellite cell fusion may be required for skeletal muscle maintenance over time. In fact, it has been suggested that the decline in satellite cell content seen with advancing age may contribute to the loss of skeletal muscle mass (sarcopenia)<sup>28,30</sup>. However, when our group depleted satellite cells in mature mice throughout adulthood, we found this did not influence the onset or progression of sarcopenia in sedentary mice<sup>31</sup>. A limitation to this study is that its findings can be extended only to sedentary cohorts. As exercise is known to influence myonuclear and satellite cell content, a long term exercise stimulus may alter the requirements for satellite cells throughout adulthood in physically active mice<sup>32,33</sup>. We explore this idea in Chapter 3<sup>34</sup>.

## **1.3 Evidence for Myonuclear Domain Flexibility During Hypertrophy**

Adult humans, mice, and rats have nearly identical myonuclear domain sizes<sup>35</sup>. Numerous studies in humans and rodents report that satellite cell proliferation and myonuclear accretion occur with skeletal muscle fiber hypertrophic growth [reviewed in<sup>30,36</sup>]. The often-observed incidence of large muscle fibers with a high proportion of myonuclei after training reinforces the notion that the myonuclear domain may expand modestly<sup>37</sup>, but generally remains stable during hypertrophy. Muscle fiber hypertrophy and myonuclear accretion via testosterone supplementation further implies that myonuclear accretion directly contributes to adult muscle growth<sup>38,39</sup>, a hypothesis that we

directly tested in Chapter 2. Conversely, time-course studies in rats <sup>40</sup> and humans <sup>41</sup> show a substantial degree of loading-induced muscle fiber hypertrophy can occur prior to or in the absence of myonuclear accretion, resulting in significant expansion of the myonuclear domain.

Type 1 and 2 muscle fibers demonstrate differential hypertrophic plasticity under a wide variety conditions in humans <sup>42-44</sup>, and myonuclear domain flexibility during hypertrophy may differ by fiber type. Our laboratory <sup>45</sup> and others <sup>46,47</sup> showed that the myonuclear domain of human Type 2 muscle fibers, which comprise ~50% of muscle fibers in most muscles, is highly flexible. Herman-Montemayor et al. reported Type 2 fiber hypertrophy >30% with non-statistically significant myonuclear accretion (9.5%,  $P < 0.10$ ) and a 29% expansion of the myonuclear domain after resistance training in untrained women <sup>47</sup>. These findings do not necessarily rule out the existence of a “myonuclear domain ceiling”, but do challenge the idea of a muscle fiber growth “threshold” beyond which myonuclear accretion is theoretically required to sustain hypertrophy <sup>37,41,48</sup>. This threshold was derived most recently from correlations in human work and, while translational outcomes in humans are the ultimate goal, loss-of-function studies in mice are necessary to compliment the indirect, correlative evidence gained in humans and to determine causality. It has also been proposed that differences between “low” and “high” hypertrophic responders to resistance training was explained by the extent of myonuclear accretion <sup>48,49</sup>, but this has recently been challenged in the literature by evidence showing myonuclear accretion is uncoupled from muscle fiber hypertrophy <sup>50</sup>.

Following conditional genetic deletion of satellite cells, our laboratory reports substantial hypertrophy in the plantaris muscle, primarily composed of Type 2 fibers,

following synergist ablation surgery in adult mice (>4 month old)<sup>2,18,30,51-54</sup>. Importantly, the lack of myonuclear accretion during hypertrophy does not negatively affect single muscle fiber contractile function<sup>2,52</sup>. Furthermore, resident myonuclei possess a transcriptional reserve that compensates for a lack of satellite cells during Type 2 fiber hypertrophy<sup>53</sup>.

A maximal transcriptional rate for a given myonucleus that corresponds to a specific myonuclear domain size has yet to be identified. Manipulating signaling pathways that are central to muscle fiber size regulation (e.g. Myostatin, AKT, JunB), in the absence of muscle overload or damage, also induces significant hypertrophy without myonuclear accretion and provides further evidence for myonuclear domain flexibility<sup>55-61</sup>. Interestingly, when Type 2 fibers are genetically modified to be more oxidative, hypertrophy is associated with myonuclear accretion<sup>57</sup>. This suggests there may be a greater reliance on myonuclear addition during a response to exercise (where numerous metabolic adaptations occur) than to pharmacological interventions. Different roles for satellite cells during a pharmacological (Chapter 2) vs an exercise intervention (Chapters 3 and 4) are explored in this dissertation<sup>34,62</sup>. In order to determine whether increased biosynthetic activity associated with the high metabolic demands of oxidative muscles and coordinating a response to exercise influences requirements for myonuclear accretion during hypertrophy we utilized an alternative non-surgical method of inducing hypertrophy in muscles other than the plantaris (Chapter 4)<sup>63</sup>.

## 1.4 Evidence for Prerequisite Myonuclear Accretion to Support Adult Muscle Fiber Hypertrophy

It is clear that the myonuclear domain is more flexible than previously appreciated, but some evidence suggests that myonuclear accretion is absolutely required for, and in fact precedes hypertrophy. Type 2 fibers in young mice (<4 months old) appear to have an absolute requirement for myonuclear accretion to mount a hypertrophic response<sup>19-22,64</sup>. Further, findings from the Myomaker<sup>scKO</sup> mouse strain (a model of impaired satellite cell fusion) suggest the absence of myonuclear addition completely inhibits muscle growth in response to synergist ablation and uphill treadmill running<sup>20,24</sup>. Counter to the idea that myonuclear accretion drives hypertrophy, significant myonuclear accretion can ensue during heavy endurance training, in the absence of hypertrophy<sup>65-67</sup>.

The effects of anabolic steroid usage provide circumstantial evidence that myonuclear accretion facilitates hypertrophy. A hypothesis that we directly test in Chapter 2. Supraphysiological testosterone levels elicit hypertrophy in conjunction with myonuclear addition<sup>38,39</sup>, which is compounded during heavy resistance training and pronounced hypertrophy<sup>68,69</sup>. However, androgen signaling can increase myogenic cell proliferation and differentiation *in vitro* and *in vivo*<sup>70-73</sup>, making it difficult to tease out the contribution of testosterone-directed fusion versus inflammation/damage versus hypertrophy on myonuclear accretion. Recent evidence also suggests that an inflammatory environment alone causes myonuclear accretion in the absence of exercise training and altered muscle fiber size<sup>74</sup>. We interpret these findings to mean that satellite cell fusion to muscle fibers *in vivo* can be mediated solely by the signaling milieu and uncoupled from muscle fiber size. During short-term muscle atrophy induced by hind limb suspension in

mice, the myonuclear domain is dramatically reduced in size, further demonstrating the flexibility of the myonuclear domain<sup>30,75-77</sup>. That is to say, if the myonuclear domain were truly rigid, one may expect myonuclear loss to consistently scale with atrophy in order to maintain the myonucleus-to-protein ratio, which would be consistent with the original “DNA unit” concept that is the foundation of the myonuclear domain theory (Cheek et al. 1971).

### **1.5 Perspectives on the Early Satellite Cell Response to Resistance Exercise**

Following severe muscle fiber injury, satellite cells mediate skeletal muscle regeneration via myogenesis and interactions with fibroblasts to coordinate proper extracellular matrix remodeling<sup>3</sup>. Resistance exercise in humans is not typically associated with muscle degeneration, but muscle injury, inflammation, and sarcolemmal damage may ensue<sup>78</sup>. One hypothesis is that the magnitude of early satellite cell proliferation after unaccustomed resistance exercise reflects myonuclear accretion potential and predicts hypertrophic adaptation; however, the relationship to muscle fiber growth is unclear<sup>79</sup>. Once muscle damage subsides, satellite cell proliferation after resistance exercise is attenuated<sup>46,80</sup>, and is not predictive of the ~16% Type 2 muscle fiber growth reported by Damas et al.<sup>46</sup>. Consistent with initial conjectures on early satellite cell proliferation with overload<sup>81</sup>, it seems that muscle fiber damage and satellite cell niche disruption primarily dictates satellite cell responses to resistance exercise, and not hypertrophy *per se*. The relationship between exercise-mediated muscle fiber damage and satellite cell proliferation is underscored by greater satellite cell density after highly- versus minimally-damaging contractions in exercise-naïve men<sup>82,83</sup>.

Under certain conditions, the propensity to fuse is an inherent property of activated satellite cells<sup>84</sup>. As such, it is conceivable that satellite cell-mediated myonuclear accretion observed with resistance training is simply a response to muscle fiber damage and the accompanying milieu, and not a requirement to maintain myonuclear domain size. In support of this hypothesis, Type 2 fiber myonuclear accretion occurs during 12 weeks of eccentric (i.e. damaging) but not concentric (i.e. minimally damaging) resistance training, despite similarly modest hypertrophic responses to both modes<sup>85</sup>. The most strenuous exercise may induce the most damage, and subsequently the most myonuclear accretion. Worth mentioning is that the synergist ablation model of skeletal muscle overload used to induce hypertrophy in rodents can be rather severe and damage-inducing depending on how the surgery is conducted<sup>81</sup>, which is an obvious drawback of the model that may affect translatability to humans. Interestingly, our laboratory showed that the early satellite cell proliferative response to synergist ablation is crucial for proper extracellular matrix remodeling during hypertrophy<sup>51</sup>. Instead of myonuclear addition to muscle fibers, we contend that the critical role for activated satellite cells during hypertrophy is to participate in extracellular matrix remodeling which facilitates growth independent of fusion<sup>30,51,52</sup>. To determine if these findings extend to a more translatable hypertrophy model, we will utilize progressive weighed wheel running, to avoid excessive muscle damage (Chapter 4).



**CHAPTER 2. RESIDENT MUSCLE STEM CELLS ARE NOT REQUIRED FOR  
TESTOSTERONE-INDUCED SKELETAL MUSCLE HYPERTROPHY**

## **Abstract of Chapter 2**

It is postulated that testosterone-induced skeletal muscle hypertrophy is driven by myonuclear accretion as the result of satellite cell fusion. To directly test this hypothesis we utilized the Pax7-DTA mouse model to deplete satellite cells in skeletal muscle followed by testosterone administration. Pax7-DTA mice (6 months of age) were treated for 5 days with either vehicle (satellite cell replete, SC+) or tamoxifen (satellite cell depleted, SC-). Following a washout period, a testosterone propionate or sham pellet was implanted for 21 days. Testosterone administration caused a significant increase in muscle fiber cross sectional area (CSA) in SC+ and SC- mice in both oxidative (soleus) and glycolytic (plantaris and extensor digitorum longus (EDL)) muscles. In SC+ mice treated with testosterone, there was a significant increase in both satellite cell abundance and myonuclei that was completely absent in testosterone-treated SC- mice. These findings provide direct evidence that testosterone-induced muscle fiber hypertrophy does not require an increase in satellite cell abundance or myonuclear accretion.

## 2.1 Introduction

Satellite cells are required for post-natal skeletal muscle growth and regeneration, but their role during periods of adult skeletal muscle hypertrophy remains to be fully elucidated<sup>86-89</sup>. Most studies that have investigated the requirement for satellite cells during hypertrophic growth in both juvenile and mature mice have utilized the surgical synergist ablation model to induce hypertrophy, which is supra-physiological and non-reversible<sup>19,20,87,90-92</sup>. These studies have shown that satellite cells are required for muscle hypertrophy prior to complete skeletal muscle maturation (< 4 months of age)<sup>19,20,91,92</sup>. In mature skeletal muscle, considerable muscle growth can occur over a relatively short time frame in the absence of satellite cell-dependent myonuclear accretion; however, satellite cells are required for sustained periods of muscle growth<sup>87,90,91</sup>. To further our understanding of satellite cell-mediated muscle hypertrophy we utilized the Pax7-DTA mouse model to enable depletion of satellite cells and a pharmacological approach to induce muscle hypertrophy. We chose continuous-release (21 days) testosterone pellet implantation as our treatment strategy since high doses of testosterone have been consistently shown to promote an increase in muscle fiber cross sectional area (CSA), myonuclear number and satellite cell content.<sup>93-95</sup>

There are multiple mechanisms by which testosterone treatment has been reported to stimulate muscle hypertrophy<sup>93,96-98</sup>. The primary mechanism is dependent upon androgen receptor (AR) content to induce androgen stimulated increases in protein synthesis<sup>99,100</sup>. Once bound by testosterone, the AR is released from the membrane to induce genomic and non-genomic actions that include increasing IGF-1 expression, Akt/mTORC1 phosphorylation events and subsequent elevated protein synthesis<sup>100-102</sup>. It

is well-documented that muscle fibers, satellite cells and other mononuclear cell populations (fibroblasts, endothelial cells and mast cells) found within skeletal muscle all express the AR; in particular, testosterone treatment of satellite cells *in vitro* induces a 25% increase in proliferation and global knockout of the AR in mice alters regulators of proliferation and differentiation<sup>103-105</sup>. While testosterone administration induces satellite cell proliferation and muscle growth, more work is needed to determine the direct relationship between increased satellite cell content and muscle hypertrophy in response to testosterone<sup>98,104</sup>.

Based on the effects of testosterone on satellite cell proliferation and fusion, and indirect evidence in humans and in mice demonstrating a relationship between myonuclear accretion and increased muscle size, the general consensus is that testosterone-induced muscle hypertrophy is driven directly by satellite cell activation and subsequent myonuclear accretion; however, direct evidence to support this consensus is currently lacking.<sup>93,94</sup> We therefore set out to test the hypothesis that testosterone-induced myonuclear accretion by satellite cells is required for skeletal muscle hypertrophy. Female Pax7-DTA mice were treated with vehicle (satellite cell replete, SC+), to serve as controls or tamoxifen (satellite cell depleted, SC-) and were supplied with testosterone propionate or sham pellets for 21 days after which hindlimb muscles were isolated and analyzed.

## 2.2 Methods

The Pax7CreER/+R26RDTA/+ strain, called Pax7-DTA, was generated by crossing the Pax7CreER/CreER mouse strain with the Rosa26DTA/DTA mouse strain<sup>3</sup>. The Pax7-DTA mouse allows for the specific and inducible depletion of satellite cells

upon tamoxifen treatment, through *Cre*-mediated activation of the diphtheria toxin A gene in Pax7-expressing cells.<sup>87</sup> Mice were housed at 14:10 hour light:dark cycle and had access to water and food ad libitum. All animal procedures were conducted in accordance with institutional guidelines approved by the Institutional Animal Care and Use Committee of the University of Kentucky.

### **Experimental design**

Thirty-two mature (6-months old) female Pax7-DTA mice were treated via intraperitoneal injection with either vehicle (15% ethanol in sunflower seed oil) or tamoxifen at a dose of 2.5 mg/day for five days<sup>87</sup>. Following a 2-week washout period, either 2.5 mg testosterone propionate pellet or sham pellet, with a release time of 21 days (A-211 Innovative Research America), was implanted subcutaneously into the lateral side of the neck with a precision trocar (MP-182 Innovative Research America) under anesthesia (1–2% inhaled isoflurane). After 21 days, mice were euthanized and muscles (plantaris, soleus, and EDL) were excised and weighed, then pinned to a cork at resting length and covered with Tissue Tek Optimal Cutting Temperature (Sakura Finetek, Torrance, CA, USA), frozen in liquid nitrogen cooled isopentane and stored at -80°C.

### **Testosterone Enzyme-Linked Immunosorbent Assay (ELISA)**

To determine the efficacy of the testosterone pellets, eight mice were implanted with either sham (n = 3) or testosterone (n = 5) pellets. Three days post implantation, mice were sacrificed and blood draws were conducted under light anesthesia (1–2% inhaled isoflurane). Blood samples were spun at 2,000xg for 15 min. Serum was collected and analyzed using Mouse/Rat Testosterone Elisa (ALPCO, Salem, NH) per manufacturer's protocol.

## **Immunohistochemistry**

Immunohistochemical (IHC) analyses for determination of cross sectional area (CSA) and myonuclear number were performed as previously described<sup>91</sup>. Frozen muscle samples were sectioned at the mid-belly of the muscle at -23°C (7 µm), air-dried and stored at -20°C. For determining muscle fiber CSA and myonuclear density, cross sections were incubated overnight in an anti-dystrophin antibody (1:100, ab15277, Abcam, St. Louis, MO, USA). Sections were incubated with a secondary antibody (1:150, anti-rabbit IgG, CI-1000, Vector), diluted in phosphate-buffered saline (PBS). Sections were mounted using VectaShield with DAPI (H-1200, Vector).

Detection of Pax7+ cells was performed as previously described<sup>87</sup>. Sections were fixed in 4% paraformaldehyde (PFA) followed by antigen retrieval. Endogenous peroxidase activity was blocked with 3% hydrogen peroxide in PBS followed by a blocking step with 1% Tyramide Signal Amplification (TSA) blocking reagent (TSA kit, T20935, Invitrogen) and Mouse-on-Mouse blocking reagent (Vector Laboratories, Burlingame, CA, USA). Pax7 primary antibody (1:100, DSHB, Iowa City, Iowa, USA) and laminin primary antibody (1:100, Sigma-Aldrich, St. Louis, MO, USA) were diluted in 1% TSA blocking buffer and applied overnight. Samples were then incubated with an isotype specific anti-mouse biotin-conjugated secondary antibody against the Pax7 primary antibody (1:1000, 115-065-205, Jackson ImmunoResearch, West Grove, PA, USA) and anti-rabbit secondary for laminin (1:250, A11034, Alexa Fluor 488, Invitrogen, Carlsbad, CA, USA). Slides were washed in PBS followed by streptavidin-horseradish peroxidase (1:500, S-911, Invitrogen) for 1 hour. AlexaFluor 594 was used to

visualize antibody-binding for Pax7 (1:100, TSA kit, Invitrogen). Sections were mounted and nuclei were stained with Vectashield with DAPI (H-1200, Vector).

### **Image quantification**

All images were captured at 20x magnification at room temperature using a Zeiss AxioImager M1 upright fluorescent microscope (Zeiss, Oberkochen, Germany). Whole muscle sections were obtained using the mosaic function in Zeiss Zen 2.3 imaging software (Zeiss). To minimize bias and increase reliability, muscle fiber CSA and myonuclear number were quantified on cross sections using MyoVision automated analysis software<sup>106</sup>. MyoVision enables muscle fibers and myonuclei in the whole muscle cross section to be counted and quantified for measures of CSA and myonuclei/fiber<sup>106</sup>. To determine satellite cell density (Pax7+ cells/fiber), satellite cells (Pax7+/DAPI+) were counted manually on entire muscle cross sections using tools in the Zen software. Satellite cell counts were normalized to fiber number via laminin. All manual counting was performed by a blinded, trained technician.

### **Statistical analysis**

Results are presented as mean  $\pm$  standard error of the mean (SEM). Data were analyzed with GraphPad Prism software (GraphPad Software, San Diego, California, USA) via a two factor ANOVA for Pax7<sup>+</sup> cells/fiber, muscle weight, mean fiber CSA and myonuclei/fiber, and a two factor repeated measures ANOVA for body weight over time. When interactions were detected, post hoc comparisons were made with Holm-Sidak post hoc tests. Serum testosterone levels were compared using an unpaired two-tailed Student's t-test. Statistical significance was accepted at  $P < 0.05$ .

## 2.3 Results

### **Testosterone pellet implantation leads to higher satellite content in SC+ mice**

The implantation of testosterone pellets resulted in significantly higher levels of serum testosterone, measured in a sub-group of mice 3 days after implantation of the pellet (Figure 2.1A). A representative image of immunohistochemical (IHC) detection of Pax7 positive cells in the soleus muscle is shown in Figure 2.1B. IHC image quantification demonstrated effective depletion in the soleus following tamoxifen treatment (Figure 2.1C). Tamoxifen treatment effectively depleted satellite cells in the oxidative soleus (Figure 2.1D) and the glycolytic plantaris (Figure 2.1E). Three weeks of testosterone administration led to higher satellite cell number in soleus (22%,  $p = 0.007$ ) and plantaris (29%,  $p < 0.001$ ) from satellite cell replete (SC+), but not depleted (SC-) mice (Figure 2.1 D&E).

### **Testosterone administration induces higher whole-body weight, muscle weights and muscle fiber CSA, independent of satellite cell content.**

Three weeks of testosterone administration led to a significant increase in body weight ( $p = 0.044$ ), resulting in a higher body weight when compared to sham treated mice ( $p = 0.023$ ) (Figure 2.2A), and higher soleus ( $p = 0.023$ ), plantaris ( $p < 0.001$ ) and EDL ( $p < 0.001$ ) wet weights (Figure 2.2B-D, respectively), independent of satellite cell content. Representative images of plantaris muscle immunoreacted with an antibody against dystrophin to measure CSA are shown in Figure 2.3A&B. Testosterone led to higher muscle fiber CSA in the soleus (17%,  $p = 0.002$ ), plantaris (16%,  $p = 0.001$ ), and EDL (14%,  $p = 0.038$ ) regardless of the presence of satellite cells (Figure 2.3C-E, respectively).



## **Myonuclear addition in response to testosterone administration is dependent on the presence of satellite cells**

Representative images of soleus muscle immunoreacted with an antibody against dystrophin and DAPI staining to determine myonuclear number are shown in Figure 2.4A&B. Myonuclear density was higher in the soleus (43%,  $p < 0.001$ ), plantaris (32%,  $p < 0.001$ ) and EDL (31%,  $p < 0.001$ ) muscles of testosterone-treated SC+ mice (Figure 2.4C-E). In mice depleted of satellite cells, no myonuclear accretion occurred with testosterone treatment, which did not affect growth, as SC- mice exhibited the same hypertrophic response to testosterone as SC+ mice (see Figs. 2.2 and 2.3).

## **2.4 Discussion**

This study reports the novel finding that neither the presence of satellite cells nor myonuclear addition via satellite cell fusion are required for testosterone-induced muscle hypertrophy, contrary to our hypothesis. It has previously been hypothesized that satellite cells play a direct role in stimulating muscle hypertrophy in response to testosterone<sup>93,94</sup>. However, the findings of the current study demonstrate that the hypertrophic response to testosterone is unaffected by absence of satellite cells arguing against such a mechanism. It is also worth noting that testosterone administration did not lead to the accrual of myonuclei through fusion of an extraneous stem cell population in tamoxifen treated muscle, as evidenced by the lack of myonuclear addition in satellite cell-depleted mice treated with testosterone.

Our report supports the finding of Egner et al. that robust myonuclear accretion is observed in response to testosterone administration in muscles that have a full complement of satellite cells<sup>95</sup>. Interestingly, the hypertrophic growth response noted by

Egner et al. (~77% hypertrophy in the soleus) greatly exceeds what we report here (~17% hypertrophy in soleus). This discrepancy is most likely due to differences in the skeletal muscle maturity of the mice used at the onset of testosterone administration. We utilized fully mature 6 month old mice, resulting in a correspondingly larger mean muscle fiber CSA (~1,400  $\mu\text{m}$ ) in sham-treated mice than those used by Egner et al. (mean muscle fiber CSA ~1,000  $\mu\text{m}$ )<sup>95</sup>. It therefore seems likely that skeletal muscle maturation in combination with testosterone administration acted synergistically to augment muscle fiber growth in the report by Egner et al<sup>95</sup>.

It is currently unknown whether the higher number of satellite cells and myonuclei observed after testosterone administration is driven by a direct effect of androgen action on the satellite cells or an indirect effect from increased levels of androgen acting directly on the muscle fiber (e.g. elevated IGF-1 expression)<sup>102</sup>. Based on our findings, it is apparent that testosterone increases satellite cell abundance and myonuclear content, providing further evidence for the proliferative effects of testosterone on satellite cells, either directly or indirectly. Our findings in satellite cell-depleted mice also demonstrate that the genomic and/or non-genomic actions of testosterone within the muscle fibers are sufficient to drive skeletal muscle hypertrophy<sup>100-102</sup>. This finding is supported by a study in rat myotubes *in vitro*, in which no change in myonuclear number occurred following 12 hours of testosterone administration despite the reported 35% higher myotube diameter than vehicle-treated cells<sup>100</sup>. Further, our lab has shown that satellite cells are not required for an increase in the activation of the Akt/mTOR signaling pathway and others have shown muscle fiber hypertrophy resulting from the overexpression of Akt occurs without satellite cell participation<sup>87,107</sup>. The

importance of testosterone activity directly on the muscle fiber itself seems to be somewhat lost in the literature, as many groups have hypothesized that increases in skeletal muscle size are a direct consequence of satellite cell fusion and not the transcriptional activity of resident myonuclei<sup>39</sup>. This is an important concept, since mechanisms internal to the muscle fiber should also be considered, particularly in designing interventions to increase muscle size. In line with this, we previously showed that resident myonuclei appear to have a transcriptional reserve capacity which can compensate for lack of satellite cells, enabling hypertrophy in response to synergist ablation (8). We show here that resident myonuclei also appear to be able to compensate in satellite-depleted muscle to enable hypertrophy in response to testosterone administration. Interestingly, it is known that satellite cells are required to support sustained periods of muscle growth in response to mechanical overload (5). Whether satellite cells are also required for continued muscle growth in response to testosterone is currently unknown. Emerging technology and novel transgenic mouse models will allow for future in-depth analysis of resident myonuclei during periods of skeletal muscle growth<sup>108</sup>. In particular, the transcriptional profile of resident myonuclei in response to a hypertrophic stimulus in the absence of satellite cell fusion is of interest.

In summary, this paper provides novel insight into the role of satellite cells in the muscle growth response to testosterone. Although testosterone normally increases satellite cell number and promotes myonuclear accretion during hypertrophy, satellite cell-dependent myonuclear accretion is not required in adult muscle for hypertrophic muscle growth. Thus, understanding the compensatory mechanism that enables healthy adult resident myonuclei to support growth in the absence of satellite cells may point to

new targets for intervention in conditions where satellite cell abundance and/or activity declines and growth is compromised, such as aging.

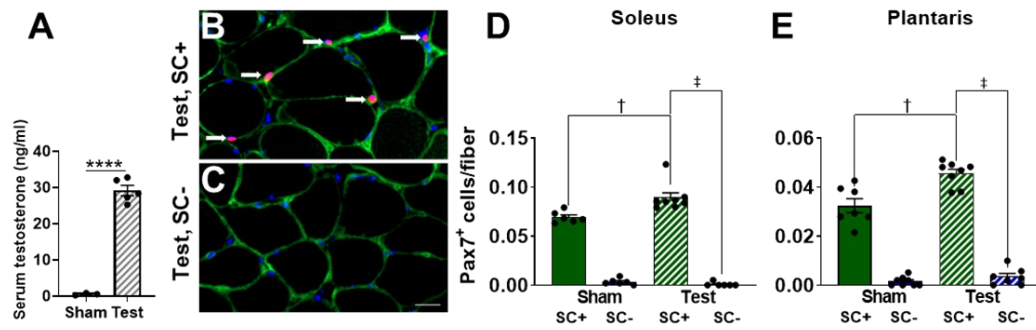


**Figure 2.1**

Higher serum testosterone (Test) and higher satellite cell density in vehicle (SC+) compared to tamoxifen-treated (SC-) mice after Test administration. (A) Serum Test concentration after 3 days of Test or Sham administration. (B&C) Representative images of satellite cell immunohistochemistry in the soleus showing laminin (green) nuclei (blue) and Pax7 (red; white arrows). Scale bar = 20  $\mu\text{m}$ . (D&E) Satellite cell density in the soleus and plantaris. Data represent mean  $\pm$  SEM.  $n = 6-8$  mice per group. †  $P < 0.05$ , Test SC+ vs Sham SC+; ‡  $P < 0.05$ , Test SC+ vs Test SC-. \*\*\*\*  $P < 0.0001$  Test ( $n = 5$ ) vs. Sham ( $n = 3$ ) mice at 3-days.

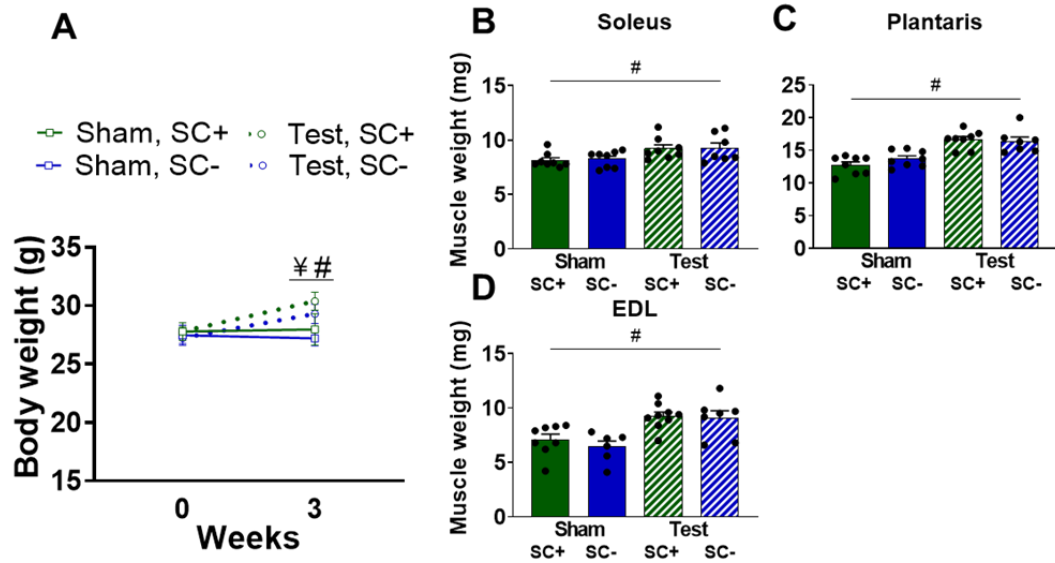


**Figure 2.2**

Testosterone (Test) increases whole-body and muscle weight in mice with (SC+) or without (SC-) satellite cells. (A) Body weight at baseline and after 3-weeks of Test or Sham administration. (B-D) Muscle wet weights in the soleus, plantaris and EDL. Data represent mean  $\pm$  SEM.  $n = 6-8$  mice per group. ¥  $P < 0.05$ , within group change over time in test treated mice. #  $P < 0.05$  Test vs Sham mice at 3-weeks.

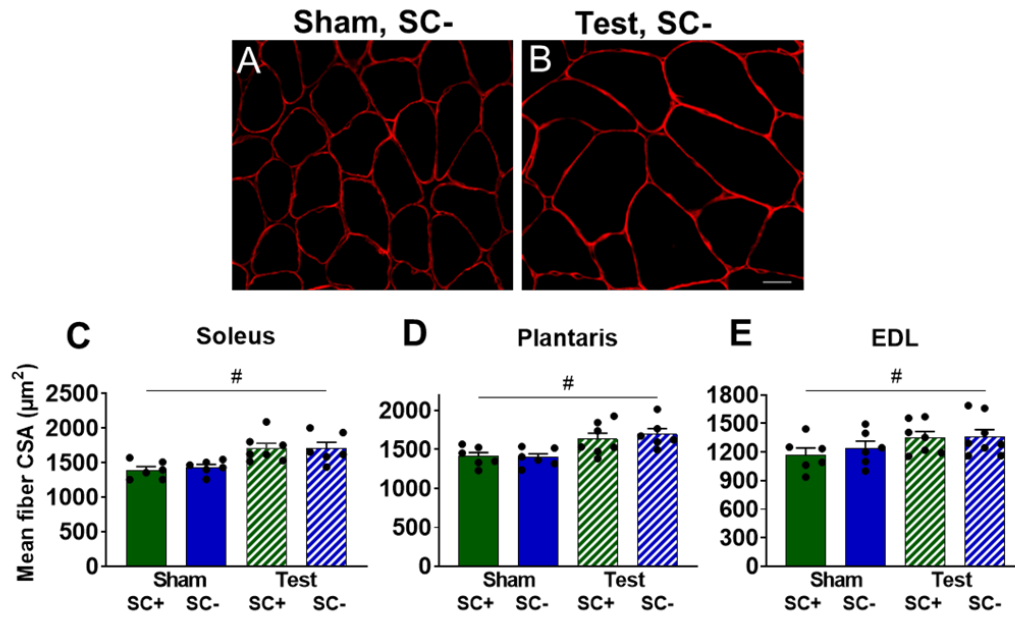


**Figure 2.3**

Testosterone (Test) leads to greater muscle fiber size independent of satellite cell content.

(A&B) Representative images of muscle fiber cross sectional area (CSA) in the plantaris visualized with an antibody against dystrophin. Scale bar = 20 µm. (C-E) Mean fiber CSA in the soleus, plantaris and EDL. Data represent mean ± SEM. n = 6-8 mice per group. # P < 0.05 Test vs Sham mice.

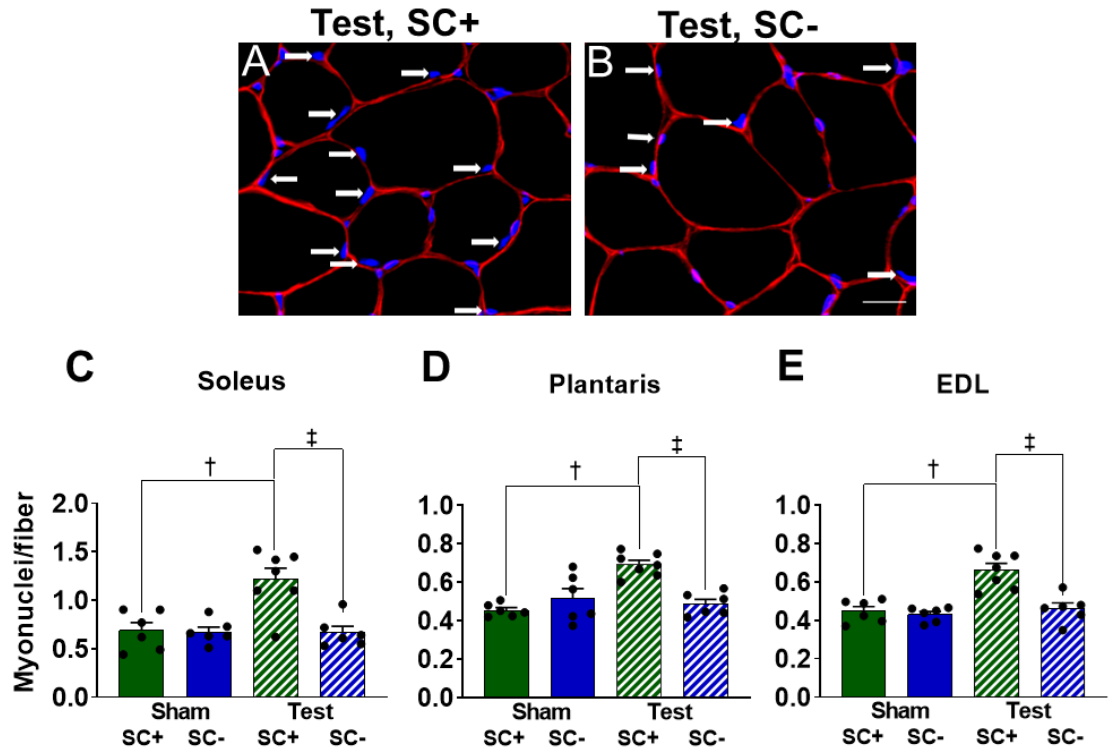


**Figure 2.4**

Elevated myonuclear number in response to testosterone (Test) is dependent on satellite cell content. (A&B) Representative images of dystrophin immunohistochemistry (red) and DAPI (blue) staining from soleus cross sections to identify myonuclei (white arrows). Scale bar = 20  $\mu$ m. (C-E) Myonuclear density of the soleus, plantaris and EDL.

Data represent mean  $\pm$  SEM. n = 6-7 mice per group. † P < 0.05, Test SC+ vs Sham SC+;

‡ P < 0.05, Test SC+ vs Test SC-.



**CHAPTER 3. DEPLETION OF RESIDENT MUSCLE STEM CELLS  
NEGATIVELY IMPACTS RUNNING VOLUME, PHYSICAL FUNCTION AND  
MUSCLE FIBER HYPERTOPHY IN RESPONSE TO LIFELONG PHYSICAL  
ACTIVITY**

### **Abstract of Chapter 3**

To date, studies that have aimed to investigate the role of satellite cells during adult skeletal muscle adaptation and hypertrophy have utilized a non-translational stimulus and/or have been carried out over a relatively short time frame. While it has been shown that satellite cell depletion throughout adulthood does not drive skeletal muscle loss in sedentary mice, it remains unknown how satellite cells participate in skeletal muscle adaptation to long term physical activity. The current study was designed to determine if reduced satellite cell content throughout adulthood would influence the transcriptome-wide response to physical activity and diminish the adaptive response of skeletal muscle. We administered vehicle or tamoxifen to adult Pax7-DTA mice to deplete satellite cells and assigned them to sedentary or wheel-running conditions for 13 months. Satellite cell depletion throughout adulthood reduced balance and coordination, overall running volume and the size of muscle proprioceptors (spindle fibers). Further, satellite cell participation was necessary for optimal muscle fiber hypertrophy but not adaptations in fiber type distribution in response to lifelong physical activity. Transcriptome-wide analysis of the plantaris and soleus revealed that satellite cell function is muscle type-specific; satellite cell-dependent myonuclear accretion was apparent in oxidative muscles, whereas initiation of GPCR signaling in the glycolytic plantaris may require satellite cells to induce optimal adaptations to long term physical activity. These findings suggest satellite cells play a role in preserving physical function during aging and influence muscle adaptation during sustained periods of physical activity.

### 3.1 Introduction

Genetic mouse models enabling an inducible depletion of satellite cells, the resident skeletal muscle stem cell, have demonstrated that satellite cells are required for regeneration after injury and hypertrophic growth prior to skeletal muscle maturity (4 months of age)<sup>86,87,91</sup>. Once mature, robust muscle fiber hypertrophy and alterations in fiber type distribution can occur over a relatively short time frame in the absence of satellite cells<sup>62,87,109</sup>. However, satellite cells become necessary during sustained periods of muscle growth and adaptation<sup>51,90</sup>. While intriguing, the translational relevance of these findings is limited due to the applied stimulus and/or an inadequate length of intervention needed to determine the long term implications of reduced satellite cell content<sup>87,90,109</sup>. The majority of these studies have utilized synergist ablation as a model of mechanical overload, which induces a supraphysiological and damaging stimulus and restricts findings to the overloaded plantaris muscle, which is comprised of 100% type 2 fibers<sup>87,90,91</sup>. As type 1 fibers comprise ~50% of human skeletal muscle and are known to positively influence physical function and health, determining the role of satellite cells during type 1 fiber adaptation is clinically relevant<sup>110,111</sup>. Further, it is becoming clear the length of satellite cell depletion, stimulus applied and muscle(s) analyzed influence findings on the necessity of satellite cells to support muscle adaptation<sup>90,109,112</sup>. Many signaling cascades have been identified that promote muscle adaptation, among the most studied are the IGF1/PI3K/AKT hypertrophy signaling pathways and AMPK/PGC-1 $\alpha$  metabolic signaling pathways. More recently, G protein coupled receptors (GPCRs) and specific G proteins have emerged as regulators of muscle adaptation<sup>113-116</sup>. How the presence or absence of satellite cells influences these signaling cascades and phenotypic adaptation over a prolonged period of time is unknown.

While there is a well-documented association between reduced satellite cell content and the loss of muscle mass with advancing age, we reported that significantly reducing satellite cell content at 4 months of age did not influence the onset or progression of muscle loss in sedentary mice as they aged<sup>31,33</sup>. However, to date, no study has taken a translational approach to directly assess the impact of satellite cell loss on skeletal muscle adaptability in physically active mice with aging. The current study

was designed to determine if satellite cell depletion throughout adulthood would diminish improvements in physical function and skeletal muscle adaptation, assessed across several hindlimb muscles, in response to lifelong physical activity. Further, we wanted to determine to what degree satellite cell participation influenced the transcriptome-wide response to physical activity and signaling pathways specific to muscle adaptation, enabling the identification of satellite cell-dependent processes. In order to address these questions, we utilized the Pax7-DTA mouse to deplete satellite cells for over one year and gave the mice free access to a running wheel during this time to simulate lifelong physical activity. Our results show that satellite cell depletion reduced measures of balance and coordination, as well as overall running volume. These outcomes were likely influenced by the smaller muscle proprioceptors found in the absence of satellite cells. Further, we show the presence of satellite cells is critical for optimal muscle fiber hypertrophy, but not for alterations in fiber type distribution, in response to lifelong physical activity. Our findings suggest a muscle-specific role for satellite cell participation during growth, with fusion playing a more direct role in the oxidative soleus, whereas initiation of GPCR signaling is influenced by satellite cell depletion in the glycolytic plantaris. Taken together, these findings suggest satellite cells play a role in preserving physical function during aging and influence muscle adaptation during sustained periods of physical activity.

### **3.2 Methods**

#### **Animals**

The Pax7<sup>CreER/+</sup>-R26<sup>DTA/+</sup> strain, called Pax7-DTA, was generated by crossing the Pax7<sup>CreER/CreER</sup> mouse strain with the Rosa26<sup>DTA/DTA</sup> mouse strain <sup>3</sup>. The Pax7-DTA mouse allows for the specific and inducible depletion of satellite cells upon tamoxifen treatment, through *Cre*-mediated recombination to induce expression of the diphtheria toxin A (DTA) gene in Pax7-expressing cells, effectively killing satellite cells. All animal procedures were conducted in accordance with institutional guidelines approved by the Institutional Animal Care and Use Committee of the University of Kentucky.

## **Experimental design**

Thirty-nine adult (5-months old) female Pax7-DTA mice were treated via intraperitoneal injection with vehicle (15 % ethanol in sunflower seed oil) or tamoxifen at a dose of 2.5 mg/day for five days, as previously described<sup>87</sup>. Following a 2-month washout period, mice were singly housed and randomly assigned to the sedentary group (cage with locked running wheel) or the running group (free access to running wheel) at 7-months of age (n=9-10 per group). A mechanical counter was used to record wheel rotations and was connected to a desktop computer via ClockLab software (Actimetrics, Wilmette, IL). The animals had access to food and water ad libitum and were checked daily for health and wellness. Mice were sacrificed 13 months later, at a mean age of 20 months. Running wheels were locked 48 hours before sacrifice and mice were fasted overnight. Hindlimb muscles (plantaris, soleus, tibialis anterior (TA) and extensor digitorum longus (EDL) were harvested and prepared for immunohistochemical (IHC) analysis and the contralateral limb for RNA extraction, and then stored at -80 °C. Five mice (3 vehicle-treated and 2 tamoxifen-treated) died over the duration of the study and upon sacrifice tumors were found in one additional mouse (vehicle-treated); these six mice were excluded from analyses.

## **Immunohistochemistry**

IHC analyses were performed as previously described<sup>91</sup>. Briefly, hindlimb muscles were extracted and weighed, then were pinned to a cork block at resting length and covered with Tissue Tek Optimal Cutting Temperature compound (Sakura Finetek, Torrance, CA, USA), and quickly frozen in liquid nitrogen cooled isopentane and stored at -80°C. Frozen muscles were sectioned at -23°C (7 µm), air-dried for at least one hour, and then stored at -20°C. For determining fiber type distribution, muscle fiber cross-sectional area (CSA), fiber type-specific CSA, and myonuclear density, cross sections were incubated overnight in a cocktail of isotype specific anti-mouse antibodies for MyHC 1 (1:75, IgG2B, BA.D5), MyHC 2a (neat, IgG1, SC.71), and MyHC 2b (neat, IgM, BF.F3) from Developmental Studies Hybridoma Bank (DSHB, Iowa City, Iowa, USA), along with an antibody against dystrophin (1:100, ab15277, Abcam, St. Louis, MO, USA), to delineate fiber borders for CSA quantification. Sections were subsequently

incubated with secondary antibodies (1:250, goat anti-mouse IgG2b Alexa Fluor 647, #A21242; 1:500, IgG1 Alexa Fluor 488, #A21121; 1:250, IgM Alexa Fluor 555, #A21426) from Invitrogen (Carlsbad, CA, USA), along with the secondary antibody for dystrophin (1:150, anti-rabbit IgG AMCA, CI-1000, Vector), diluted in PBS. Sections were mounted using VectaShield with DAPI (H-1200, Vector). For an additional measure of myonuclear density, soleus cross sections were stained for pericentriolar material 1 (PCM1, Sigma-Aldrich), as previously described <sup>117</sup>.

Detection of Pax7+ cells was performed as previously described <sup>87</sup>. Briefly, sections were fixed in 4% paraformaldehyde (PFA) followed by antigen retrieval using sodium citrate (10 mM, pH 6.5) at 92°C. Endogenous peroxidase activity was blocked with 3% hydrogen peroxide in phosphate-buffered saline (PBS) followed by an additional blocking step with 1% Tyramide Signal Amplification (TSA) blocking reagent (TSA kit, T20935, Invitrogen) and Mouse-on-Mouse blocking reagent (Vector Laboratories, Burlingame, CA, USA). Pax7 primary antibody (1:100, DSHB) and laminin primary antibody (1:100, Sigma-Aldrich) were diluted in 1% TSA blocking buffer and applied overnight. Samples were then incubated with anti-mouse biotin-conjugated secondary antibody against the Pax7 primary antibody (1:1000, 115-065-205, Jackson ImmunoResearch, West Grove, PA, USA) and anti-rabbit secondary for laminin (1:250, A11034, Alexa Fluor 488, Invitrogen, Carlsbad, CA, USA). Slides were washed in PBS followed by streptavidin-horseradish peroxidase (1:500, S-911, Invitrogen) for 1 hour. AlexaFluor 594 was used to visualize antibody-binding for Pax7 (1:100, TSA kit, Invitrogen). Sections were mounted and nuclei were stained with Vectashield with DAPI (H-1200, Vector).

Detection of N-acetyl-d-glucosamine was evaluated on muscle sections using Texas Red-conjugated wheat germ agglutinin (WGA (eBiosciences, San Diego, CA)). Sections were fixed in 4 % PFA and then incubated with WGA conjugate for 2 hours at room temperature. Sections were also stained with Picrosirius red (PSR) for 1 hour per the manufacturer's instructions (24901-500; Polysciences, Warrington, PA, USA). For quantification, the area of red-stained collagen was quantified relative to the total muscle area.

## **Image quantification**

All WGA and PSR-stained images were captured at 10x magnification, and the total stained area quantified using the thresholding feature of the AxioVision Rel software, as described previously<sup>109</sup>. Muscle spindles were identified by the presence of a thick basement membrane (the muscle spindle capsule) which surrounds the intrafusal fibers<sup>118,119</sup>. Spindles and lobes (located within muscle spindles) were manually traced for CSA analysis. All remaining images were captured at 20x magnification at room temperature using a Zeiss upright fluorescent microscope (Zeiss AxioImager M1 Oberkochen, Germany). Whole muscle sections were obtained using the mosaic function in Zeiss Zen 2.3 imaging software. To minimize bias and increase reliability, fiber type distribution, muscle fiber CSA, fiber type-specific CSA and myonuclear density were quantified on cross sections using MyoVision automated analysis software<sup>106</sup>. To determine satellite cell density (Pax7+ cells/fiber), satellite cells (Pax7+/DAPI+) were counted manually on entire muscle cross sections using tools in the Zen software. Satellite cell counts were normalized to fiber number, delineated by laminin boundaries. All manual counting was performed by a blinded, trained technician.

## **RNA isolation**

Soleus and plantaris muscles were homogenized in QIAzol (Qiagen, Hilden, Germany) and RNA was isolated using RNeasy Mini Kit (Qiagen) according to the manufacturer's instructions. RNA was eluted in nuclease-free water for subsequent microarray and RT-qPCR analyses. RNA quantity and purity was checked by measuring the optical density (260 and 280 nm) using Nanodrop. All 260/280 ratios were above 1.8.

## **RT-qPCR**

Complementary DNA was synthesized from 500 ng of total RNA using the SuperScript IV VILO cDNA Synthesis Kit (Invitrogen, Carlsbad, California). RT-qPCR was performed on a QuantStudio 5 Real-Time PCR System (Thermo Fisher Scientific, Carlsbad, California), with Fast SYBR Green master mix (Thermo Fisher Scientific), a 10- fold dilution of cDNA into a 10 $\mu$ l final reaction, using primers against *Gpr4*, *Gnai2*, *Dgkh*, *Prkcsb* and *Vcp* (Table 3.1). RT-qPCRs were performed using the following

thermal cycler conditions: 50°C for 2 minutes, 95°C for 2 minutes, 40 cycles of a two-step reaction, denaturation at 95°C for 15 seconds, annealing at 60°C for 30 seconds. RT-qPCR efficiency was calculated by linear regression from fluorescence increase in the exponential phase in the LinRegPCR software v11.1<sup>120</sup>. Expression was normalized to *Vcp* using the delta-delta Ct method<sup>121</sup>.

### **Microarray analysis**

The microarray hybridization and processing were performed at the University of Kentucky Microarray Core Facility, according to the manufacturer's protocol (Affymetrix, Santa Clara, CA). Affymetrix chips (mouse Clariom S array) were used with 50 ng/μl of RNA (500 ng total RNA) derived from a pooled sample of right plantaris and soleus muscles (n=7/8 group). In an additional analysis, we pooled RNA (50 ng/μl) samples from a subset of mice that performed an equal volume of running (n=3/group). We pooled RNA samples based on the experimental results reported by Kendzioriski et al. showing that gene expression from RNA pools are similar to averages of individuals that comprise the pool<sup>122</sup>.

### **Gene expression analysis**

Enriched ( $\geq 1.5$  fold) gene expression data sets were transferred to the Venn diagram tool created by the Van de Peer lab (<http://bioinformatics.psb.ugent.be/webtools/Venn/>). Data sets were then transferred to ConsensusPathDB for over-representation and enrichment analyses, carried out with default parameters<sup>123</sup>.

### **Functional testing**

Rotarod and balance beam measurements were performed by a trained technician (blinded to the group assignments) at the University of Kentucky Rodent Behavior Core a week prior to sacrifice.

#### *Rotarod test*

Sensorimotor coordination was assessed using a rotarod apparatus consisting of a rotating rod suspended 18 inches above a padded floor (San Diego Instruments, San



Diego, CA). This system uses a mouse's natural fear of falling as a motivational tool to test gross motor function. Mice were placed on the rotating rod at a speed of 4 revolutions per minute (rpm) for 60 seconds for their training sessions (two training sessions separated by at least 10 minutes). After successful completion of the training sessions and adequate rest, the speed of the rod was gradually increased to a maximum of 40 rpms for each of the three testing sessions. The trial was complete when the animal fell, or the time period ended (300 second max). Latency to fall (seconds) was recorded, and the average of the three testing trials was reported for each animal.

### *Balance beam*

A beam walking protocol was used to evaluate mice on their ability to traverse beams of decreasing widths. The beam walking protocol evaluates motor balance and coordination by assessing both the time it takes the mice to traverse the beam. Following standard acclimatization and training, three beam widths were used to assess balance (28, 17, and 11 mm) and the mice were given 1 minute per trial to complete the crossing of the beam to a bedding filled safe-room on the far end of the beam. The mean of the five trials for the 11 mm beam was used for analysis. Difficulty traversing only occurred with the 11 mm beam.

### **Data Analysis**

Results are presented as mean  $\pm$  SEM. Data were analyzed with GraphPad Prism software via a two factor ANOVA, a two factor repeated measures ANOVA (running over time), or an unpaired Student's t-test (cross sectional running data). When interactions were detected, post hoc comparisons were made with Sidak post-tests. Statistical significance was accepted at  $P < 0.05$ .

### **3.3 Results**

#### **Satellite cell replete mice (SC+) had higher satellite cell and myonuclear density in response to lifelong physical activity than satellite cell depleted mice (SC-)**

Pax7-DTA mice treated with tamoxifen at 5 months of age demonstrated  $\geq 90\%$  depletion of satellite cells (SC-) in hindlimb skeletal muscles (plantaris, soleus, TA and

EDL) at the time of sacrifice at 20 months of age (representative image of Pax7 staining shown in Figure 3.1A and B; quantified in Figures 3.1C and D, Table 3.2). Free access to a running wheel for 13 months, beginning at 7 months of age, did not result in higher satellite cell content in SC- mice (Figures 3.1C and D, Table 3.2). By contrast, in satellite cell replete mice (SC+), satellite cell density (satellite cells/fiber) in both the plantaris and soleus muscles was higher in response to lifelong physical activity, (Figures 3.1C and D). Satellite cell content was not affected by running in the SC+ TA or EDL muscles (Table 3.2).

Lifelong physical activity resulted in higher myonuclear density in the soleus, but not the plantaris, of SC+ mice; as expected there was no change in myonuclear density in these muscles in SC- mice (representative images of myonuclear staining in Figures 3.2A and B; quantified in Figures 3.2C and D, Table 3.2). The observation that myonuclear density was not higher in the soleus of SC- runners suggests that an alternative stem cell population did not substitute for satellite cells in contributing myonuclei in response to lifelong physical activity. To confirm the higher myonuclear density in the soleus of SC+ mice following running, we performed pericentriolar material 1 (PCM1) staining to definitively identify myonuclei <sup>117</sup>. As reported previously, PCM1 staining identified more myonuclei compared to DAPI/dystrophin staining; however, the change in myonuclear density was the same between the two methods (Figure 3.2D) <sup>117</sup>. Similar to satellite cell content, there was no myonuclear addition in the EDL and TA hindlimb muscles in response to running (Table 3.2).

### **Lifelong physical activity influenced whole-body and heart weight independent of satellite cell content**

Lifelong physical activity led to lower body weight (Figure 3.3A) and higher normalized heart weight (Figure 3.3B). These findings highlight that lifelong voluntary wheel running was a powerful stimulus capable of inducing positive phenotypic adaptations independent of satellite cell content.

### **Satellite cells were not required for an oxidative shift in fiber type composition in response to lifelong physical activity**

In response to lifelong physical activity, IHC analysis showed a robust shift from glycolytic 2b fibers to oxidative 2a fibers in the plantaris (representative images shown in Figures 3.4A and B; quantified in Figure 3.4C). This is the first report to demonstrate that a lack of satellite cells in combination with aging does not impair this metabolic adaptation to wheel running. There was no significant shift in the fiber-type composition of the soleus with physical activity, likely due to its inherently oxidative phenotype (Figure 3.4D).

### **Satellite cell depletion limited hypertrophic growth in response to lifelong physical activity**

Muscle fiber type-specific CSA was larger in plantaris and soleus muscles following lifelong physical activity in SC<sup>+</sup> compared to SC<sup>-</sup> mice (representative images shown in Figures 3.5A-D; quantified in Figures 3.5E-H). Total mean muscle fiber CSA was larger in the SC<sup>+</sup> compared to SC<sup>-</sup> soleus (Figure 3.5H); however, due to the prominent shift towards smaller 2a fibers in the plantaris of SC<sup>+</sup> runners (as shown above in Figure 3.4C), plantaris mean fiber CSA was not different between sedentary and running mice (Figure 3.5E). We also analyzed whole-muscle wet weights, corroborating our findings at the CSA level (Figure 3.6). Neither lifelong physical activity nor satellite cell depletion influenced muscle fiber size in the TA or EDL (Table 3.2).

### **Satellite cell content influenced the transcriptome-wide response to lifelong physical activity**

We next performed a transcriptome-wide analysis to identify signaling pathways involved in satellite cell-mediated muscle fiber hypertrophy in response to lifelong physical activity. We pooled RNA samples from the plantaris (n=7/group) and soleus (n=7/group) and performed microarray analysis to uncover pathways preferentially enriched in SC<sup>+</sup> compared to SC<sup>-</sup> runners. We compared the highly expressed genes ( $\geq 1.5$ -fold) in the plantaris to those of the soleus and found considerable differences

between the muscles in their satellite cell-dependent response to lifelong physical activity (Figure 3.7A). Next, we utilized an over-representation analysis to identify signaling pathways significantly enriched in SC+ compared to SC- muscles (Figures 3.7B and C) and a gene set enrichment analysis which identified a distinct  $G\alpha_{i2}$  signaling pathway with a well-established role in hypertrophic growth to be preferentially enriched in SC+ plantaris (Figure 3.7D) <sup>114,115</sup>. We validated this finding by performing qPCR on key genes involved in the  $G\alpha_{i2}$  signaling cascade (Figure 3.7E). Collectively, these data suggest that  $G\alpha_{i2}$  signaling is a potential satellite cell-dependent process promoting muscle fiber growth in the plantaris in response to lifelong physical activity.

### **Satellite cell depletion throughout adulthood negatively influenced physical function and running volume**

We utilized a rotarod test to quantify motor coordination and a balance beam test to assess balance and coordination. SC- mice performed worse on both tests of function, spending less time on the rotarod and taking a longer period of time to transverse the balance beam (Figure 3.8A and 3.8B). Lifelong physical activity did not improve performance on the tests of physical function in SC+ or SC- mice. These findings could, in part, explain declines in physical function with aging that are independent of muscle mass and/or a physically active lifestyle. Depletion of satellite cells reduced voluntary wheel running volume (km/day) over the duration of the study (Figures 3.8C and 3.8D). This is likely explained by the demonstrated impairments in balance and coordination. In an effort to control for differences in running volume we performed microarray analysis on a subset of SC+ and SC- mice (n = 3/group) that ran equal volumes (~9 km/day) over the course of the study. We analyzed the genes enriched ( $\geq 1.5$  fold) in SC+ mice when compared to SC- mice of equal running volume and found that the most highly enriched pathways and key genes in the  $G\alpha_{i2}$  signaling network appeared to be mediated by the presence of satellite cells, as they were still enriched in SC+ compared to SC- mice when accounting for running volume (Figure 3.9)

### **Satellite cell depletion led to aberrant muscle spindle characteristics**

To investigate the underlying cause for reduced physical function in the absence of satellite cells, we tested whether satellite cell depletion influenced spindle fiber (muscle proprioceptor) morphology. We quantified N-acetyl-D-glucosamine (a key component of glycosaminoglycan polymers) utilizing a fluorescent wheat germ agglutinin (WGA) to stain the extracellular matrix (ECM). We found no differences in ECM accumulation within the spindle fibers themselves (ECM index (Figure 3.10C)). However, satellite cell depleted mice had lower muscle spindle size and trended towards lower spindle-lobe size (Figure 3.10D and 3.10E). Interestingly, lifelong physical activity did not rescue this phenotype, having no impact on muscle spindle size in SC- or SC+ mice.

### **Satellite cell depletion did not lead to fibrosis in response to lifelong physical activity**

As ECM accumulation, or fibrosis, has previously been shown to be associated with blunted muscle fiber hypertrophy in response to mechanical overload in the absence of satellite cells, we utilized Picrosirius red (PSR) and WGA staining to quantify levels of ECM<sup>90</sup>. We found no differences in ECM accumulation in the entire cross section (total PSR and WGA staining) regardless of satellite cells or running status, ruling this out as a potential mechanism underlying blunted hypertrophic growth in the absence of satellite cells (Figure 3.11A-J).

## **3.4 Discussion**

We report for the first time that a lack of satellite cells throughout adulthood limits muscle fiber hypertrophy in response to lifelong physical activity. Further, satellite cell depletion adversely affects muscle proprioceptor size, physical function (balance and coordination), as well as running volume. On the other hand, we show that satellite cells are not required for an oxidative shift in fiber type in response to wheel running during aging, demonstrating that processes regulating hypertrophic growth and the metabolic properties of the muscle can be uncoupled. It is not surprising that lifelong physical activity leads to higher heart weight and attenuates age-related gains in body weight that accompany murine aging. Satellite cell ablation does not influence these long term

outcomes in response to physical activity. While wheel running induced robust training adaptations in the soleus and plantaris, the TA and EDL were not influenced by the training stimulus, likely due to the different functional demands being placed on the muscles via the wheel running stimulus <sup>124,125</sup>.

Greater muscle fiber CSA in response to voluntary wheel running is a common but not universal finding in mice <sup>109,126-128</sup>. We previously reported that 2 months of running did not result in larger fiber CSA, suggesting that a protracted period of running is necessary to elicit a significant increase in muscle fiber size <sup>109</sup>. Importantly, the mice analyzed in this report were 20 months old at the time of sacrifice, enabling the study of skeletal muscle adaptation prior to the confounding effects of age-related reduction in muscle fiber size that occur  $\geq 24$  months of age <sup>31,129,130</sup>. Given the decline in satellite cell content with advancing age, our findings suggest increasing satellite cell content specifically in physically active older adults could be a potential therapeutic strategy to increase muscle mass in response to exercise <sup>33,131,132</sup>. Beyond this, falls and fractures are common in older adults, which can result in extended bouts of physical rehabilitation in otherwise sedentary individuals <sup>133</sup>. Our results suggest targeting satellite cells may augment the hypertrophic response to sustained periods of rehabilitation. Further, satellite cell depletion throughout adulthood reduces muscle proprioceptor size, voluntary physical activity and physical function. Declines in balance and coordination with advancing age increase the risk of falls and are associated with slower walking speeds, a major risk factor for mobility disability and the loss of independence <sup>134-136</sup>. Whether restoring satellite cell number may improve physical function remains to be determined but has important clinical implications.

Satellite cell depletion for 13 months does not influence ECM accumulation in sedentary or physically active mice. While the ablation of satellite cells has been shown to induce excessive ECM development in response to mechanical overload as a result of synergist ablation surgery, the adaptive response to wheel running is distinct from that of synergist ablation <sup>90</sup>. This distinction is likely due to the damaging and supraphysiological nature of synergist ablation-induced muscle overload <sup>137</sup>. In line with our previous findings, which also utilized female Pax7-DTA mice, there was no effect of

satellite cell depletion on ECM accumulation in running or sedentary mice at 8 months of age in the plantaris or at 8 and 24 months in the diaphragm muscle<sup>109,138</sup>. However, ECM accumulation may be exacerbated by lifelong satellite cell depletion in mice  $\geq 2$  years of age, as reported previously<sup>31,139</sup>.

Satellite cell participation in muscle fiber hypertrophy differed between the soleus and plantaris in response to lifelong physical activity, consistent with the idea that distinct mechanisms regulate muscle growth in different muscles and fiber types<sup>29,140,141</sup>. While satellite cell content is higher in both the SC+ soleus and plantaris muscles in response to running, significant myonuclear accretion only occurs in the soleus. It may be that in response to lifelong physical activity, satellite cells potentiate growth in the soleus directly through fusion, whereas they may stimulate growth in the plantaris through other mechanisms, such as influencing the muscle microenvironment to facilitate remodeling<sup>51</sup>. This finding supports previous work that has indicated the reliance on myonuclear addition during muscle growth is greater in oxidative than in glycolytic muscles<sup>89,112,139</sup>.

Based on the results of our transcriptome analysis, it appears that satellite cells are critical for the initiation of certain anabolic signaling events in response to lifelong physical activity and may function via GPCR and downstream  $G\alpha_{i2}$  signaling, specifically in the plantaris. This effect may be indirect, through negative impact on spindle fiber function, thereby reducing running volume, or through direct effects on myofiber CSA in response to running, or a combination thereof. Subgroup analysis of SC- and SC+ mice that ran equal volumes suggests a direct effect on muscle GPCR signaling. GPCR-mediated signaling events are integral to anabolic signaling and muscle growth<sup>113,116</sup>. Further, the work of Minetti et al. suggests activation of the  $G\alpha_{i2}$  signaling cascade in the presence of satellite cells likely initiates downstream phosphorylation events necessary for the stimulation of muscle protein synthesis<sup>114,115</sup>. While available deep sequencing data provide insight into the molecular profile of activated satellite cells and information can be gleaned as to the signaling molecules/ligands that are likely candidates influencing GPCR-related signaling, the GPCRs upregulated in the plantaris are orphan receptors, making the identification of bonafide ligands challenging<sup>142,143</sup>. Further research is required to identify and integrate the mechanisms whereby satellite

cells maximize physical activity and promote increases in muscle fiber size over the lifespan, that extend beyond fusion to muscle fibers.

Our findings are limited by assigning the two muscles that adapted to life-long wheel running (the plantaris and soleus) to either IHC or transcriptomic analysis, preventing further validation of findings at the protein level. Also, as all mice were female, sacrificed at 1 time point (20-months old) and given free access to running wheels, we are unable to investigate sex-specific or long term skeletal muscle adaptation in a temporal fashion while controlling for running volume. This study has several strengths including a thorough characterization of skeletal muscle adaptation to a translation stimulus with and without satellite cell participation. This work has produced clinically relevant findings with important implications for the skeletal muscle field.

In conclusion, while our previous work shows that satellite cells are not required for short term adaptation to a growth stimulus in adult mice, or maintenance of muscle mass during aging in sedentary mice, satellite cells are necessary for the maintenance of physical function and the increase in muscle fiber size in response to lifelong physical activity<sup>31,87</sup>. Our study provides novel insight into the muscle-specific role of satellite cells in skeletal muscle hypertrophy in response to lifelong physical activity. In more oxidative muscles, satellite cell fusion may be essential, whereas in glycolytic muscles, satellite cells may promote signaling in muscle fibers to facilitate growth. These findings suggest that preserving satellite cell content with aging could preserve physical function and improve muscle growth in older adults engaged in regular physical activity.



Table 3.1 qPCR primer list

Sequence 5' → 3'		
Gpr4	Forward primer	CTGTGCAGAGTCGGGACCAA
	Reverse primer	AGATTGCTAGGCCTGCTCCG
Gnai2	Forward primer	CTGGCAGGATGGGCCAC
	Reverse primer	CATGGTCTTCTTGCCCCAT
<u>Dgkh</u>	Forward primer	CAGCCTGGACCTGGGGATT
	Reverse primer	AAGTTGGGAGGGTTCCGTT
<u>Prkcsh</u>	Forward primer	CGGAGCGTTCCGTTCTCTTA
	Reverse primer	ATGGCCTCTCAGCGAGGTA
<u>Vcp</u>	Forward primer	TGCCAGGCCAACTTCATCTC
	Reverse primer	CCGGACATTGGCCTCAGATT

**Table 3.2 TA and EDL characteristics**

	TA				EDL			
	Sed, SC+	Sed, SC-	Run, SC+	Run, SC-	Sed, SC+	Sed, SC-	Run, SC+	Run, SC-
Pax7 <sup>+</sup> cells/100 fibers	3.36 ± 0.19	0.09 ± 0.02	3.81 ± 0.33	0.27 ± 0.18	3.28 ± 0.51	0.14 ± 0.05	3.30 ± 0.12	0.13 ± 0.08
Myonuclei/fiber	0.91 ± 0.09	0.88 ± 0.05	0.88 ± 0.06	0.92 ± 0.07	0.85 ± 0.04	0.71 ± 0.09	0.81 ± 0.05	0.80 ± 0.06
Mean fiber CSA, $\mu\text{m}^2$	1,666 ± 60.3	1,678 ± 55.9	1,647 ± 102.9	1,636 ± 42	1,240 ± 54.7	1,192 ± 41.2	1,244 ± 42.6	1,248 ± 40.17

Values are mean ± SEM. N = 6-9 mice/group. Sed, Sedentary conditions; Run, Running conditions.

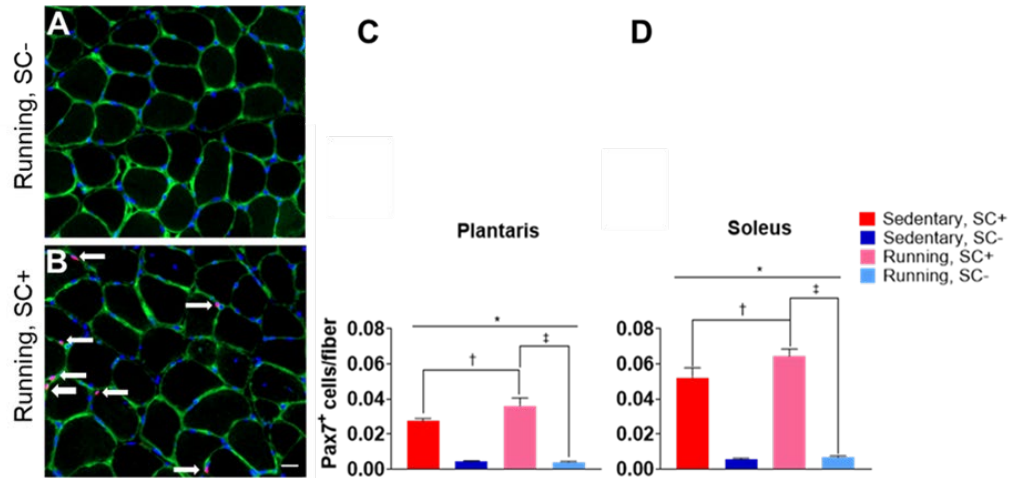


**Figure 3.1**

Higher satellite cell density in the plantaris and soleus muscles of running satellite cell replete (SC+) compared to depleted (SC-) mice. (A-B) Representative image of satellite cell immunohistochemistry showing laminin (green), nuclei (blue), and Pax7 (red; white arrows). Scale bar = 20  $\mu$ m. (C-D) Satellite cell density in the plantaris and soleus. Data represent mean  $\pm$  SEM. n = 6-9 mice per group. Data were analyzed via a two factor ANOVA. Post hoc comparisons were made with Sidak post-tests. \*P < 0.05, interaction effect between condition and treatment; † P < 0.05, running SC+ vs sedentary SC+; ‡ P < 0.05, running SC+ vs running SC-.

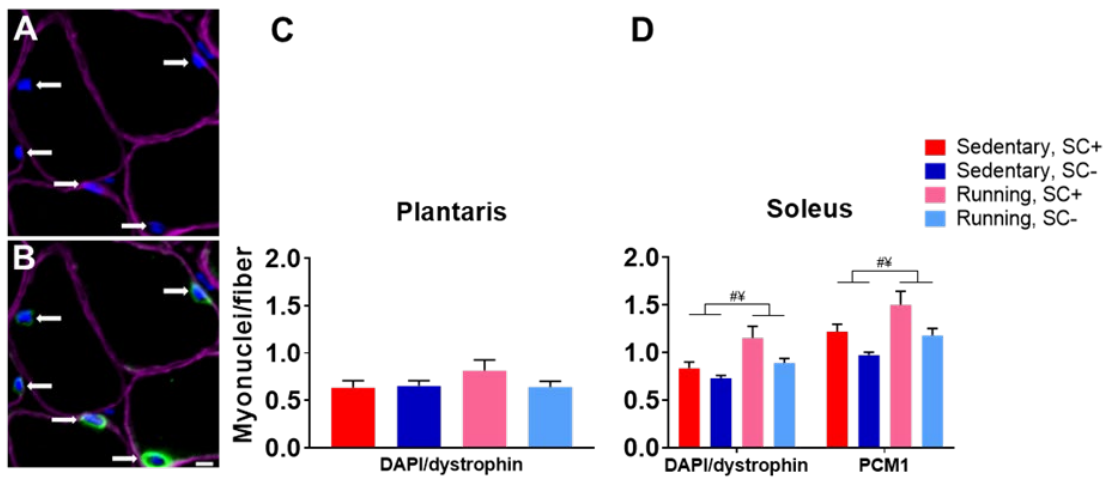


**Figure 3.2**

Myonuclear accretion with lifelong physical activity was dependent on the presence of satellite cells. (A) Representative image of dystrophin (purple) and DAPI (blue) staining from muscle cross sections to identify myonuclei (white arrows). (B) Representative image of dystrophin (purple) and DAPI (blue) and PCM1 (green) staining from muscle cross sections to identify myonuclei (white arrows). Scale bar = 5  $\mu$ m. (C-D) Myonuclear density of the plantaris and soleus. Data represent mean  $\pm$  SEM. n = 6-9 mice per group. Data were analyzed via a two factor ANOVA. #P < 0.05, running vs sedentary mice; ¥P < 0.05, SC+ vs SC- mice.

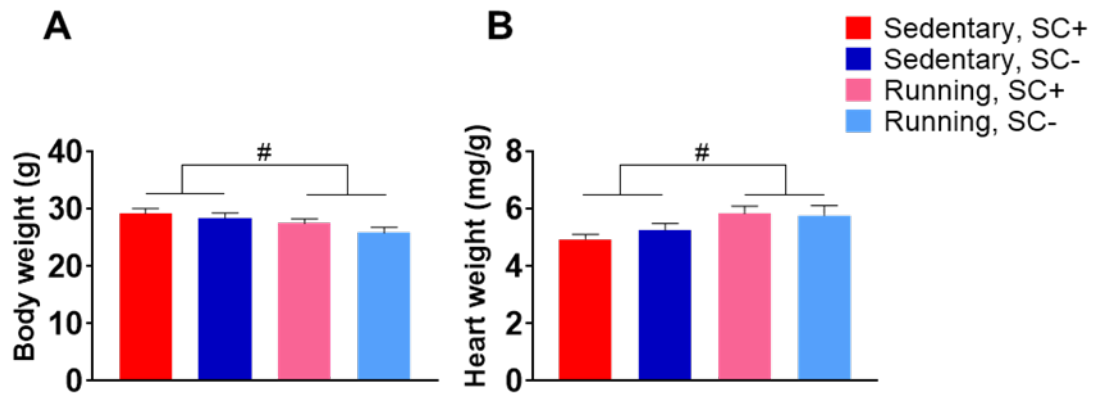


**Figure 3.3**

Lifelong physical activity led to a lower body weight and higher heart weight independent of satellite cells. (A) Body weight. (B) Heart weight normalized to body weight. Data represent mean  $\pm$  SEM. n = 7-9 mice per group. Data were analyzed via a two factor ANOVA. #P < 0.05, running vs sedentary mice.

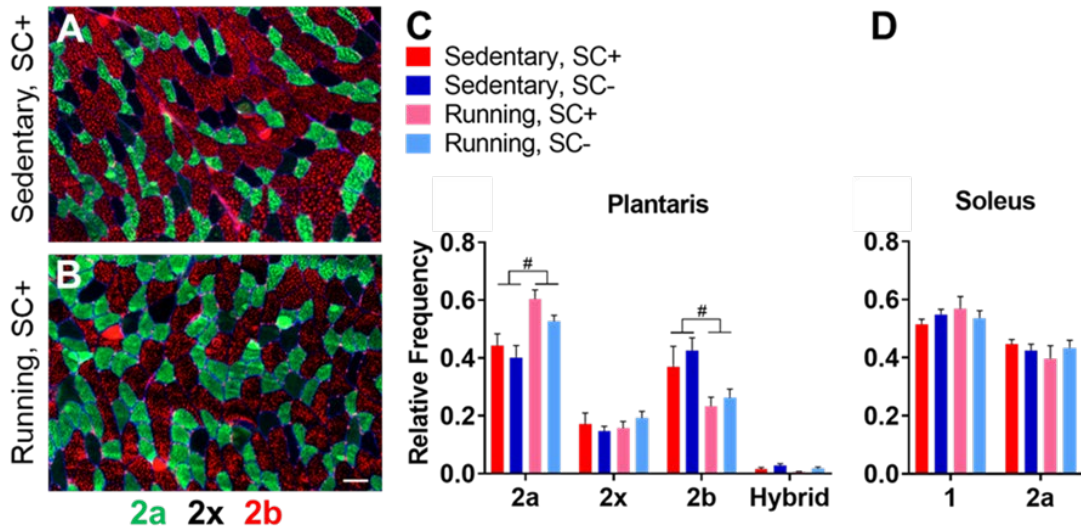


**Figure 3.4**

Lifelong physical activity led to an oxidative shift in muscle fiber composition in the plantaris. (A-B) Representative images of the plantaris muscle stained for dystrophin (blue), myosin heavy chain 2a (green) and myosin heavy chain 2b (red). Scale bar = 50  $\mu$ m. (C-D) Relative frequency of fiber type in the plantaris and soleus. Data represent mean  $\pm$  SEM. n = 6-9 mice per group. Data were analyzed via a two factor ANOVA. #P < 0.05, running vs sedentary mice.

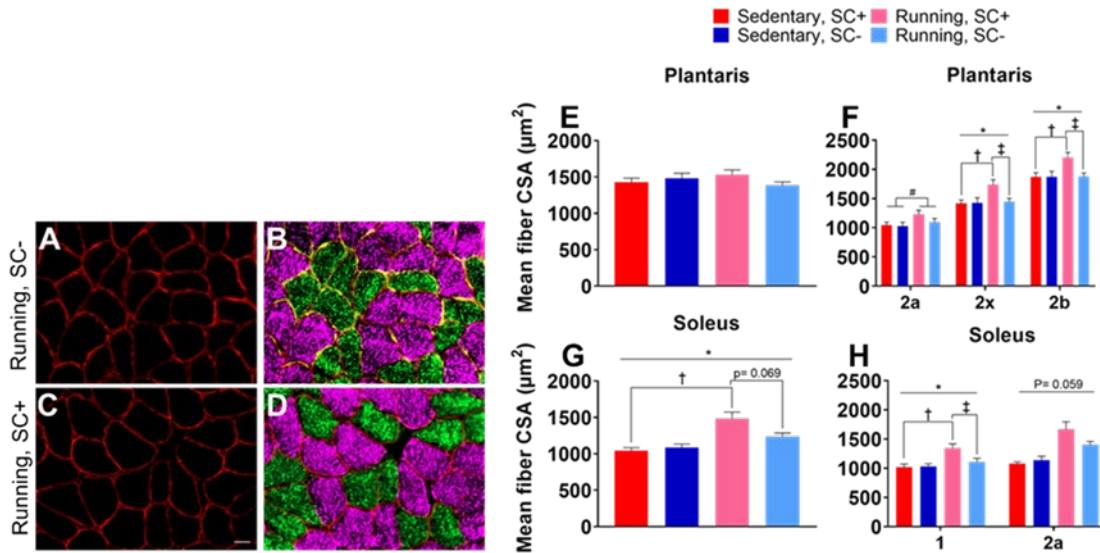


**Figure 3.5**

Satellite cell depletion limited the hypertrophic response induced by lifelong physical activity. (A-D) Representative images of muscle fiber size in the soleus stained for dystrophin (red), type 1 myosin heavy chain (pink) and type 2a (green) myosin heavy chain. Scale bar = 20 µm. (E) Whole muscle mean fiber CSA in the plantaris. (F) Mean fiber CSA by fiber type in the plantaris. (G) Whole muscle mean fiber CSA in the soleus. (H) Mean fiber CSA by fiber type in the soleus. Data represent mean ± SEM. n = 6-9 mice per group. Data were analyzed via a two factor ANOVA. Post hoc comparisons were made with Sidak post-tests. \*P < 0.05, interaction effect between condition and treatment; † P < 0.05, running SC+ vs sedentary SC+; ‡ P < 0.05, running SC+ vs running SC-.

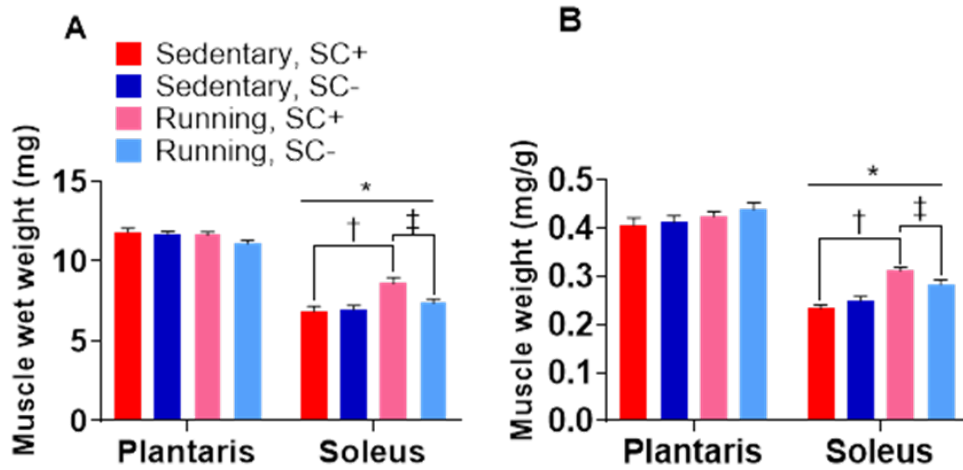


**Figure 3.6**

Satellite cell depletion limited muscle growth in the soleus induced by lifelong physical activity. (A) Muscle wet weights in the plantaris and soleus. (B) Muscle weights normalized to body weight. Data represent mean  $\pm$  SEM.  $n = 7-9$  mice per group. Data were analyzed via a two factor ANOVA. Post hoc comparisons were made with Sidak post-tests. \* $P < 0.05$ , interaction effect between condition and treatment; †  $P < 0.05$ , running SC+ vs sedentary SC+; ‡  $P < 0.05$ , running SC+ vs running SC-.





**B**

P-value	Pathway
1.47E-17	Olfactory transduction - Mus musculus (mouse)
2.57E-09	GPCR downstream signaling
3.88E-09	Signaling by GPCR
6.62E-09	Olfactory Signaling Pathway
1.58E-07	Signal Transduction
0.000	Formyl peptide receptors bind formyl peptides and many other ligands
0.001	Arachidonic acid metabolism - Mus musculus (mouse)
0.002	G alpha (i) signalling events
0.002	GPCR ligand binding
0.002	Cytokine-cytokine receptor interaction - Mus musculus (mouse)

**C**

P-value	Pathway
7.46E-06	mRNA 3'-end processing
7.46E-06	Post-Elongation Processing of Intron-Containing pre-mRNA
6.65E-05	Cleavage of Growing Transcript in the Termination Region
6.65E-05	RNA Polymerase II Transcription Termination
6.65E-05	Post-Elongation Processing of the Transcript
8.67E-05	mRNA Splicing - Major Pathway
8.67E-05	mRNA Splicing
0.001	Nucleotide-like (purinergic) receptors
0.002	Processing of Capped Intron-Containing Pre-mRNA
0.003	P2Y receptors

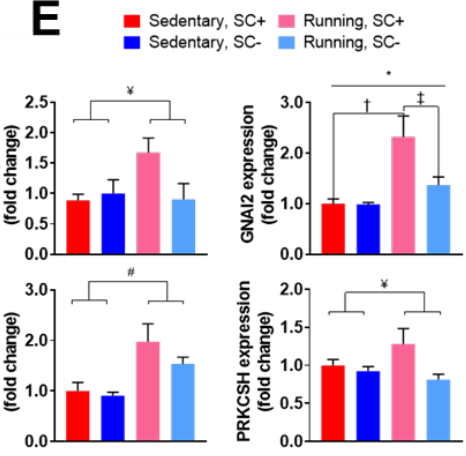
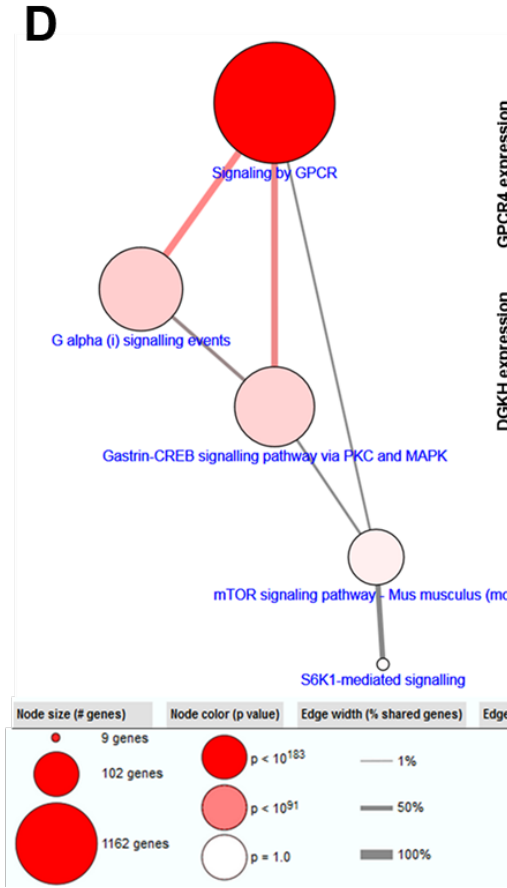


### Figure 3.7

Lifelong exercise in the presence of satellite cells influenced global transcription and up-regulated expression of genes involved in GPCR signaling pathways in the plantaris. (A) Venn diagram of genes enriched in the soleus and plantaris of satellite cell replete runners. Top 10 gene sets overrepresented in the (B) plantaris and (C) soleus. (D) Gene set enrichment analysis highlighting the  $G\alpha_{i2}$  signaling network in the plantaris. (E) RT-qPCR results of  $G\alpha_{i2}$  genes verified the results seen in our gene set enrichment analysis. Data represent mean  $\pm$  SEM. n = 6-9 mice per group. Data were analyzed via a two factor ANOVA. Post hoc comparisons were made with Sidak post-tests. \*P < 0.05, interaction effect between condition and treatment; † P < 0.05, running SC+ vs sedentary SC+; ‡ P < 0.05, running SC+ vs running SC-. #P < 0.05, running vs sedentary mice; ¥ P < 0.05, SC+ vs SC- mice.

# A

P-value	Pathway
1.12E-22	Olfactory transduction - Mus musculus (mouse)
8.83E-14	Olfactory Signaling Pathway
1.04E-09	GPCR downstream signaling
2.13E-09	Signaling by GPCR
1.31E-07	Signal Transduction

# B

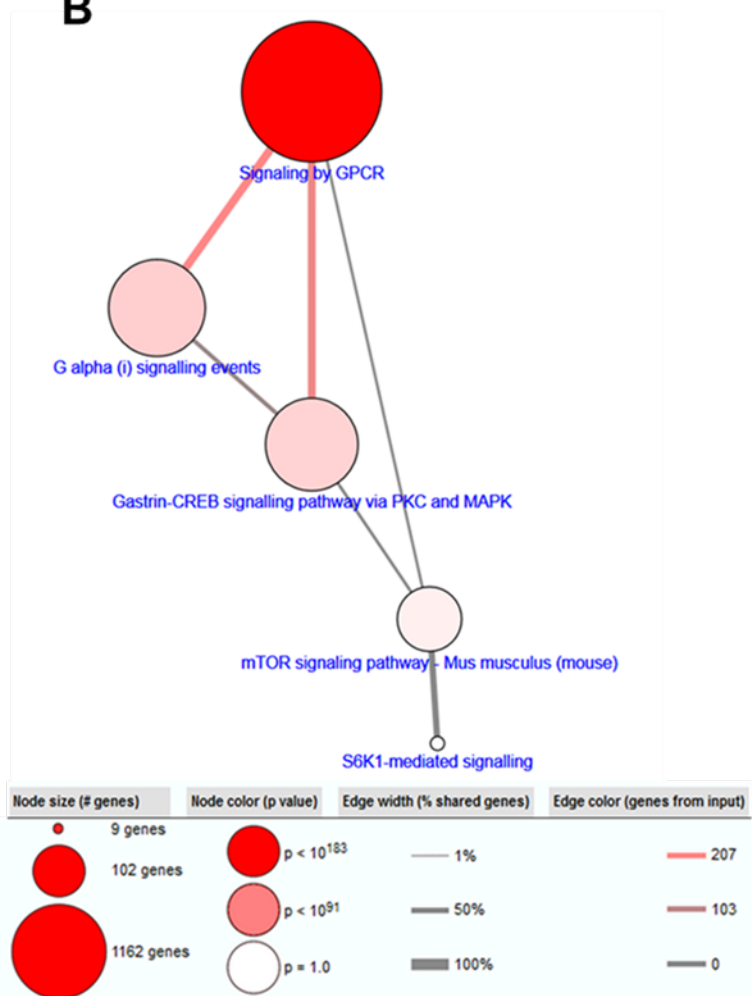


**Figure 3.8**

Differences in enriched gene sets persisted after controlling for running volume. (A) Top 5 gene sets overrepresented in the plantaris of satellite cell replete mice when compared to depleted mice that ran equal volumes. (B) Gene set enrichment analysis highlighting the  $G\alpha_{i2}$  signaling network.

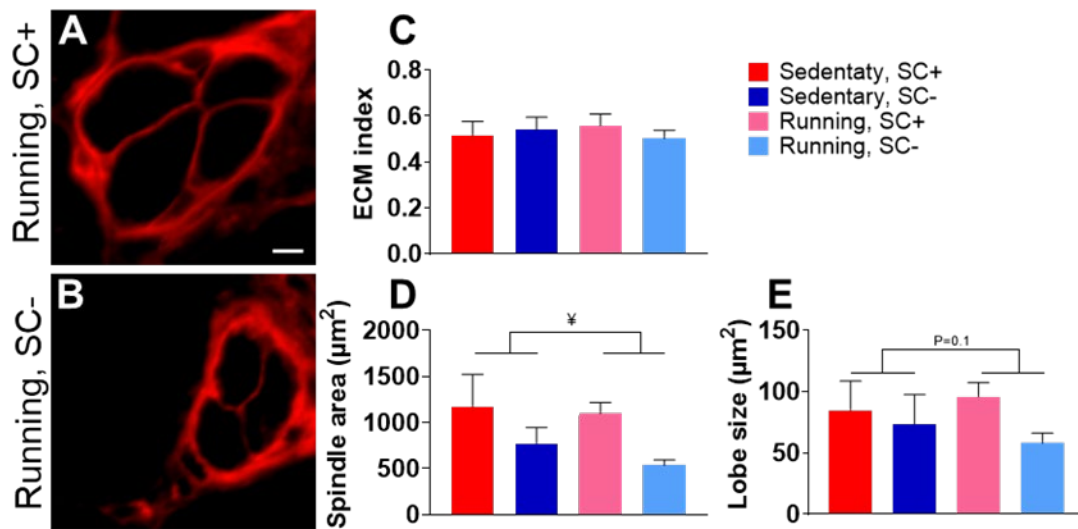


**Figure 3.9**

Satellite cell depletion affected muscle spindle characteristics but not ECM accumulation.

(A-B) Representative images of muscle spindle fibers from the plantaris muscle. Scale

bar = 5  $\mu\text{m}$ . Quantification of, (C) ECM index, (D) spindle area and (E) spindle lobe size.

Data represent mean  $\pm$  SEM. n = 4 mice per group. Data were analyzed via a two factor

ANOVA.  $\text{¥}$  P < 0.05, SC+ vs SC- mice.

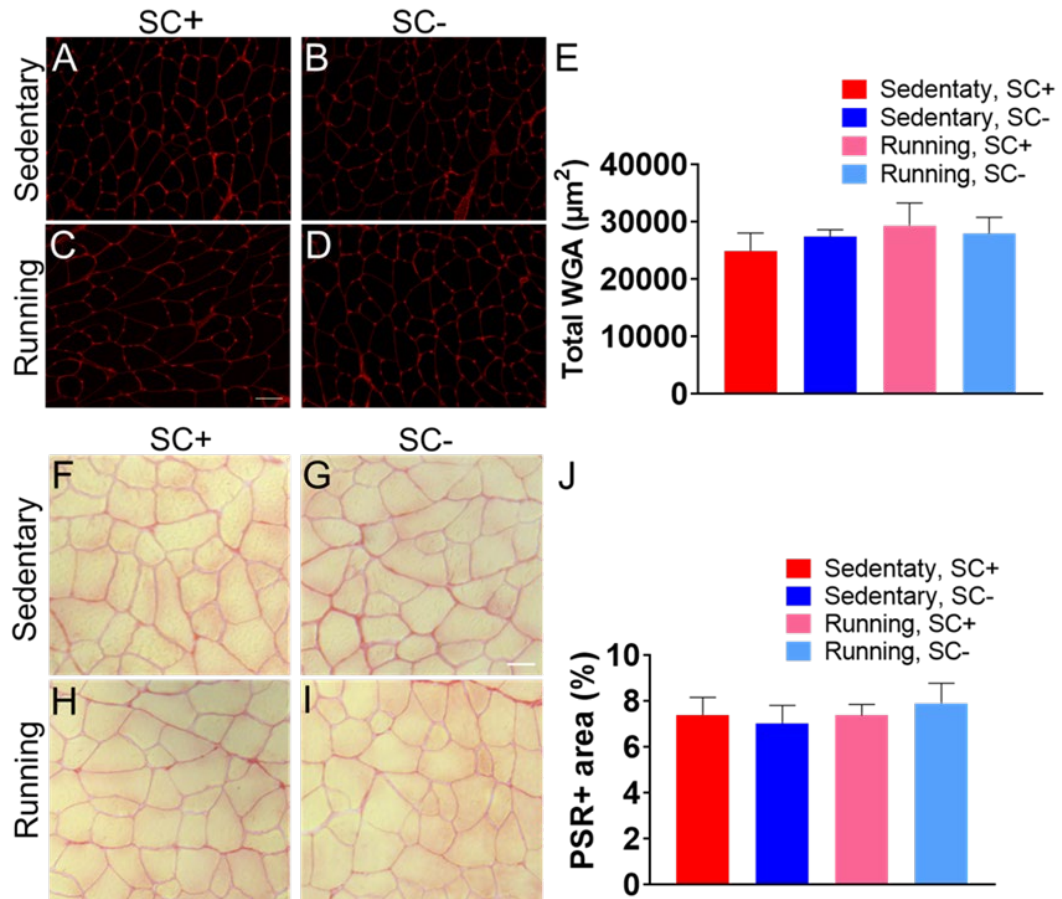


**Figure 3.10**

Satellite cell depletion did not cause fibrosis in response to lifelong physical activity. (A-E) Representative WGA-stained muscle cross sections and quantification. Scale bar = 50 µm. (F-J) Representative PSR-stained muscle cross sections and quantification. Scale bar = 20 µm. Data represent mean ± SEM. n = 7-8 mice/group.

**CHAPTER 4: RESIDENT MUSCLE STEM CELL DEPLETION BLUNTS  
MUSCLE FIBER HYPERTOPHY AFTER SHORT AND LONG TERM  
WEIGHTED WHEEL RUNNING**

## Abstract of Chapter 4

Satellite cells, the resident muscle stem cell, are required for post-natal development, skeletal muscle regeneration across the lifespan and skeletal muscle growth before maturity ( $\geq 4$  months old). Certain groups, including our own, have aimed to specifically address whether satellite cells are required for hypertrophic growth in mature skeletal muscle. We have reported that satellite cells are not required for hypertrophy in response to short-term testosterone administration or synergist ablation induced mechanical overload; however, we have discovered that sustained periods of muscle growth during long term-term synergist ablation or wheel running requires satellite cells for maximal adaptation. Certain studies even suggest the absence of myonuclear addition completely inhibits muscle growth. These divergent results highlight distinct cellular processes regulating muscle adaptation in response to satellite cell depletion based on the chosen intervention. Here, we aimed to generate a comprehensive characterization and transcriptome-wide profiling of skeletal muscle during growth and adaptation in the presence and absence of satellite cells in order to identify distinct phenotypes and signaling networks influenced by satellite cell content. We administered vehicle or tamoxifen to adult Pax7-Diphtheria Toxin A (Pax7-DTA) mice and subjected them to 4 and 8 weeks of progressive weighted wheel running (PoWeR) and performed immunohistochemical (IHC) analysis on the soleus (oxidative phenotype) and plantaris (mixed oxidative and glycolytic phenotype) of vehicle- (SC+) and tamoxifen-treated (SC-) mice and whole-muscle RNA-seq on the soleus. We further performed single myonuclear (smn) RNA-seq on the soleus muscle of SC+ and SC- mice after PoWeR to provide distinct information on how satellite cell fusion affects myonuclear transcription.



We show that while skeletal muscle can mount a robust hypertrophic response to PoWeR in the absence of satellite cells, growth is ultimately blunted at 4 and 8 weeks in the soleus and at 8 weeks in the plantaris. Transcriptome-wide profiling revealed several signaling networks key to muscle adaptation are dysregulated in the absence of satellite cells in the soleus at the 4 and 8 week time points.

## 4.1 Introduction

Satellite cells, the resident muscle stem cell, are required for post-natal development, skeletal muscle regeneration across the lifespan and skeletal muscle growth before maturity ( $\geq 4$  months old)<sup>19,86,87,91</sup>. Certain groups, including our own, have aimed to specifically address whether satellite cells are required for hypertrophic growth in response to mechanical loading, testosterone administration (see Chapter 2), and exercise (see Chapter 3), in mature skeletal muscle<sup>20,24,34,62,87,90</sup>. Findings vary and seem to be influenced by a host of confounding variables across studies, such as the mode and length of perturbation utilized to induce muscle growth, the duration of satellite cell depletion, the timing of depletion (pre, post or at some point during adaptation) and the mouse model utilized<sup>20,24,34,62,90,109</sup>. Our group has leveraged the Pax7-Diphtheria Toxin A (Pax7-DTA) strain to deplete satellite cells at several time points and over various durations to gain a fundamental understanding for the requirements of satellite cells during adaptation and growth<sup>31,34,90,91,139</sup>. To date, we have reported that satellite cells are not required for hypertrophy in response to short-term testosterone administration or synergist ablation induced mechanical overload; however, we have discovered that sustained periods of muscle growth during long term-term synergist ablation or wheel running requires satellite cells for maximal adaptation<sup>34,62,90</sup>.

Our findings in response to synergist ablation show activated satellite cells play a critical role in regulating fibrosis during growth via exosome delivery of miR-206 to fibroblasts, targeting *Rrbp1* and suppressing collagen biosynthesis<sup>51</sup>. Interestingly, the presence of satellite cells was only required for the first week of muscle overload in order to mount effective extracellular matrix remodeling and growth<sup>51</sup>. This suggests that

blunted long-term growth in the absence of satellite cells is related more to secretory signaling via activated satellite cells than to a lack of satellite cell fusion and myonuclear accretion, at least in response to synergist ablation<sup>51,90</sup>. Interestingly, in response to a more translational model of muscle adaptation, long term wheel running, hypertrophy in the absence of satellite cells was attenuated, independent of fibrosis, as shown in Chapter 3<sup>34</sup>. Adding to this complexity, in Chapter 3, our data show there may be muscle-specific roles for satellite cells, with glycolytic muscles being more reliant on the secretory function of satellite cells and oxidative muscles more reliant on fusion. Conversely, findings from the Myomaker<sup>scKO</sup> mouse strain (a model of impaired satellite cell fusion) suggest the absence of myonuclear addition completely inhibits muscle growth in response to synergist ablation and uphill treadmill running<sup>20,24</sup>. These divergent results highlight distinct cellular processes regulating muscle adaptation in response to satellite cell depletion based on the applied stimuli and potentially the mouse strain being used.

While synergist ablation has classically been utilized to study muscle hypertrophy in mice, several groups have recently developed models of muscle growth and adaptation that can be more easily translated to humans<sup>24,63,144-146</sup>. Our group published a report characterizing a progressive weighted wheel running (PoWeR) protocol that induces robust skeletal muscle adaptation and growth with a resulting phenotype very similar to that of progressive cycle training in humans<sup>112</sup>. This new model, along with others, provide an opportunity to perform rigorous and translational studies to generate novel information that further elucidates how satellite cells influence skeletal muscle adaptation.

Here, we aimed to generate a comprehensive characterization and transcriptome-wide profiling of skeletal muscle during growth and adaptation in the presence and absence of satellite cells in order to identify distinct phenotypes and signaling networks influenced by satellite cell content. We subjected Pax7-DTA mice to 4 and 8-weeks of PoWeR and performed immunohistochemical (IHC) analysis on the soleus (oxidative phenotype) and plantaris (mixed oxidative and glycolytic phenotype) of vehicle- (SC+) and tamoxifen-treated (SC-) mice and whole-muscle RNA-seq on the soleus. We further performed single myonuclear (smn) RNA-seq on the soleus muscle of SC+ and SC- mice after PoWeR to provide distinct information on how satellite cell fusion affects myonuclear transcription. We show that while skeletal muscle can mount a robust hypertrophic response to PoWeR in the absence of satellite cells, growth is ultimately blunted at 4 and 8 weeks in the soleus and at 8 weeks in the plantaris. Transcriptome-wide profiling revealed several signaling networks key to muscle adaptation are dysregulated in the absence of satellite cells in the soleus at the 4 and 8 week time points.

## 4.2 Methods

### Animals

The Pax7<sup>CreER/+</sup>-R26<sup>DTA/+</sup> strain, called Pax7-DTA, was generated by crossing the Pax7<sup>CreER/CreER</sup> mouse strain with the Rosa26<sup>DTA/DTA</sup> mouse strain <sup>3</sup>. The Pax7-DTA mouse allows for the specific and inducible depletion of satellite cells upon tamoxifen treatment, through *Cre*-mediated recombination to induce expression of the diphtheria toxin A (DTA) gene in Pax7-expressing cells, effectively killing satellite cells. All animal procedures were conducted in accordance with institutional guidelines approved by the Institutional Animal Care and Use Committee of the University of Kentucky.

## Experimental design

For initial whole-muscle RNA-seq and IHC experiments, forty-eight adult (6-months old) female Pax7-DTA mice were treated via intraperitoneal injection with vehicle (SC+) (15 % ethanol in sunflower seed oil) or tamoxifen (SC-) at a dose of 2.5 mg/day for five days, as previously described<sup>87</sup>. Following a 1-wk washout period, mice were singly housed and randomly assigned to 4-wk Sedentary SC+/SC- or 8-wk Sedentary groups (cage with locked running wheel), 4-wk PoWeR SC+/SC- groups or 8-wk PoWeR SC+/SC- groups (n=8 per group). After 1-week of acclimation to an unweighted wheel, 4-wk PoWeR consisted of 2 g of weight in week 1, 3 g in week 2, 4 g in week 3, 5 g in week 4; 8-wk PoWeR consisted of 2 g of weight in week 1, 3 g in week 2, 4 g in week 3, 5 g in weeks 4 and 5, and 6 g in weeks 6–8 (**Figure 1A**). The wheels were loaded with 1 g magnets (product no. B661, K&J Magnetics, Pipersville, PA). ClockLab software (Actimetrics, Wilmette, IL) was used to record running behavior. The animals had access to food and water ad libitum and were checked daily for health and wellness. Running wheels were locked 24 hours before sacrifice and mice were fasted overnight. The soleus and plantaris muscles were excised, weighed and prepared for IHC analysis and the contralateral limb for RNA extraction, and then stored at –80 °C. As there were no differences in body or muscle weights between the 4 and 8-week time points for both SC+ and SC- sedentary mice, time points were collapsed and treated as one group. An additional 6 mice were randomly assigned to the 4-wk PoWeR SC+/SC- groups. Wheels were locked 4 or 24 hours before sacrifice and mice were fasted overnight. The soleus muscle was excised at both time points and prepared immediately

for smnRNA-seq. Another group of 6 mice were randomly assigned to the 8-wk PoWeR SC+/SC- groups for in vivo force testing. Wheels were locked 48 hours before testing.

### **Immunohistochemistry**

IHC analyses were performed as previously described<sup>91</sup>. Briefly, hindlimb muscles were extracted and weighed, then were pinned to a cork block at resting length and covered with Tissue Tek Optimal Cutting Temperature compound (Sakura Finetek, Torrance, CA, USA), and quickly frozen in liquid nitrogen cooled isopentane and stored at -80°C. Frozen muscles were sectioned at -23°C (7 µm), air-dried for at least one hour, and then stored at -20°C. For determining fiber type distribution, muscle fiber cross-sectional area (CSA), fiber type-specific CSA, and myonuclear density, cross sections were incubated overnight in a cocktail of isotype specific anti-mouse antibodies for MyHC 1 (1:75, IgG2B, BA.D5), MyHC 2a (neat, IgG1, SC.71), and MyHC 2b (neat, IgM, BF.F3) from Developmental Studies Hybridoma Bank (DSHB, Iowa City, Iowa, USA), along with an antibody against dystrophin (1:100, ab15277, Abcam, St. Louis, MO, USA), to delineate fiber borders for CSA quantification. Sections were subsequently incubated with secondary antibodies (1:250, goat anti-mouse IgG2b Alexa Fluor 647, #A21242; 1:500, IgG1 Alexa Fluor 488, #A21121; 1:250, IgM Alexa Fluor 555, #A21426) from Invitrogen (Carlsbad, CA, USA), along with the secondary antibody for dystrophin (1:150, anti-rabbit IgG AMCA, CI-1000, Vector), diluted in PBS. Sections were mounted using VectaShield with DAPI (H-1200, Vector).

Detection of Pax7+ cells was performed as previously described<sup>87</sup>. Briefly, sections were fixed in 4% paraformaldehyde (PFA) followed by antigen retrieval using sodium citrate (10 mM, pH 6.5) at 92°C. Endogenous peroxidase activity was blocked

with 3% hydrogen peroxide in phosphate-buffered saline (PBS) followed by an additional blocking step with 1% Tyramide Signal Amplification (TSA) blocking reagent (TSA kit, T20935, Invitrogen) and Mouse-on-Mouse blocking reagent (Vector Laboratories, Burlingame, CA, USA). Pax7 primary antibody (1:100, DSHB) and laminin primary antibody (1:100, Sigma-Aldrich) were diluted in 1% TSA blocking buffer and applied overnight. Samples were then incubated with anti-mouse biotin-conjugated secondary antibody against the Pax7 primary antibody (1:1000, 115-065-205, Jackson ImmunoResearch, West Grove, PA, USA) and anti-rabbit secondary for laminin (1:250, A11034, Alexa Fluor 488, Invitrogen, Carlsbad, CA, USA). Slides were washed in PBS followed by streptavidin-horseradish peroxidase (1:500, S-911, Invitrogen) for 1 hour. AlexaFluor 594 was used to visualize antibody-binding for Pax7 (1:100, TSA kit, Invitrogen). Sections were mounted and nuclei were stained with Vectashield with DAPI (H-1200, Vector).

Detection of N-acetyl-d-glucosamine was evaluated on muscle sections using Texas Red-conjugated wheat germ agglutinin (WGA (eBiosciences, San Diego, CA)). Sections were fixed in 4 % PFA and then incubated with WGA conjugate for 2 hours at room temperature. Sections were stained with Picrosirius red (PSR) for 1 hour per the manufacturer's instructions (24901-500; Polysciences, Warrington, PA, USA). PSR staining was used according to the manufacturer's recommendations to visualize the collagen network under polarized light. Detection of capillaries was evaluated on muscle sections using lectin<sup>147</sup>. Fresh muscle sections were cut and allowed to air dry for 4 hours, rehydrated with PBS, blocked in 2.5% normal horse serum (Vector Laboratories,

S-2012) and incubated in Texas Red conjugated Lectin from Griffonia Simplicifolia Lectin I (1:50) diluted in 2.5% NHS (Sigma, L4889).

### **Image quantification**

All WGA images were captured at 10x magnification, and the total stained area quantified using the thresholding feature of the AxioVision Rel software, as described previously<sup>109</sup>. PSR images were captured at 10x magnification and quantifications were obtained with ImageJ software. For analysis, polarized images were analyzed and the amounts of densely (red) and loosely (green) packed collagen were quantified in the muscle cross sections relative to muscle area with ImageJ. Lectin images were captured at 10x magnification and the thresholding feature of the AxioVision Rel software was used to identify Lectin+ capillaries. All remaining images were captured at 20x magnification at room temperature using a Zeiss upright fluorescent microscope (Zeiss AxioImager M1 Oberkochen, Germany). Whole muscle sections were obtained using the mosaic function in Zeiss Zen 2.3 imaging software. To minimize bias and increase reliability, fiber type distribution, muscle fiber CSA, fiber type-specific CSA and myonuclear density were quantified on cross sections using MyoVision automated analysis software<sup>106</sup>. To determine satellite cell density (Pax7+ cells/fiber), satellite cells (Pax7+/DAPI+) were counted manually on entire muscle cross sections using tools in the Zen software. Satellite cell counts were normalized to fiber number, delineated by laminin boundaries. All manual counting was performed by a blinded, trained technician.

### **RNA isolation**

Soleus muscles were homogenized in QIAzol (Qiagen, Hilden, Germany) and RNA was isolated using RNeasy Mini Kit (Qiagen) according to the manufacturer's



instructions. Two  $\mu\text{g}$  of RNA was eluted in 50  $\mu\text{L}$  of nuclease-free water (concentration 50ng/ $\mu\text{L}$ ) and purity checked: RIN  $\geq 6.8$  OD260/280  $> 2.0$  and sent to Novogene for subsequent library construction, sequencing and preliminary bioinformatic analysis. RNA samples were pooled (n=4/group) based on the experimental results reported by Kendzierski et al. showing that gene expression from RNA pools are similar to averages of individuals that comprise the pool <sup>122</sup>.

### **RNA-seq analysis**

Downstream analysis was performed using a combination of programs including STAR, HTseq, Cufflink and our wrapped scripts. Alignments were parsed using Tophat program and differential expressions were determined through DESeq2/edgeR. Reference genome and gene model annotation files were downloaded from genome website browser (NCBI/UCSC/Ensembl) directly. Indexes of the reference genome was built using STAR and paired-end clean reads were aligned to the reference genome using STAR (v2.5). STAR used the method of Maximal Mappable Prefix(MMP) which can generate a precise mapping result for junction reads. HTSeq v0.6.1 was used to count the read numbers mapped of each gene. And then FPKM of each gene was calculated based on the length of the gene and reads count mapped to this gene. FPKM, Reads Per Kilobase of exon model per Million mapped reads, considers the effect of sequencing depth and gene length for the reads count at the same time, and is currently the most commonly used method for estimating gene expression levels <sup>148</sup>. Differential expression analysis between two conditions/groups (two biological replicates per condition) was performed using the DESeq2 R package (2\_1.6.3). DESeq2 provide statistical routines for determining differential expression in digital gene expression data using a model based

on the negative binomial distribution. The resulting P-values were adjusted using the Benjamini and Hochberg's approach for controlling the False Discovery Rate (FDR). Genes with an adjusted P-value <0.1 found by DESeq2 were assigned as differentially expressed.

### **Myonuclear isolation**

Soleus muscles were excised immediately following euthanasia and the protocol developed by Cutler et al. was followed for isolation of myonuclei<sup>149</sup>. Briefly, muscles were minced with scissors in homogenization buffer (500 µl HEPES (1 M) 3 ml KCl (1 M) 250 µl spermidine (100 mM) 750 µl spermine tetrahydrochloride (10 mM) 10 ml EDTA (10 mM) 250 µl EGTA (100 mM) 2.5 ml MgCl (100 mM) 5.13 g sucrose Ultra-pure water to 50 ml Filter sterilize and store at 4 °C for up to 1 month. Immediately prior to use add: 100 µl DTT (1 M) 5 Roche complete mini protease inhibitor tablets), dounced on ice in homogenization buffer and passed through a 40 µm filter into sorting buffer. DAPI was added to label nuclei and fluorescently-labeled nuclei were purified via Fluorescence-activated cell sorting (FACS) and collected in reverse transcription (RT) buffer.

### **Construction of libraries and generation of cDNA on the 10x genomics platform**

Nuclei were loaded into the 10X Chromium system using the Single Cell Reagent Kit v3 according to the manufacturer's protocol. Following library construction, libraries were sequenced on the Illumina NovaSeq 6000 system at the University of Florida.

### **Single myonuclear (smn)RNA-seq analyses**

The Cell Ranger Single-Cell Software Suite was used to perform sample demultiplexing, barcode processing and single-cell 3' gene counting

(<http://software.10xgenomics.com/single-cell/overview/welcome>). The cDNA insert was aligned to an appropriate reference genome using STAR. For mouse cells, mm10 was used. Partek Flow was used for all downstream analysis from Filtered\_Barcode\_Matrix.h5 files. Filter criteria included total reads: (Min: 499, Max: 20,567), expressed genes: (Min: 400, Max: 4,018) and mitochondrial reads percent: (Min: 0%, Max: 15.00%). Additional filtering was performed which excluded features where values were  $< 1.0$  in at least 99.9% of the samples yielding a total of 9,358 genes for downstream analysis. Samples were normalized using counts per million and log transformation. Principal component analysis was used prior to t-SNE for visual based clustering. Myonuclei for each sample were classified by Acta1 expression. Gene set analysis was performed between selected time points and treatments. Low-value filtering was set to 1.0 for lowest average coverage and FDR step-up ( $\text{Adj } p < 0.01$ ) was used for multiple test correction.

### **Pathway analysis**

Differentially expressed gene lists (DEGs) were uploaded to g:Profiler for pathway analysis and uploaded to Cytoscape v3.8 for subsequent enrichment analysis and data visualization. The GeneMANIA application within Cytoscape was also used for network category analysis and data visualization. Nodes were generated with an adjusted  $p$  value  $< 0.1$  for enrichment. The size of each node is scaled to the gene set size, the shape of each node is specific to GO (circle) or pathway (diamond) enrichment. The color of the node is scaled to the adjusted  $p$  value. Edges connecting nodes are scaled to the similarity coefficient (genes shared between nodes). Network categories included: co-expression: genes are linked if their expression levels are similar across conditions in a

gene expression study. Co-localization: genes are linked if they are both expressed in the same tissue or if their gene products are both identified in the same cellular location. Genetic interaction: genes are functionally associated if the effects of perturbing one gene were found to be modified by perturbations to a second gene. Pathway: two gene products are linked if they participate in the same reaction within a pathway. Physical interaction: genes are linked if they were found to interact in a protein-protein interaction study. Predicted: predicted functional relationships between genes.

### **Strength testing**

Following PoWeR training, strength of plantar flexor muscles was determined by in vivo isometric tetanic torque. Mice were anesthetized by 2.5% isoflurane with oxygen set at 1.5 l/min (VetEquip vaporizer) in an induction chamber and transferred to a nose cone. The right hind limb was assessed for all mice. Fur on the lower two-thirds of the hind limb was trimmed (Wahl Bravmini), and the mouse was placed on a 37°C temperature regulated platform (809c in-situ mouse apparatus, Aurora Scientific, Aurora, ON, Canada). The hind limb was securely positioned using a clamp at the knee, and the foot was placed in a footplate attached to a dual-mode lever and motor (300D-300C-LRFP, Aurora Scientific). Tape was wrapped around the foot and footplate to prevent compensatory movement or placement shifting, and the apparatus was adjusted to ensure the tibia was parallel with the platform with a 90-degree angle at the ankle. Platinum needle electrodes were placed percutaneously lateral to the knee to stimulate the tibial nerve via an electric stimulator (High Power Bi-Phase Stimulator, Aurora Scientific). Needles were adjusted to identify the optimal placement to generate maximum torque production and eliminate activation of dorsiflexors, using the Instant Stim function with

Live View in Dynamic Muscle Control LabBook (DMC v6.000). The level of electrical current to stimulate maximal torque output was determined by a series of twitches (0.05 s pulse duration) beginning at 10 mA and increasing to approximately 50 mA until the maximum isometric torque stimulated by the minimum current was determined. This current setting remained constant throughout the subsequent torque-frequency curve to determine maximum isometric tetanic torque (10 Hz, 40 Hz, 80 Hz, 120 Hz, 150 Hz, 180 Hz, and 200 Hz, 0.25s pulse duration with a 2 min rest period between each stimulus). All data were collected with DMC v6.000 and analyzed using Dynamic Muscle Analysis (DMA v5.501).

### **Statistical Analysis**

Results are presented as mean  $\pm$  SEM. Data were analyzed with GraphPad Prism software, via a two-way ANOVA with Tukey's correction for multiple comparisons, a one-way repeated measures ANOVA with Sidak's correction for multiple comparisons or an unpaired two-tailed Student's t-test. Significance was set at a p value  $<0.05$ .

## **4.3 Results**

### **PoWeR-induced muscle growth is blunted in the absence of satellite cells**

Neither satellite cell depletion nor PoWeR influenced body weight over the duration of the study (Figure 4.1B). There was no difference in average daily running volume over the 4-wk and 8-wk PoWeR protocols and this was not influenced by the presence of satellite cells (Figure 4.1C). PoWeR induced higher normalized soleus weight after 4-wks and 8-wks of PoWeR; this effect was blunted at both time points in the absence of satellite cells (Figure 4.1D). PoWeR induced higher normalized plantaris

weight after 4-wks and 8-wks of PoWeR; this effect was blunted at 8-wks in the absence of satellite cells (Figure 4.1E).

### **Higher satellite cell density in the soleus and plantaris of SC+ PoWeR trained mice**

Tamoxifen administration depleted satellite cells  $\geq 90\%$  in the soleus and plantaris in sedentary and PoWeR trained mice. This is shown qualitatively in representative satellite cell IHC from the soleus (Figure 4.2A) and quantitatively in the soleus and plantaris (Figures 4.2B and C). PoWeR training led to higher satellite cell density at 4-wks and 8-wks in the soleus and plantaris of SC+ mice only. This is shown qualitatively in representative satellite cell IHC from the soleus (Figure 4.2A) and quantitatively in the soleus and plantaris (Figures 4.2B and C).

### **PoWeR led to a greater proportion of oxidative fibers in the plantaris, independent of satellite cell content**

Four-wks of PoWeR training led to an oxidative shift in fiber type distribution in the plantaris. This is shown qualitatively in representative fiber type IHC (Figure 4.3A) and quantitatively in Figure 4.3B. Fiber type distribution did not differ between 4-wks and 8-wks of PoWeR in the plantaris (Figure 3B). The soleus did not experience any alterations in fiber type distribution in response to PoWeR (Figure 4.3C).

### **Higher myonuclear density and fiber size in the soleus and plantaris of SC+ PoWeR trained mice**

PoWeR training led to higher myonuclear density at 4-wks in the soleus and plantaris in PoWeR trained mice, which did not increase further at 8-wks. This is shown

qualitatively in representative dystrophin/DAPI staining from the soleus (Figure 4.4A) and quantitatively in the soleus and plantaris (Figures 4.4B and C). PoWeR training led to higher muscle fiber size at 4-wks and 8-wks in both the soleus and plantaris. Satellite cell depletion blunted growth at 4-wks and 8-wks in the soleus and at 8-wks in the plantaris. Fiber size assessment is shown qualitatively in the soleus (Figure 4.4A) and quantified for both the soleus and plantaris (Figures 4.4D and E).

### **Extracellular matrix accumulation did not limit muscle fiber hypertrophy in response to PoWeR**

As we have previously shown excess extracellular matrix (ECM) accumulation is associated with blunted skeletal muscle hypertrophy in response to 8-wks of overload induced by synergist ablation in the absence of satellite cells, we wanted to assess ECM accumulation in response to PoWeR<sup>90</sup>. Neither PoWeR nor satellite cell depletion led to increased levels of glycosaminoglycans surrounding the muscle fibers, measured by wheat germ agglutinin (WGA) staining. This is shown qualitatively in WGA-stained plantaris cross sections (Figure 4.5A), quantified in Figure 4.5B.

### **Whole-muscle and smnRNA-seq reveal dysregulated signaling during adaptation to 4-wks of PoWeR in SC- skeletal muscle**

In an effort to gain an understanding of the underlying mechanisms blunting muscle fiber hypertrophy in SC- skeletal muscle we performed whole-muscle RNA-seq and single myonuclear (smn)RNA-seq on satellite cell replete and deplete soleus. After 4-wks of PoWeR training 1902 genes were overexpressed in SC+ skeletal muscle and 2600 were overexpressed in SC- skeletal muscle relative to their sham controls (Figure 4.6A). Gene ontology (GO) and pathway analyses revealed substantial differences in gene

expression in response to 4-wks of PoWeR between SC+ and SC- skeletal muscle (Figures 4.6B and C). Genes involved in ECM remodeling (both in GO and pathway analyses) and capillarization (GO analysis) were significantly overexpressed only in the presence of satellite cells in response to PoWeR. The SC- group had no statistically enriched pathways. Enrichment mapping, combining GO and pathway analyses, allowed more detailed analyses of the pathways that comprise the nodes of gene networks differentially enriched in SC+ (blue) or SC- (pink) soleus (Figure 4.7A). Figure 4.7B expands the ECM remodeling network and Figure 4.7C expands the capillarization network, with the color of each node scaled to the adjusted p value and the node size scaled to the gene set size. Edge sizes connecting nodes were scaled to the similarity coefficient (genes shared between nodes). Highly enriched nodes in the ECM remodeling network, collagen activated tyrosine kinase receptor signaling pathway (Figure 4.7D), and the capillarization network, artery morphogenesis (Figure 4.7E), specific to SC+ soleus muscle were further analyzed in GeneMANIA to visualize and provide information around the genes within each node. The color of the node for each gene is scaled to an interaction score, defined as the effect of a given gene on the selected pathway. Edges represent network categories (see Methods for detailed description).

After 4-wks of PoWeR training 1844 genes were underexpressed in SC+ skeletal muscle and 2502 were underexpressed in SC- skeletal muscle compared to their sham controls (Figure 4.8A). Enrichment mapping and pathway analysis showed a great deal of similarity in the pathways downregulated in response to 4-wks of PoWeR between SC+ and SC- skeletal muscle (Figures 4.8B-C and 4.9A). Pathways involved in ribosome



biogenesis (Figure 4.9B) and oxidative metabolism (Figure 4.9C) were suppressed in SC+ and SC- skeletal muscle after 4-wks of PoWeR.

In order to examine the myonuclear transcriptome in relation to the whole-muscle transcriptome, we performed RNAseq on individual isolated myonuclei (smnRNA-seq) from SC+ and SC- soleus muscles after 4-wks of PoWeR. Represented are a schematic of the work flow (Figure 4.10A). An unbiased cluster of smnRNA-seq data, including all cell types and myonuclei from SC+ and SC- mice represented on a UMAP plot (Figure 4.10B, left) and a distinct myonuclear cluster showing myonuclei from SC+ muscle in blue and SC- muscle in pink (Figure 4.10B, right). Myonuclei from SC- soleus showed 964 underexpressed genes and 83 overexpressed genes when compared to SC+ myonuclei (Figure 4.10C). Pathway analysis revealed a lower expression of genes in oxidative and ribosomal pathways, revealing a greater suppression of these pathways after exercise in myonuclei in the absence of satellite cells (Figures 4.10D-F).

#### **After 8-wks of PoWeR SC- skeletal muscle displayed delayed transcriptional activity**

After 8-wks of PoWeR training only 166 genes were overexpressed in SC+ skeletal muscle while 1415 were overexpressed in SC- skeletal muscle relative to 4-wk PoWeR (Figure 4.11A). Consistent with a robust transcriptional response, GO and pathway analyses displayed a greater degree of pathway enrichment in SC- muscle in response to 8-wks of PoWeR (Figures 4.11B and C), which was confirmed by enrichment mapping (Figure 4.12A). In particular, the ribosome biogenesis network was only enriched in the absence of satellite cells (Figures 4.11B-C and 4.12C and E) and there

was higher degree of enrichment in oxidative pathways in SC- skeletal muscle (Figures 4.11B and C).

Pathways most highly enriched in the presence of satellite cells (e.g., RNA/mRNA stability) were also upregulated in SC- skeletal muscle (Figures 4.12B and D).

After 8-wks of PoWeR training 157 genes were underexpressed in SC+ skeletal muscle and 1368 were underexpressed in SC- skeletal muscle (Figure 4.13A), consistent with the large difference in overexpressed genes seen between groups (see Figure 4.11A). GO and pathway analyses revealed few pathways to be heavily enriched in either group but heterogeneity existed in enrichment analysis between SC+ and SC- skeletal muscle (Figures 4.13B and C). This was driven largely by the downregulation of gene sets involved in collagen remodeling at the 8-wk time point in the absence of satellite cells. The enriched pathways and biological processes in SC+ skeletal muscle were driven by a small group of genes related to immune function and another small gene set involved in suppressing glycolysis. Given the relatively large number of underexpressed genes in SC- skeletal muscle, the low level of pathway enrichment is surprising and indicates that the vast majority of these underexpressed genes do not map to known biological processes or pathways. This may represent an uncoordinated transcriptional response or be related to meaningful unmapped pathways being altered in response to PoWeR in the absence of satellite cells.

## **Aberrant skeletal muscle adaptation in response to PoWeR in the absence of satellite cells**

Based on the dysregulation of pathways key to skeletal muscle adaptation in the absence of satellite cells, we aimed to determine if there was a resultant phenotype after PoWeR. We found that total collagen area was slightly lower in SC<sup>+</sup> skeletal muscle after PoWeR. This is shown qualitatively in PSR-stained cross sections of the soleus imaged under bright field excitation (Figure 4.14A), quantified in Figure 4.14B. This finding may have been influenced by the larger fibers present in SC<sup>+</sup> muscle, as total PSR was quantified in regions of interest and not the whole muscle cross section.

We found that only in the presence of satellite cells was there an increase in densely and loosely organized collagen networks, suggesting altered collagen organization/remodeling in the absence of satellite cells. This is shown qualitatively in PSR-stained cross sections of the soleus imaged under polarized-light excitation (Figure 4.14C), quantified in Figure 4.14D. We also assessed capillarization and found a trend for reduced capillary density in response to PoWeR in SC<sup>-</sup> skeletal muscle. This is shown qualitatively in lectin-stained cross sections (Figure 4.14E) and quantitatively (Figure 4.14F). To determine if this maladaptive response to exercise influence muscle strength, we assessed peak torque over a force frequency curve and found that plantar flexor muscles from SC<sup>-</sup> mice produced lower levels of peak torque in response to supramaximal stimulation when compared to SC<sup>+</sup> muscles (Figure 4.14G).

## **4.4 Discussion**

Whether satellite cells are required for skeletal muscle hypertrophy is a long-standing debate in the field. It is now apparent that robust muscle fiber hypertrophy can

occur in the absence of satellite cell participation in response to anabolic pharmacological interventions<sup>56,62,107,150-153</sup>. What remains less clear is the need for satellite cells in order to mount a growth response to an exercise (or overload) stimulus<sup>20,24,90</sup>. The findings of this study show that while the soleus and plantaris hypertrophy and adapt to a considerable degree in the absence of satellite cells, these effects are blunted when compared to satellite cell replete muscle. Further, we identify the dysregulation of several exercise-induced gene networks in the soleus in the absence of satellite cells which may contribute to a maladaptive response to exercise.

At the end of 4-wks of PoWeR, soleus muscles from SC- mice have blunted muscle fiber hypertrophy and fail to mount a transcriptional response conducive to optimal skeletal muscle adaptation to exercise. When compared to SC+ mice, there is a failure to increase gene networks regulating collagen turnover/remodeling. In order to determine if this aberrant transcriptional response to PoWeR in SC- mice led to phenotypic alterations, we assessed ECM composition, quantifying both glycosaminoglycans and total collagen content. Although the amount of ECM was not different between groups, immunohistochemical analysis revealed lower proportions of densely and loosely organized collagen networks in soleus muscles from SC+ compared to SC- mice after 8-weeks of PoWeR. ECM remodeling during skeletal muscle hypertrophy is a well characterized phenomenon that is critical for transmitting force generated by muscle fibers<sup>154,155</sup>. Forces are transmitted laterally through basement membrane collagens and longitudinally via fibrillar collagens and the capacity to transmit force is determined by the molecular composition and arrangement of the ECM<sup>154,156</sup>.

Based on the different composition of collagens comprising of satellite cell deplete and replete skeletal muscle after PoWeR, we wanted to determine if there was a resultant strength phenotype by examining measures of in vivo plantar flexion torque. Our data show that while both SC+ and SC- mice reach comparable levels of peak force, force levels drop off rapidly in SC- mice over the duration of strength testing, while peak force levels are maintained in SC+ mice. In line with this, we have previously shown that force generation of the plantaris muscle is attenuated after synergist ablation in SC- skeletal muscle. Here, we show increased remodeling and stiffness of collagen in skeletal muscle only occurs in the presence of satellite cells. It seems likely that in response to PoWeR or synergist ablation altered ECM organization in the absence of satellite cells is contributing to reduced strength outcomes <sup>157 156</sup>.

Gene expression profiling also showed that artery morphogenesis/capillarization pathways were activated in SC+ compared to SC- soleus, which was associated with a trend for lower capillary density in the absence of satellite cells. Capillaries are a critical component of adaptation as they allow for adequate muscle fiber perfusion which supports the delivery of oxygen, growth factors and nutrients to the muscle <sup>158</sup>. In line with this, low capillary density is associated with blunted skeletal muscle growth in humans <sup>159 160</sup>. It is now well established that satellite cells are anatomically close to capillaries and participate in bidirectional signaling with endothelial cells (e.g., VEGF signaling) <sup>161-163</sup>. Satellite cell differentiation supports angiogenesis and a recent report shows high levels of VEGFA in satellite cells, which serves to recruit blood vessel endothelial cells <sup>161-163</sup>. Further, the report by Verma et al., shows ECM organization to

be a highly enriched satellite cell to endothelial cell interaction pathway, which may in part explain our ECM findings <sup>162</sup>.

Our soleus whole-muscle RNA-seq data at the 4-wk time point show both SC+ and SC- mice transcriptionally downregulate several pathways involved in oxidative metabolism and ribosome biogenesis in response to PoWeR. To determine if gene expression responses observed at the whole muscle level were generated from the muscle fiber, as opposed to other cell populations in the muscle, we analyzed the myonuclear transcriptome of the soleus after 4-wks of PoWeR in both SC+ and SC- mice, isolating myonuclei 24 hours after the last running bout, consistent with our whole-muscle data. smnRNA-seq data reveal a greater suppression of metabolic pathways in SC- myonuclei when compared to SC+ myonuclei. Ribosomal biogenesis and oxidative phosphorylation pathways are substantially lower in SC- compared to SC+ myonuclei. A downregulation of several rRNAs after chronic resistance training has been shown previously in humans, corroborating what we report here after 4-wks of PoWeR <sup>164</sup>. Unique to this study, we show a greater degree of downregulation of ribosomal pathways at the myonuclear level in the absence of satellite cells. While the extent to which these differences can be attributed to newly fused satellite cell-derived myonuclei remains to be determined, recent publications using single nuclear RNAseq have demonstrated considerable heterogeneity in myonuclei <sup>165</sup>.

The transcriptional signature of SC+ skeletal muscle at the end of 8-wks of PoWeR varies by only a few hundred genes compared to the 4-wk time point. This demonstrates SC+ muscle is capable of mounting a robust and effective transcriptional response to a novel stimulus in order to coordinate adaptation, which leads to a new

transcriptional homeostasis that is maintained for the final 4-wks of training. As the overall exercise stimulus is similar to that of the first 4-wks of training, this makes a great deal of sense. On the other hand, in SC- skeletal muscle, there is pronounced transcriptional heterogeneity (thousands of differentially expressed genes) between the 4-wk and 8-wk time points, in stark contrast to SC+ skeletal muscle, showing failure to initiate an appropriate transcriptional response to a novel stimulus. Interestingly, though, pathways downregulated at the 4-wk time point (oxidative phosphorylation and ribosome biogenesis) are now upregulated at the 8-wk time point only in SC- skeletal muscle. This may be indicative of delayed, or compensatory, transcriptional activation in resident myonuclei in the absence of satellite cell-dependent myonuclear addition to aid in adaptation.

Our findings reported here are in line with what we have shown previously during synergist ablation induced muscle overload. In response to both mechanical overload and PoWeR, resident myonuclei can transcriptionally support a hypertrophic and adaptive response in the absence of satellite cells and myonuclear addition. However, muscle growth and adaptation are ultimately blunted in satellite cell deplete muscle. The attenuated growth in response to synergist ablation is associated with fibrosis, at least partially due to a lack of communication from satellite cells to fibroblasts to suppress ECM accumulation in response to the severe model of mechanical overload. In response to PoWeR, a more translational model of exercise, muscle does not become fibrotic in the absence of satellite cells, but growth is still attenuated and associated with aberrant ECM/collagen remodeling. Our data reveal satellite cells are critical for a coordinated and effective transcriptional response to a novel stimulus, optimizing adaptations and

muscle hypertrophy. Based on findings from both models, it seems very possible that satellite cells and/or fusion in and of itself is not anabolic, per say, but that satellite cells are a prerequisite for a transcriptional response to exercise that will lead to maximal muscle adaptation.



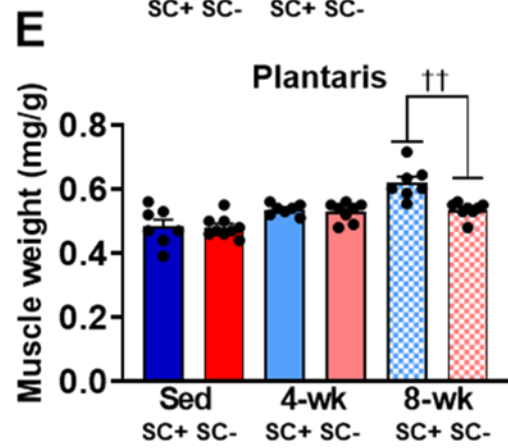
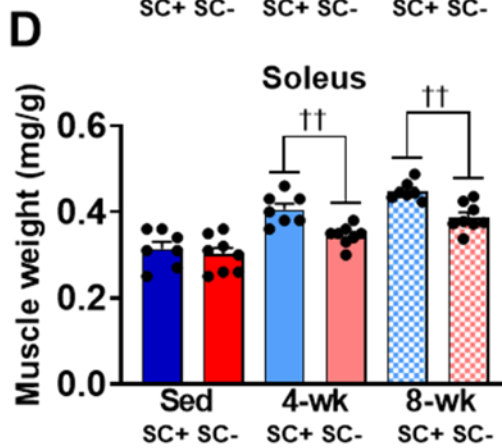
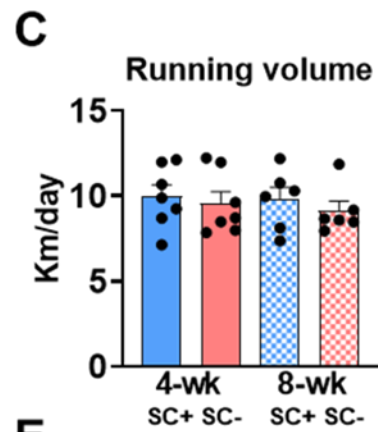
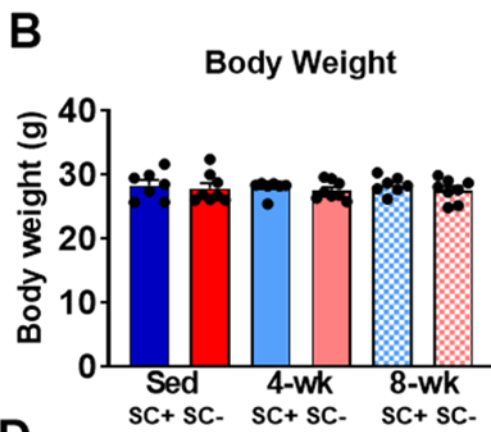
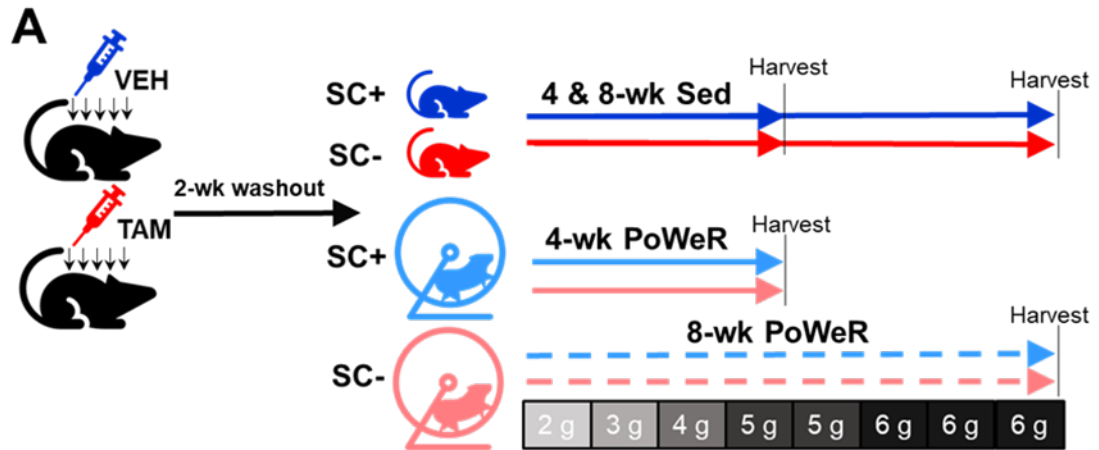


### Figure 4.1

Satellite cell depletion blunted higher muscle weights induced by PoWeR. (A) Schematic showing PoWeR protocol. (B) Endpoint body weights across all groups. (C) Average running volume after 4-wks and 8-wks of PoWeR. (D) Normalized muscle weight in the soleus. (E) Normalized muscle weight in the plantaris. Data are represented as mean  $\pm$  SEM. Statistical analysis: Two-way ANOVA with Tukey's multiple comparisons test. PoWeR led to higher muscle weights at 4-wks ( $p < 0.0001$ ) and 8-wks ( $p < 0.0001$ ) in the soleus and at 4-wks ( $p < 0.01$ ) and 8-wks ( $p < 0.0001$ ) in the plantaris. There was a significant effect for satellite cell depletion blunting this adaptation.  $\dagger\dagger p < 0.01$ .

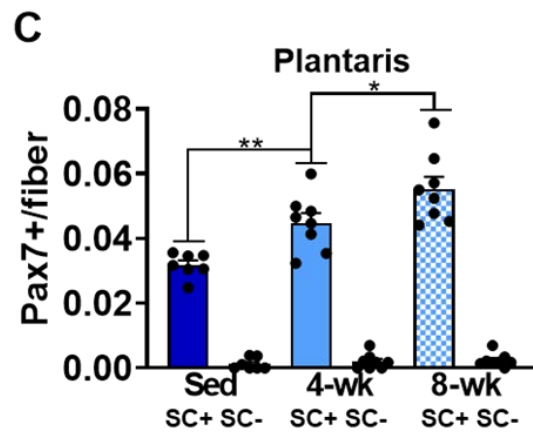
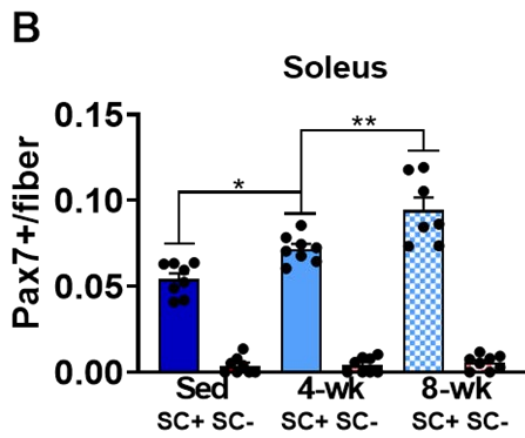
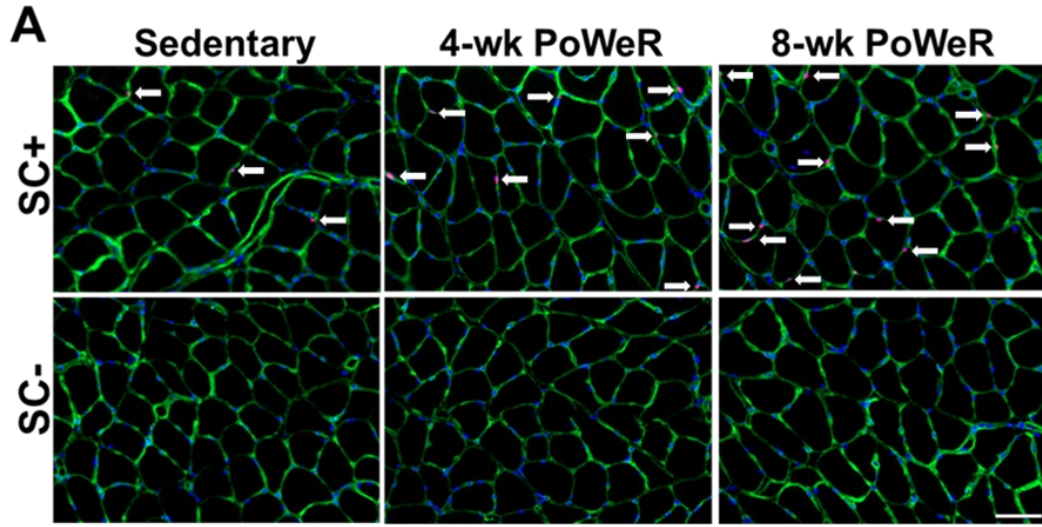


## Figure 4.2

PoWeR led to higher satellite cell content in the soleus and plantaris in SC+ mice. (A) Representative images of satellite cell immunohistochemistry from the soleus across all groups showing laminin (green), nuclei (blue), and Pax7 (red; white arrows). (B) Satellite cell density in the soleus. (C) Satellite cell density in the plantaris. Scale bar = 50  $\mu$ m.

Data are represented as mean  $\pm$  SEM. Statistical analysis: Two-way ANOVA with Tukey's multiple comparisons test. There was a main effect for PoWeR ( $p < 0.0001$ ) and satellite cell depletion ( $p < 0.0001$ ) in the soleus and a main effect for PoWeR ( $p < 0.0001$ ) and satellite cell depletion ( $p < 0.0001$ ) in the plantaris. There was a significant interaction between PoWeR and satellite cell content in the soleus ( $p < 0.001$ ) and plantaris ( $p < 0.0001$ ). \* $p < 0.05$ , \*\* $p < 0.01$ .

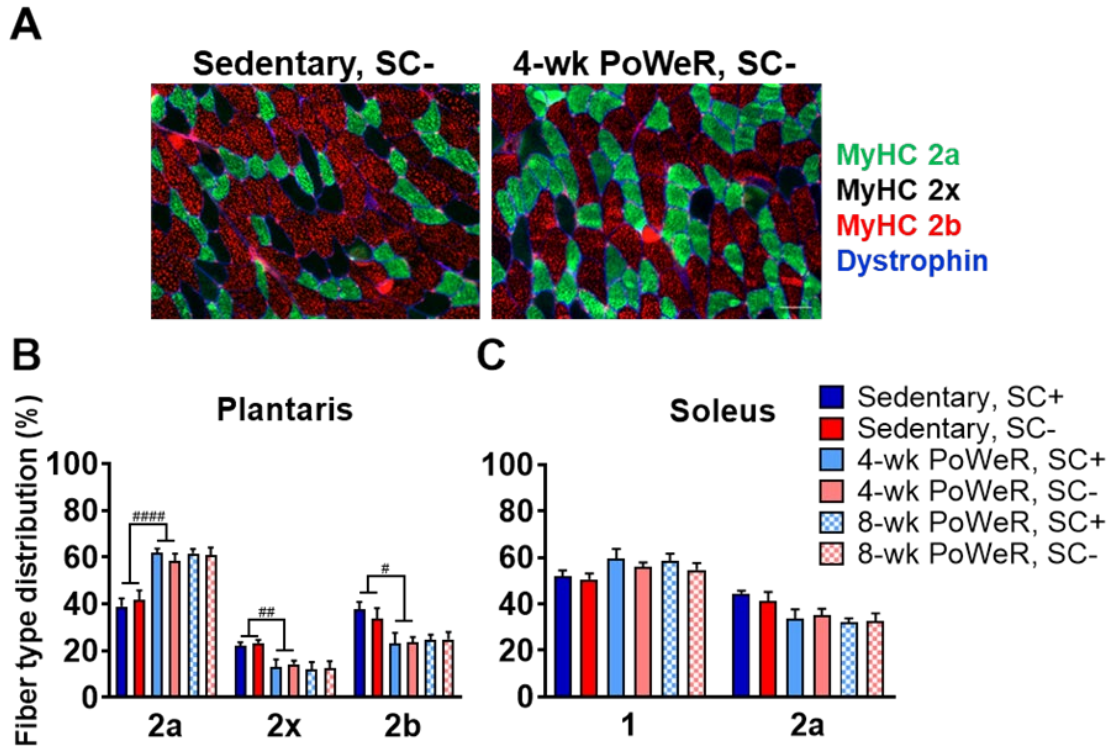


**Figure 4.3**

PoWeR led to an oxidative shift in fiber type distribution in the plantaris. (A)

Representative images of fiber type immunohistochemistry in the plantaris showing dystrophin (blue) myosin heavy chain 2a (green) and myosin heavy chain 2b (red).

Negative (black) fibers were scored as myosin heavy chain 2x. (B) Relative frequency of fiber type in the plantaris. (C) Relative frequency of fiber type in the soleus. Scale bar = 50  $\mu$ m. Data are represented as mean  $\pm$  SEM. Statistical analysis: Two-way ANOVA with Tukey's multiple comparisons test. PoWeR led to a higher proportion of oxidative fibers. # $p$ <0.05, ## $p$ <0.01, #### $p$ <0.0001.

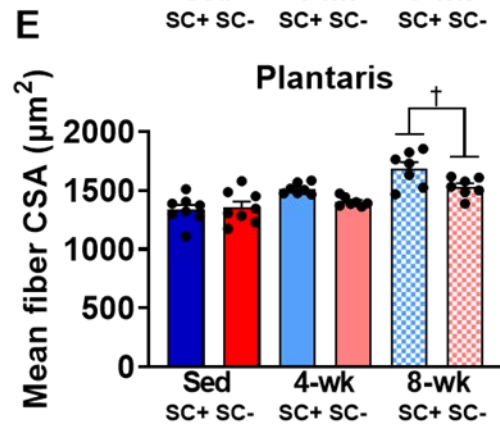
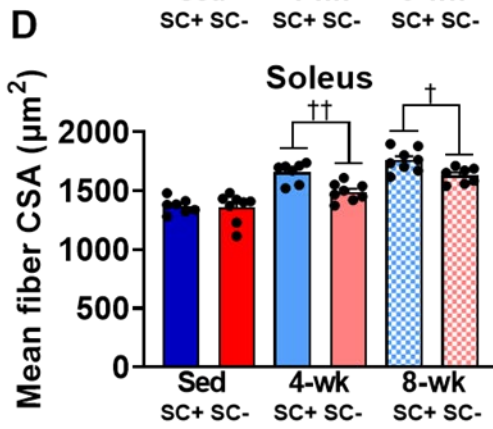
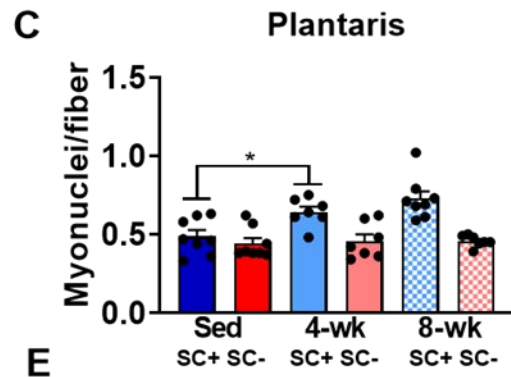
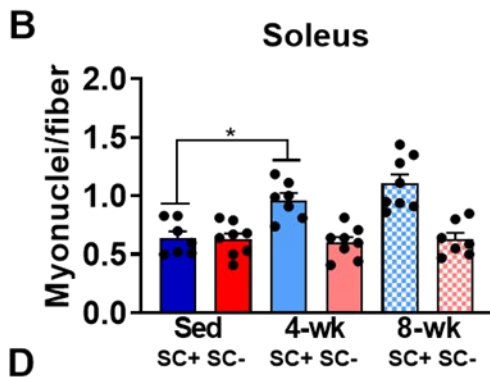
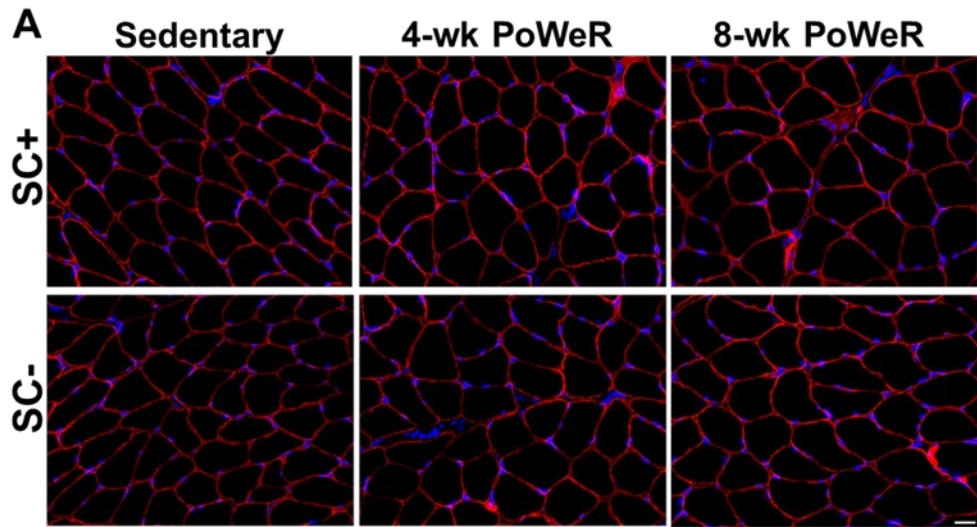


#### Figure 4.4

Satellite cell depletion inhibited myonuclear accretion and blunted muscle fiber

hypertrophy in response to PoWeR. (A) Representative images of myonuclear and fiber size immunohistochemistry from the soleus across all groups showing dystrophin (red) and nuclei (blue). (B) Myonuclear cell density in the soleus. (C) Myonuclear density in the plantaris. (D) Mean fiber cross sectional area (CSA) in the soleus. (E) Mean fiber CSA in the plantaris. Scale bar = 20  $\mu\text{m}$ . Data are represented as mean  $\pm$  SEM.

Statistical analysis: Two-way ANOVA with Tukey's multiple comparisons test. (B) and (C): there was a main effect for PoWeR ( $p < 0.05$ ) and satellite cell depletion ( $p < 0.001$ ) in the soleus and a main effect for PoWeR ( $p < 0.01$ ) and satellite cell depletion ( $p < 0.0001$ ) in the plantaris. There was a significant interaction between PoWeR and satellite cell depletion in the soleus ( $p < 0.05$ ) and plantaris ( $p < 0.05$ ). \* $p < 0.05$ . (D) and (E): PoWeR led to higher muscle fiber CSA at 4-wks ( $p < 0.0001$ ) and 8-wks ( $p < 0.0001$ ) in the soleus and at 4-wks ( $p < 0.05$ ) and 8-wks ( $p < 0.0001$ ) in the plantaris. There was a significant effect for satellite cell depletion blunting this adaptation. †  $p < 0.05$ , ††  $p < 0.01$ .

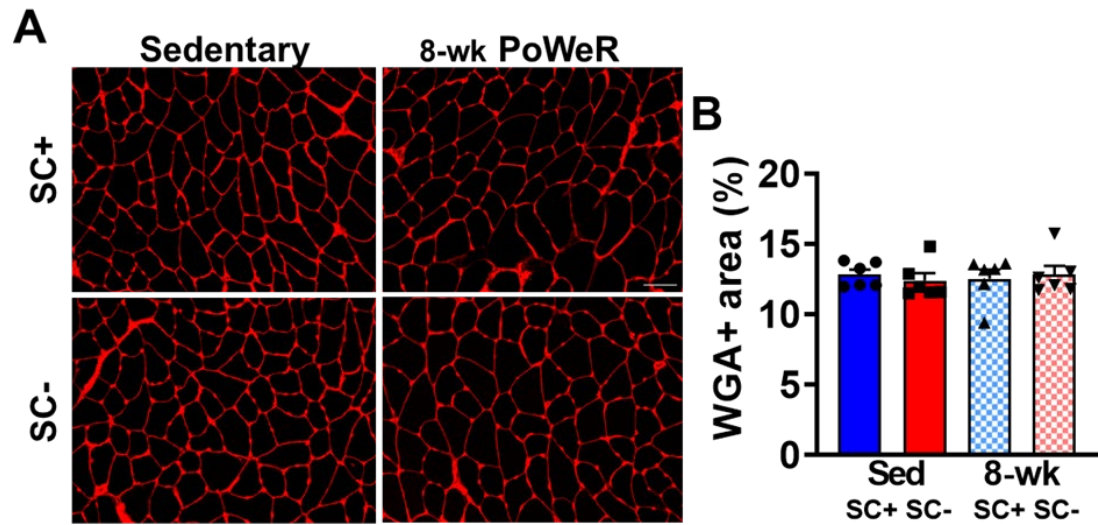
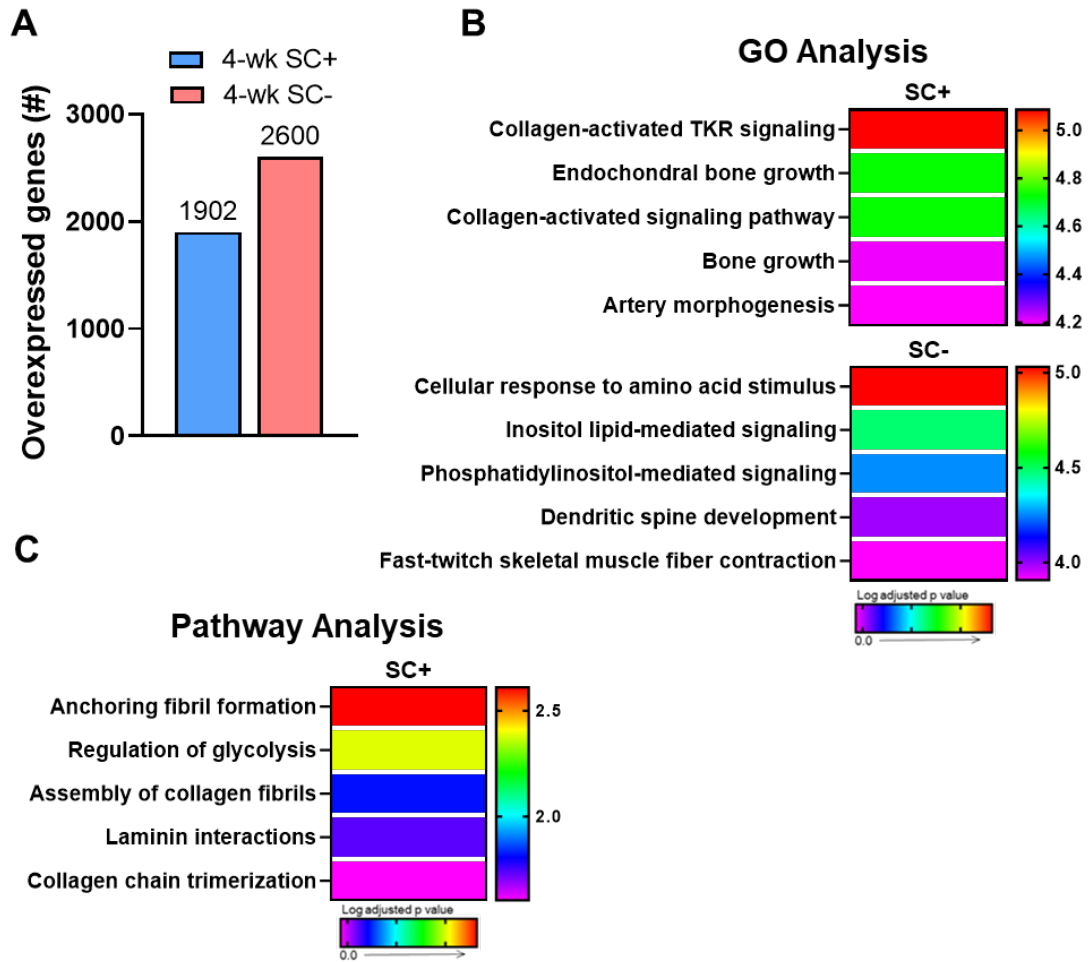


**Figure 4.5**

Neither PoWeR nor satellite cell content influenced glycosaminoglycan accumulation.

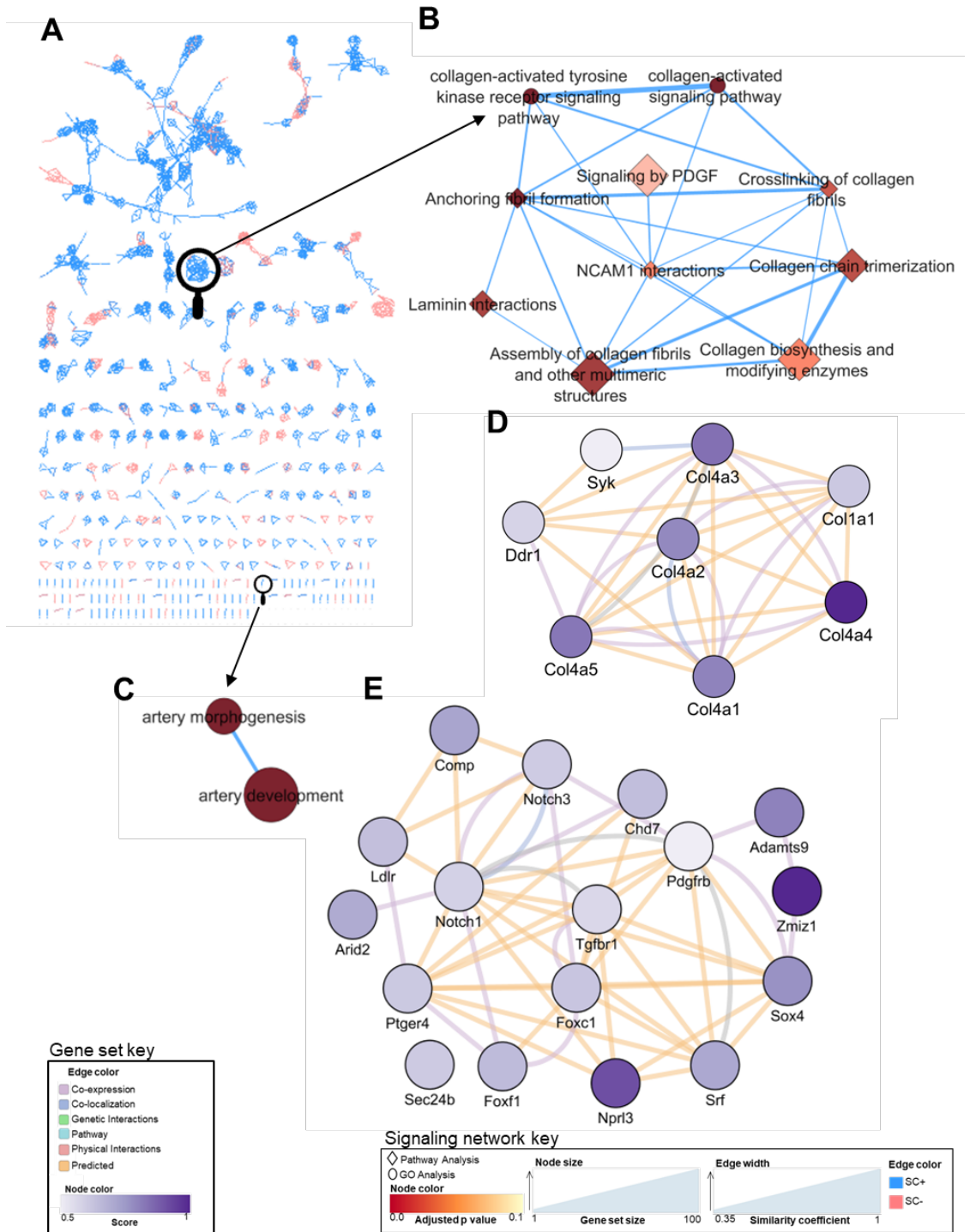
(A) Representative images WGA-stained plantaris muscle. (B) Relative area of WGA positive staining. Scale bar = 50  $\mu$ m. Data are represented as mean  $\pm$  SEM. Statistical analysis: Two-way ANOVA with Tukey's multiple comparisons test.





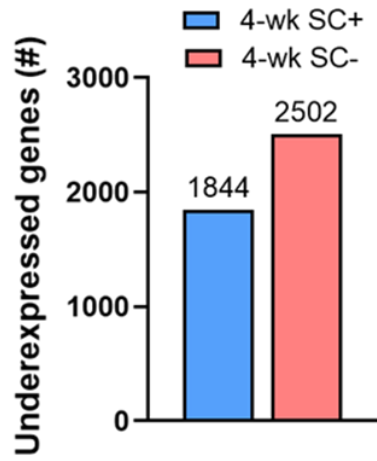
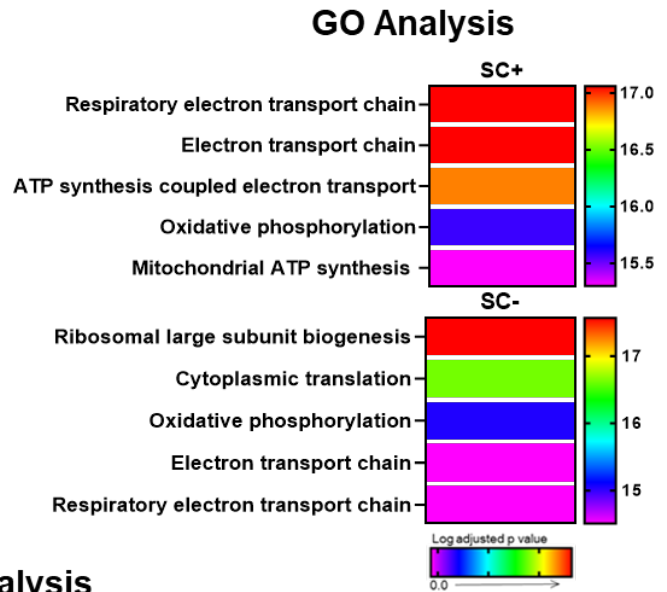
**Figure 4.6**

Collagen remodeling and capillarization pathways were enriched only in the presence of satellite cells after 4-wks of PoWeR. (A) Bar graph showing the number of overexpressed genes in the soleus (whole-muscle RNA-seq) after 4-wks of PoWeR in SC+ and SC- skeletal muscle 24 hours after the last bout of exercise relative to sham controls. (B) The most highly enriched biological processes (GO Analysis) for both groups. (C) The most highly enriched Reactome pathways (Pathway Analysis) for the SC+ group. The SC- group had no statistically enriched pathways.



### **Figure 4.7**

Enriched signaling networks and gene sets specific to SC<sup>+</sup> skeletal muscle. (A) Unbiased enrichment map representing all statistically enriched GO biological process terms and Reactome pathways (nodes) and the number of genes overlapping between biological processes and pathways (edges); shown in blue for SC<sup>+</sup> and pink for SC<sup>-</sup>. (B) Collagen signaling network. (C) Capillarization signaling network. (D) Gene set enriching the collagen activated tyrosine kinase receptor signaling pathway node. (E) Gene set enriching the artery morphogenesis node.

**A****B****C**

### Pathway Analysis

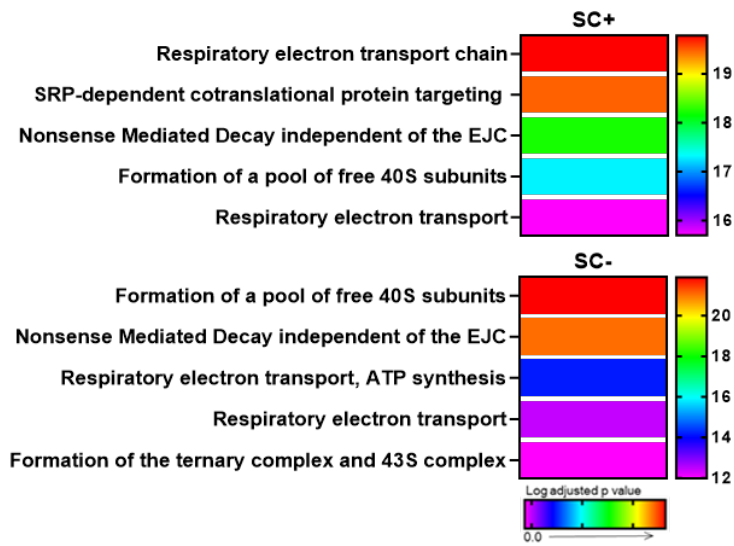


**Figure 4.8**

Oxidative phosphorylation and ribosome biogenesis are downregulated after 4-wks of PoWeR. (A) Bar graph showing the number of underexpressed genes in the soleus (whole-muscle RNA-seq) after 4-wks of PoWeR in SC+ and SC- skeletal muscle 24 hours after the last bout of exercise relative to sham controls. (B) The most highly enriched biological processes (GO Analysis) for both groups. (C) The most highly enriched Reactome pathways (Pathway Analysis) for both groups

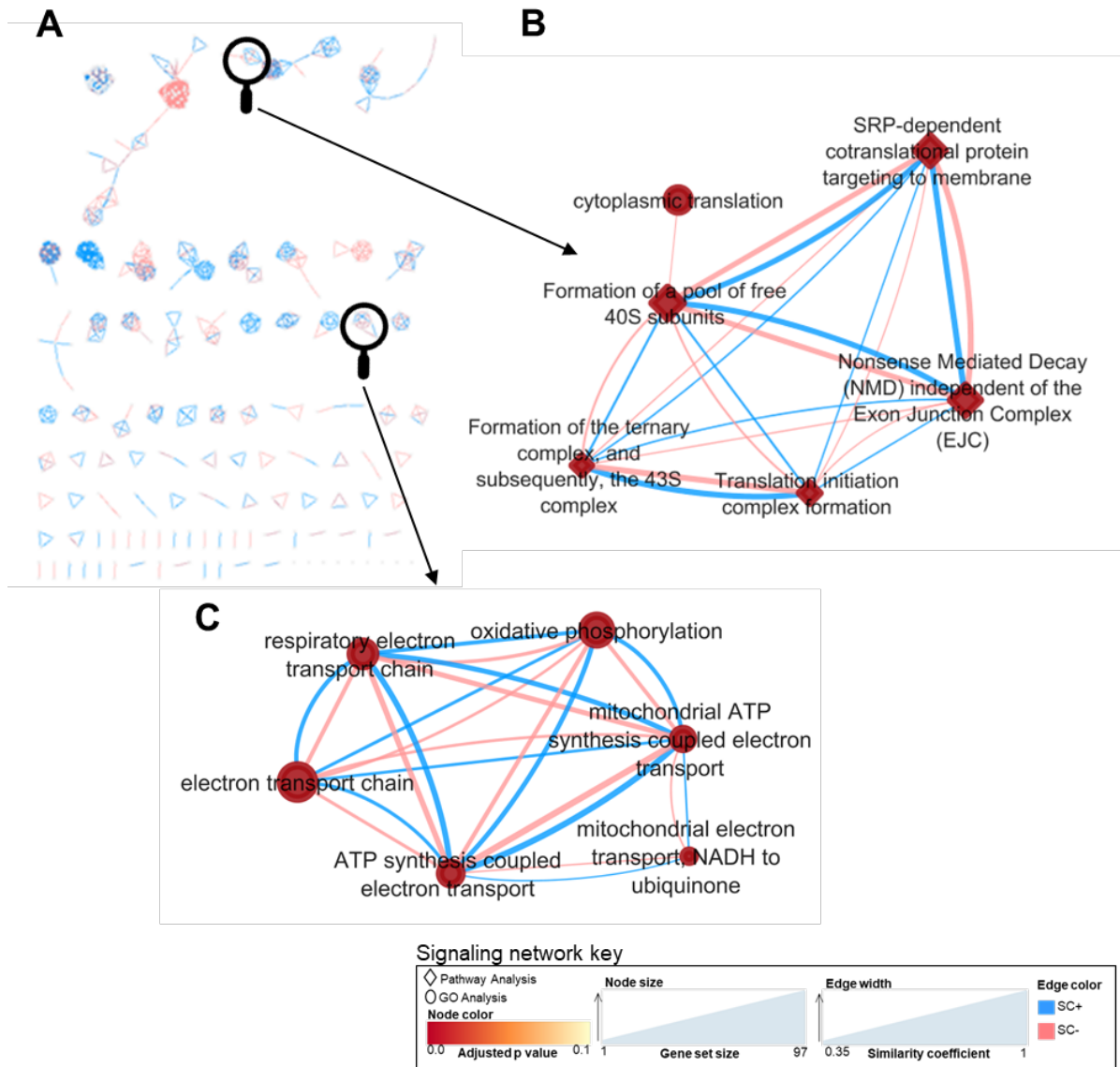


**Figure 4.9**

Enriched signaling networks are shared between SC+ and SC- skeletal muscle. (A) Unbiased enrichment map representing all statistically enriched GO biological process terms and Reactome pathways (nodes) and the number of genes overlapping between biological processes and pathways (edges); shown in blue for SC+ and pink for SC-. (B) Translation signaling network. (C) Oxidative phosphorylation signaling network.

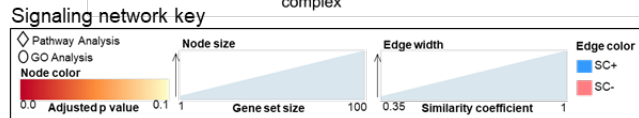
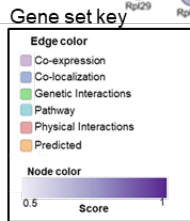
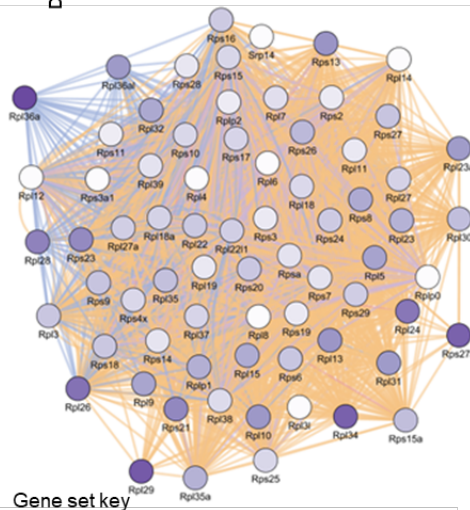
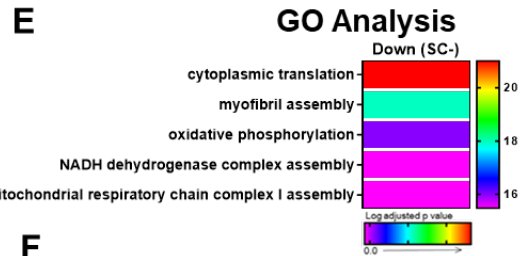
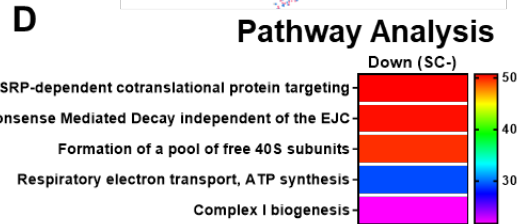
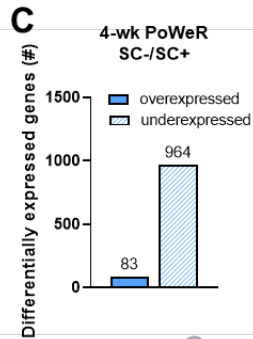
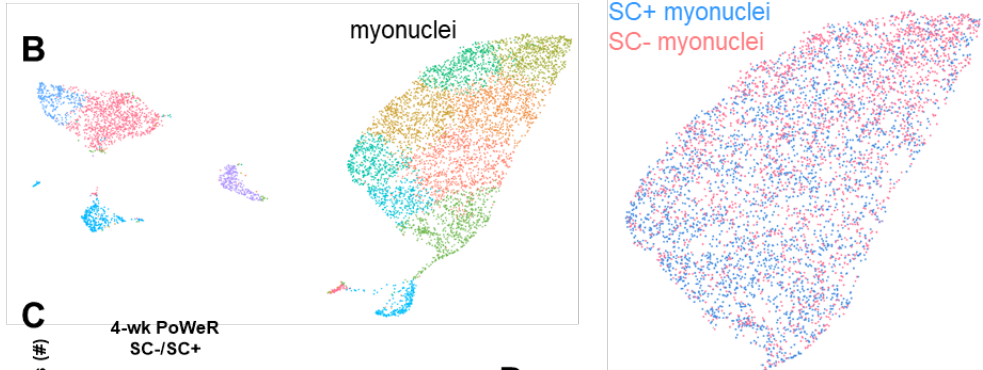
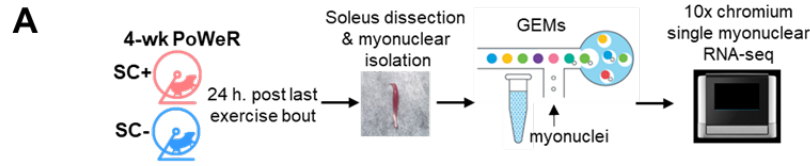


### **Figure 4.10**

Myonuclear transcriptome reveals a greater downregulation of oxidative and ribosomal pathways in the absence of satellite cells. (A) Schematic of myonuclear isolation and sequencing from skeletal muscle following PoWeR. (B) Unbiased cluster of smnRNA-seq data from SC<sup>+</sup> and SC<sup>-</sup> mice represented on a UMAP and the myonuclear cluster showing myonuclei from SC<sup>+</sup> muscle in blue and SC<sup>-</sup> muscle in pink. (C) Bar graph showing the number of over and underexpressed genes in the soleus after 4-wks of PoWeR in SC<sup>+</sup> skeletal muscle when compared to SC<sup>-</sup> skeletal muscle. The most highly enriched (D) biological processes (GO Analysis) and (E) Reactome pathways (Pathway Analysis). (F) Translation signaling network and the gene set enriching the selected node.



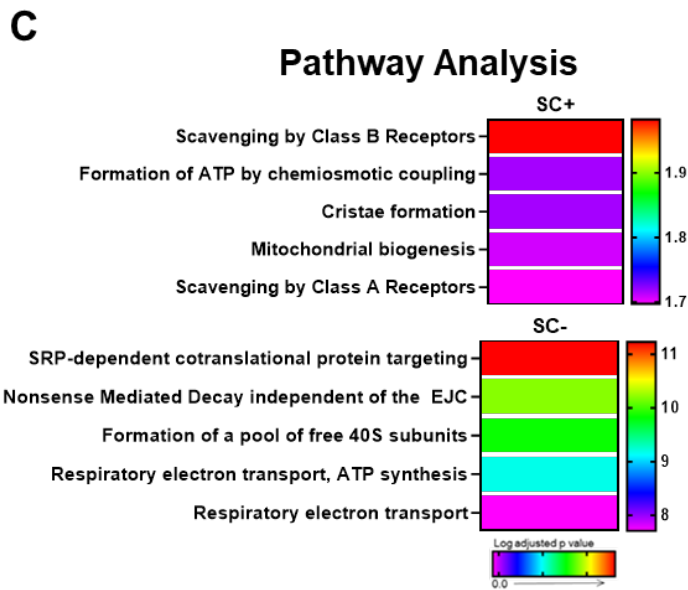
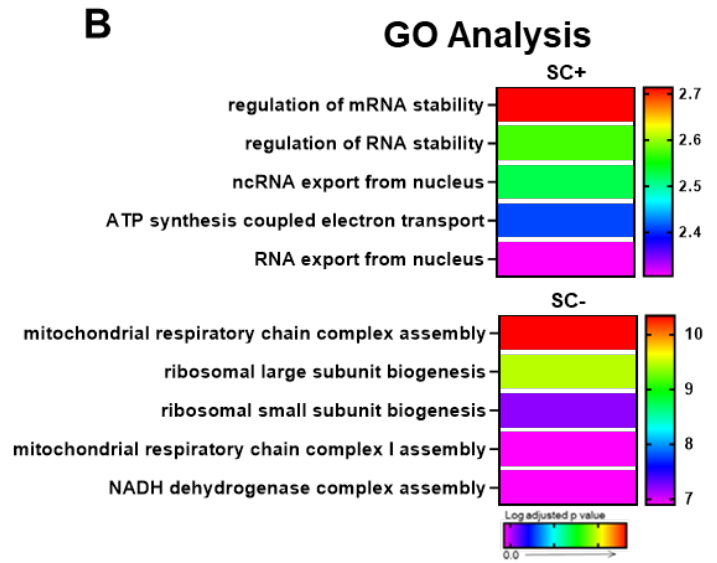
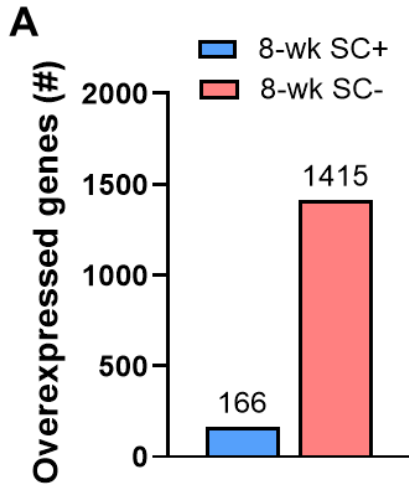


### **Figure 4.11**

Oxidative phosphorylation and ribosome biogenesis are upregulated after 8-wks of PoWeR only in the absence of satellite cells. (A) Bar graph showing the number of overexpressed genes in the soleus (whole-muscle RNA-seq) after 8-wks of PoWeR in SC+ and SC- skeletal muscle 24 hours after the last bout of exercise relative to 4-wk PoWeR. (B) The most highly enriched biological processes (GO Analysis) for both groups. (C) The most highly enriched Reactome pathways (Pathway Analysis) for both groups.

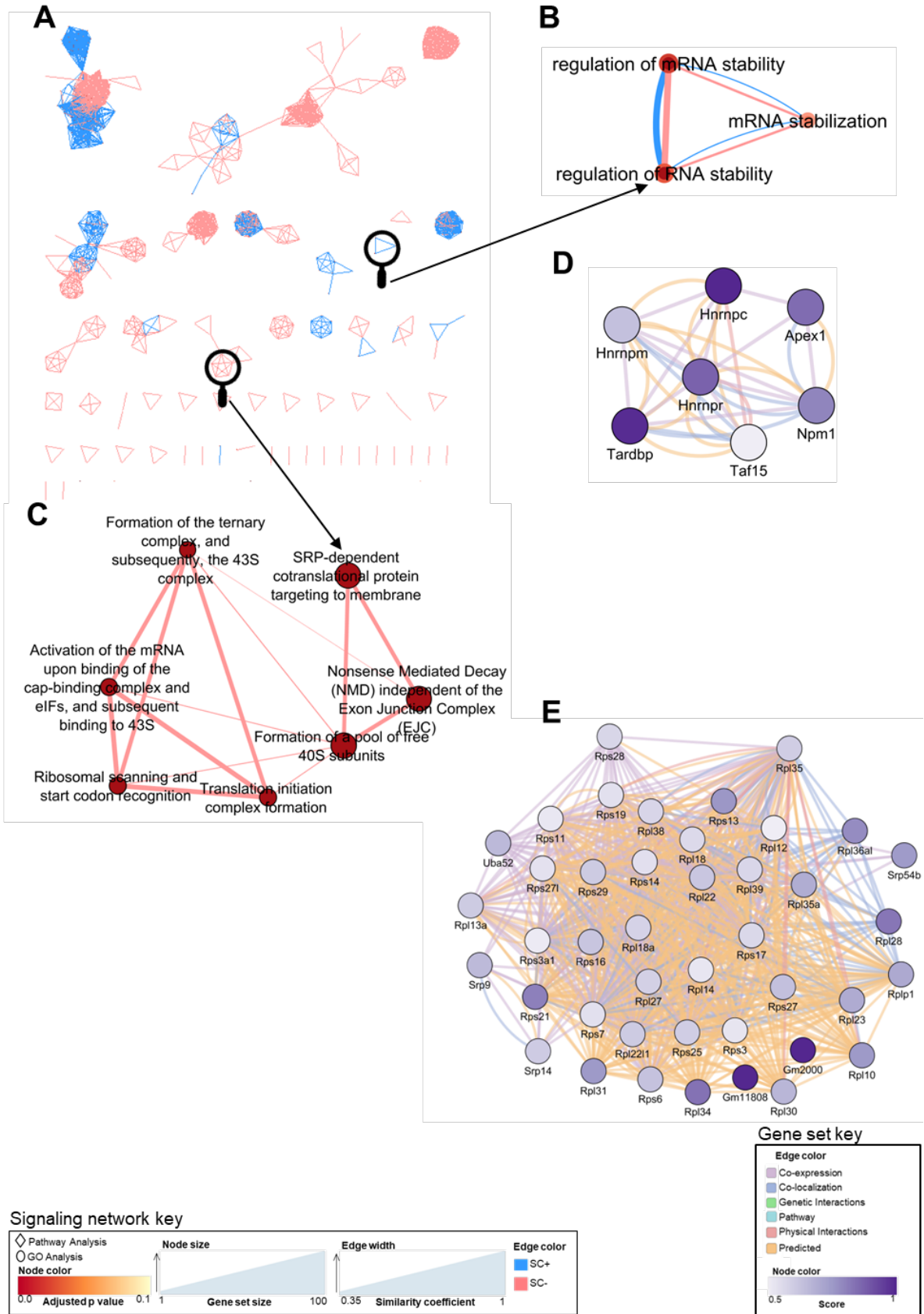


### **Figure 4.12**

Enriched signaling networks and gene sets in SC<sup>+</sup> and SC<sup>-</sup> skeletal muscle. (A) Unbiased enrichment map representing all statistically enriched GO biological process terms and Reactome pathways (nodes) and the number of genes overlapping between biological processes and pathways (edges); shown in blue for SC<sup>+</sup> and pink for SC<sup>-</sup>. (B) RNA stability signaling network. (C) translation signaling network. (D) The gene set enriching the regulation of RNA stability node. (E) The gene set enriching the SRP-dependent cotranslational protein targeting to the membrane node.

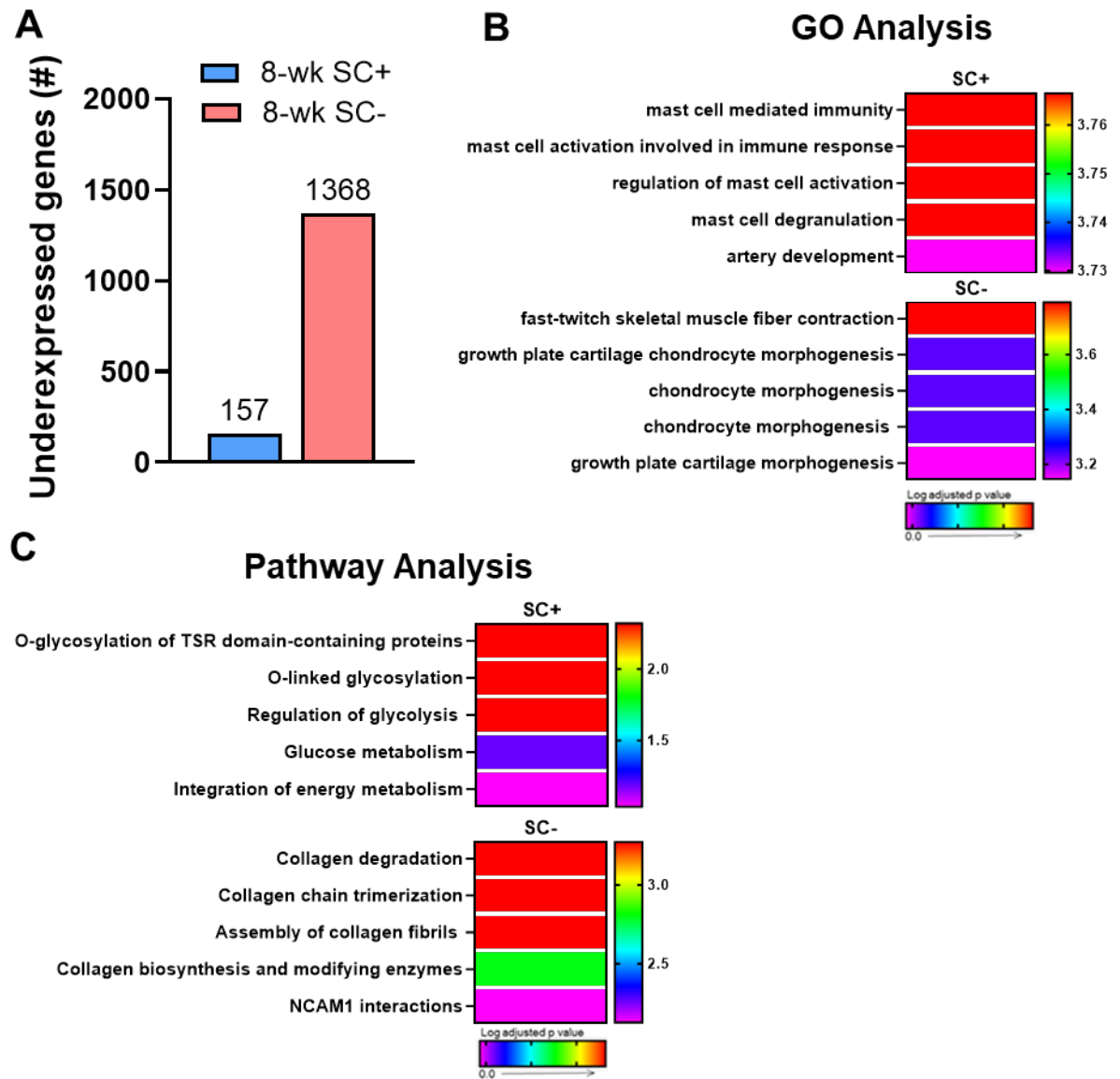


**Figure 4.13**

Collagen remodeling is suppressed after 8-wks of PoWeR only in the absence of satellite cells. (A) Bar graph showing the number of underexpressed genes in the soleus (whole-muscle RNA-seq) after 8-wks of PoWeR in SC+ and SC- skeletal muscle 24 hours after the last bout of exercise relative to 4-wk PoWeR. (B) The most highly enriched biological processes (GO Analysis) for both groups. (C) The most highly enriched Reactome pathways (Pathway Analysis) for both groups.

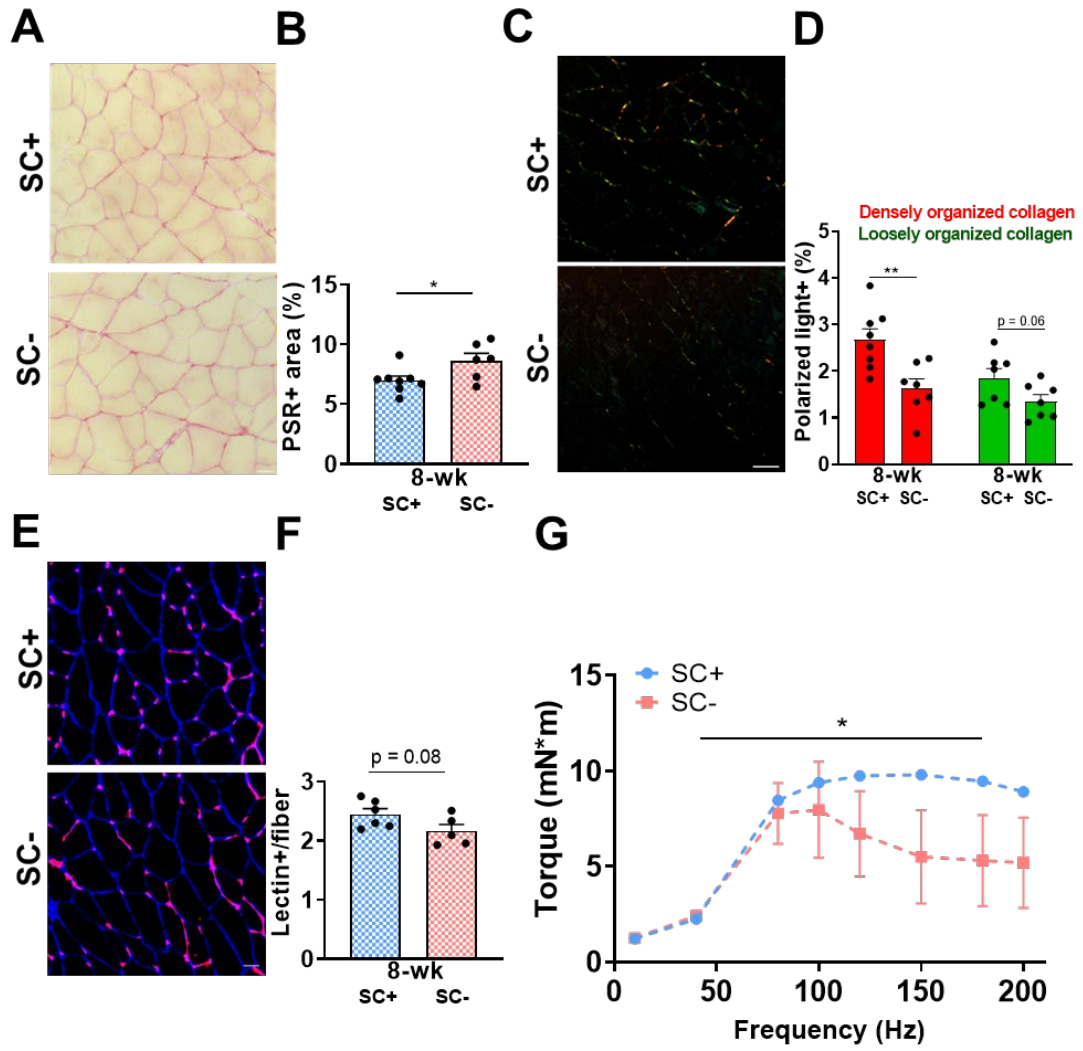


#### **Figure 4.14**

Satellite cell depletion led to aberrant collagen remodeling, capillarization and strength adaptation to PoWeR. (A) Representative PSR-stained soleus images visualized with bright field. (B) Relative area positive for PSR. (C) Representative PSR-stained soleus images visualized with polarized light. (D) Relative area of red and green emitted light. (E) Representative lectin (red) and laminin (blue) stained soleus images to identify capillaries and fibers. (F) Relative number of Lectin+ events. (G) Force frequency curve. Scale bar = 50  $\mu$ m. Data are represented as mean  $\pm$  SEM. Statistical analyses: (B), (D), (E) unpaired two-tailed Student's t-test, (G) repeated measures one-way ANOVA with Sidak's multiple comparisons test.

## REFERENCES

1. Lepper C, Partridge TA, Fan C-M. An absolute requirement for Pax7-positive satellite cells in acute injury-induced skeletal muscle regeneration. *Development*. 2011;138(17):3639-3646.
2. McCarthy JJ, Mula J, Miyazaki M, et al. Effective fiber hypertrophy in satellite cell-depleted skeletal muscle. *Development*. 2011;138(17):3657-3666.
3. Murphy MM, Lawson JA, Mathew SJ, Hutcheson DA, Kardon G. Satellite cells, connective tissue fibroblasts and their interactions are crucial for muscle regeneration. *Development*. 2011;138(17):3625-3637.
4. Sambasivan R, Yao R, Kissenpfennig A, et al. Pax7-expressing satellite cells are indispensable for adult skeletal muscle regeneration. *Development*. 2011;138(17):3647-3656.
5. Seale P, Sabourin LA, Girgis-Gabardo A, Mansouri A, Gruss P, Rudnicki MA. Pax7 is required for the specification of myogenic satellite cells. *Cell*. 2000;102(6):777-786.
6. Katz B. The terminations of the afferent nerve fibre in the muscle spindle of the frog. *Philosophical Transactions of the Royal Society of London. Series B, Biological Sciences*. 1961:221-240.
7. Mauro A. Satellite cell of skeletal muscle fibers. *The Journal of biophysical and biochemical cytology*. 1961;9:493-495.
8. Robertson JD. Electron microscopy of the motor end-plate and the neuromuscular spindle. *American Journal of Physical Medicine & Rehabilitation*. 1960;39(1):1-44.
9. Cheek D, Holt A, Hill D, Talbert J. Skeletal muscle mass and growth: the concept of the deoxyribonucleic unit. *Pediatric Research*. 1971;5:312-328.
10. Hall ZW, Ralston E. Nuclear Domains in Muscle Cells. *Cell*. 1989;59:771-772.
11. Pavlath GK, Rich K, Webster SG, Blau HM. Localization of muscle gene products in nuclear domains. *Nature*. 1989;337(6207):570-573.
12. Schiaffino S, Pierobon Bormioli S, Aloisi M. The fate of newly formed satellite cells during compensatory muscle hypertrophy. *Virchows Archiv B Cell Pathology Zell-pathologie*. 1976;21(1):113-118.
13. Epstein CJ. Cell size, nuclear content, and the development of polyploidy in the mammalian liver. *Proceedings of the National Academy of Sciences*. 1967;57(2):327-334.
14. Nagy P, Teramoto T, Factor VM, et al. Reconstitution of liver mass via cellular hypertrophy in the rat. *Hepatology*. 2001;33(2):339-345.
15. Miyaoka Y, Ebato K, Kato H, Arakawa S, Shimizu S, Miyajima A. Hypertrophy and unconventional cell division of hepatocytes underlie liver regeneration. *Current biology : CB*. 2012;22(13):1166-1175.
16. Kim S, Li Q, Dang CV, Lee LA. Induction of ribosomal genes and hepatocyte hypertrophy by adenovirus-mediated expression of c-Myc in vivo. *Proceedings of the National Academy of Sciences*. 2000;97(21):11198-11202.
17. Egnér IM, Bruusgaard JC, Gundersen K. An apparent lack of effect of satellite cell depletion on hypertrophy could be due to methodological limitations. Response to 'Methodological issues limit interpretation of negative effects of



- satellite cell depletion on adult muscle hypertrophy'. *Development*. 2017;144(8):1365-1367.
18. McCarthy JJ, Dupont-Versteegden EE, Fry CS, Murach KA, Peterson CA. Methodological issues limit interpretation of negative effects of satellite cell depletion on adult muscle hypertrophy. *Development*. 2017;144(8):1363-1365.
  19. Egner IM, Bruusgaard JC, Gundersen K. Satellite cell depletion prevents fiber hypertrophy in skeletal muscle. *Development*. 2016;143(16):2898-2906.
  20. Goh Q, Millay DP. Requirement of myomaker-mediated stem cell fusion for skeletal muscle hypertrophy. *Elife*. 2017;6:e20007.
  21. Hindi SM, Shin J, Gallot YS, et al. MyD88 promotes myoblast fusion in a cell-autonomous manner. *Nature communications*. 2017;8(1):1624.
  22. Randrianarison-Huetz V, Papaefthymiou A, Herledan G, et al. Srf controls satellite cell fusion through the maintenance of actin architecture. *The Journal of cell biology*. 2018;217(2):685-700.
  23. Moriya N, Miyazaki M. Akt1 deficiency diminishes skeletal muscle hypertrophy by reducing satellite cell proliferation. *American Journal of Physiology-Regulatory, Integrative and Comparative Physiology*. 2018.
  24. Goh Q, Song T, Petrany MJ, et al. Myonuclear accretion is a determinant of exercise-induced remodeling in skeletal muscle. *eLife*. 2019;8:e44876.
  25. McLoon LK, Rowe J, Wirtschafter J, McCormick KM. Continuous myofiber remodeling in uninjured extraocular myofibers: myonuclear turnover and evidence for apoptosis. *Muscle & Nerve: Official Journal of the American Association of Electrodiagnostic Medicine*. 2004;29(5):707-715.
  26. Schmalbruch H, Lewis D. Dynamics of nuclei of muscle fibers and connective tissue cells in normal and denervated rat muscles. *Muscle & Nerve: Official Journal of the American Association of Electrodiagnostic Medicine*. 2000;23(4):617-626.
  27. Spalding KL, Bhardwaj RD, Buchholz BA, Druid H, Frisén J. Retrospective birth dating of cells in humans. *Cell*. 2005;122(1):133-143.
  28. Keefe AC, Lawson JA, Flygare SD, et al. Muscle stem cells contribute to myofibres in sedentary adult mice. *Nature communications*. 2015;6:7087.
  29. Pawlikowski B, Pulliam C, Dalla Betta N, Kardon G, Olwin BB. Pervasive satellite cell contribution to uninjured adult muscle fibers. *Skeletal muscle*. 2015;5(1):42.
  30. Murach KA, Fry CS, Kirby TJ, et al. Starring or Supporting Role? Satellite Cells and Skeletal Muscle Fiber Size Regulation. *Physiology (Bethesda)*. 2018;33(1):26-38.
  31. Fry CS, Lee JD, Mula J, et al. Inducible depletion of satellite cells in adult, sedentary mice impairs muscle regenerative capacity without affecting sarcopenia. *Nature medicine*. 2015;21(1):76.
  32. Mackey A, Karlsen A, Coupe C, et al. Differential satellite cell density of type I and II fibres with lifelong endurance running in old men. *Acta Physiologica*. 2014;210(3):612-627.
  33. Karlsen A, Bechshøft RL, Malmgaard-Clausen NM, et al. Lack of muscle fibre hypertrophy, myonuclear addition, and satellite cell pool expansion with

- resistance training in 83-94-year-old men and women. *Acta Physiologica*. 2019:e13271.
34. Englund DA, Murach KA, Dungan CM, et al. Depletion of resident muscle stem cells negatively impacts running volume, physical function and muscle hypertrophy in response to lifelong physical activity. *American Journal of Physiology-Cell Physiology*. 2020.
  35. Liu JX, Hoglund AS, Karlsson P, et al. Myonuclear domain size and myosin isoform expression in muscle fibres from mammals representing a 100,000-fold difference in body size. *Experimental physiology*. 2009;94(1):117-129.
  36. Van der Meer S, Jaspers R, Degens H. Is the myonuclear domain size fixed? *Journal of musculoskeletal & neuronal interactions*. 2011.
  37. Conceicao MS, Vechin FC, Lixandrao M, et al. Muscle Fiber Hypertrophy and Myonuclei Addition: A Systematic Review and Meta-analysis. *Med Sci Sports Exerc*. 2018.
  38. Egner IM, Bruusgaard JC, Eftestøl E, Gundersen K. A cellular memory mechanism aids overload hypertrophy in muscle long after an episodic exposure to anabolic steroids. *The Journal of physiology*. 2013;591(24):6221-6230.
  39. Sinha-Hikim I, Roth SM, Lee MI, Bhasin S. Testosterone-induced muscle hypertrophy is associated with an increase in satellite cell number in healthy, young men. *American journal of physiology. Endocrinology and metabolism*. 2003;285(1):E197-205.
  40. van der Meer SF, Jaspers RT, Jones DA, Degens H. The time course of myonuclear accretion during hypertrophy in young adult and older rat plantaris muscle. *Annals of Anatomy-Anatomischer Anzeiger*. 2011;193(1):56-63.
  41. Kadi F, Schjerling P, Andersen LL, et al. The effects of heavy resistance training and detraining on satellite cells in human skeletal muscles. *The Journal of physiology*. 2004;558(3):1005-1012.
  42. Luden N, Hayes E, Galpin A, et al. Myocellular basis for tapering in competitive distance runners. *Journal of Applied Physiology*. 2010;108(6):1501-1509.
  43. Murach KA, Raue U, Wilkerson BS, et al. Fiber Type-Specific Gene Expression with Taper in Competitive Distance Runners. *PloS one*. 2014;9(9)(e108547).
  44. Murach KA, Minchev K, Grosicki GJ, et al. Myocellular Responses to Concurrent Flywheel Training during 70 Days of Bed Rest. *Medicine and science in sports and exercise*. 2018.
  45. Fry CS, Noehren B, Mula J, et al. Fibre type-specific satellite cell response to aerobic training in sedentary adults. *J Physiol*. 2014;592(Pt 12):2625-2635.
  46. Damas F, Libardi C, Ugrinowitsch C, et al. Early-and later-phases satellite cell responses and myonuclear content with resistance training in young men. *PloS one*. 2018;13(1):e0191039-e0191039.
  47. Herman-Montemayor JR, Hikida RS, Staron RS. Early-Phase Satellite Cell and Myonuclear Domain Adaptations to Slow-Speed vs. Traditional Resistance Training Programs. *The Journal of Strength & Conditioning Research*. 2015;29(11):3105-3114.
  48. Petrella JK, Kim JS, Cross JM, Kosek DJ, Bamman MM. Efficacy of myonuclear addition may explain differential myofiber growth among resistance-trained

- young and older men and women. *American journal of physiology. Endocrinology and metabolism*. 2006;291(5):E937-946.
49. Petrella JK, Kim JS, Mayhew DL, Cross JM, Bamman MM. Potent myofiber hypertrophy during resistance training in humans is associated with satellite cell-mediated myonuclear addition: a cluster analysis. *J Appl Physiol (1985)*. 2008;104(6):1736-1742.
  50. Mobley CB, Haun CT, Roberson PA, et al. Biomarkers associated with low, moderate, and high vastus lateralis muscle hypertrophy following 12 weeks of resistance training. *PloS one*. 2018;13(4):e0195203.
  51. Fry CS, Kirby TJ, Kosmac K, McCarthy JJ, Peterson CA. Myogenic progenitor cells control extracellular matrix production by fibroblasts during skeletal muscle hypertrophy. *Cell stem cell*. 2017;20(1):56-69.
  52. Fry CS, Lee JD, Jackson JR, et al. Regulation of the muscle fiber microenvironment by activated satellite cells during hypertrophy. *FASEB journal : official publication of the Federation of American Societies for Experimental Biology*. 2014;28(4):1654-1665.
  53. Kirby TJ, Patel RM, McClintock TS, Dupont-Versteegden EE, Peterson CA, McCarthy JJ. Myonuclear transcription is responsive to mechanical load and DNA content but uncoupled from cell size during hypertrophy. *Molecular biology of the cell*. 2016;27(5):788-798.
  54. Murach KA, White SH, Wen Y, et al. Differential Requirement for Satellite Cells During Overload-Induced Muscle Hypertrophy in Growing Versus Mature Mice. *Skeletal muscle*. 2017;7(14).
  55. Amthor H, Otto A, Vulin A, et al. Muscle hypertrophy driven by myostatin blockade does not require stem/precursor-cell activity. *Proceedings of the National Academy of Sciences of the United States of America*. 2009;106(18):7479-7484.
  56. Lee S-J, Huynh TV, Lee Y-S, et al. Role of satellite cells versus myofibers in muscle hypertrophy induced by inhibition of the myostatin/activin signaling pathway. *Proceedings of the National Academy of Sciences*. 2012;109(35):E2353-E2360.
  57. Omairi S, Matsakas A, Degens H, et al. Enhanced exercise and regenerative capacity in a mouse model that violates size constraints of oxidative muscle fibres. *Elife*. 2016;5.
  58. Raffaello A, Milan G, Masiero E, et al. JunB transcription factor maintains skeletal muscle mass and promotes hypertrophy. *The Journal of cell biology*. 2010;191(1):101-113.
  59. Wang Q, McPherron AC. Myostatin inhibition induces muscle fibre hypertrophy prior to satellite cell activation. *J Physiol*. 2012;590(9):2151-2165.
  60. Welle S, Bhatt K, Pinkert CA, Tawil R, Thornton CA. Muscle growth after postdevelopmental myostatin gene knockout. *American journal of physiology. Endocrinology and metabolism*. 2007;292(4):E985-991.
  61. Blaauw B, Canato M, Agatea L, et al. Inducible activation of Akt increases skeletal muscle mass and force without satellite cell activation. *FASEB journal : official publication of the Federation of American Societies for Experimental Biology*. 2009;23(11):3896-3905.

62. Englund DA, Peck BD, Murach KA, et al. Resident muscle stem cells are not required for testosterone-induced skeletal muscle hypertrophy. *American Journal of Physiology-Cell Physiology*. 2019.
63. Dungan CM, Murach KA, Frick KK, et al. Elevated Myonuclear Density During Skeletal Muscle Hypertrophy In Response to Training Is Reversed During Detraining. *American Journal of Physiology-Cell Physiology*. 2019.
64. Guerci A, Lahoute C, Hébrard S, et al. Srf-dependent paracrine signals produced by myofibers control satellite cell-mediated skeletal muscle hypertrophy. *Cell metabolism*. 2012;15(1):25-37.
65. McKenzie AI, D'Lugos AC, Saunders MJ, Gworek KD, Luden ND. Fiber Type-Specific Satellite Cell Content in Cyclists Following Heavy Training with Carbohydrate and Carbohydrate-Protein Supplementation. *Frontiers in physiology*. 2016;7.
66. Frese S, Valdivieso P, Flück M, et al. Expression of Metabolic and Myogenic Factors during two Competitive Seasons in Elite Junior Cyclists. *Deutsche Zeitschrift für Sportmedizin*. 2016;67(6).
67. Frese S, Ruebner M, Suhr F, et al. Long-term endurance exercise in humans stimulates cell fusion of myoblasts along with fusogenic endogenous retroviral genes in vivo. *PloS one*. 2015;10(7):e0132099.
68. Eriksson A, Kadi F, Malm C, Thornell L-E. Skeletal muscle morphology in power-lifters with and without anabolic steroids. *Histochemistry and cell biology*. 2005;124(2):167-175.
69. Kadi F, Eriksson A, Holmner S, Thornell L-E. Effects of anabolic steroids on the muscle cells of strength-trained athletes. *Medicine and science in sports and exercise*. 1999;31(11):1528-1534.
70. Fu R, Liu J, Fan J, et al. Novel evidence that testosterone promotes cell proliferation and differentiation via G protein-coupled receptors in the rat L6 skeletal muscle myoblast cell line. *Journal of cellular physiology*. 2012;227(1):98-107.
71. Lee DK. Androgen receptor enhances myogenin expression and accelerates differentiation. *Biochemical and biophysical research communications*. 2002;294(2):408-413.
72. Deane CS, Hughes DC, Sculthorpe N, Lewis MP, Stewart CE, Sharples AP. Impaired hypertrophy in myoblasts is improved with testosterone administration. *The Journal of steroid biochemistry and molecular biology*. 2013;138:152-161.
73. Serra C, Tangherlini F, Rudy S, et al. Testosterone improves the regeneration of old and young mouse skeletal muscle. *Journals of Gerontology Series A: Biomedical Sciences and Medical Sciences*. 2012;68(1):17-26.
74. Boutrup RJ, Farup J, Vissing K, Kjaer M, Mikkelsen UR. Skeletal muscle stem cell characteristics and myonuclei content in patients with rheumatoid arthritis: a cross-sectional study. *Rheumatology international*. 2018:1-11.
75. Jackson JR, Mula J, Kirby TJ, et al. Satellite cell depletion does not inhibit adult skeletal muscle regrowth following unloading-induced atrophy. *American journal of physiology. Cell physiology*. 2012;303(8):C854-861.

76. Bruusgaard JC, Egner IM, Larsen TK, Dupre-Aucouturier S, Desplanches D, Gundersen K. No change in myonuclear number during muscle unloading and reloading. *Journal of applied physiology*. 2012;113(2):290-296.
77. Bruusgaard JC, Gundersen K. In vivo time-lapse microscopy reveals no loss of murine myonuclei during weeks of muscle atrophy. *The Journal of clinical investigation*. 2008;118(4):1450-1457.
78. Damas F, Phillips SM, Libardi CA, et al. Resistance training-induced changes in integrated myofibrillar protein synthesis are related to hypertrophy only after attenuation of muscle damage. *J Physiol*. 2016;594(18):5209-5222.
79. Bellamy LM, Joannis S, Grubb A, et al. The acute satellite cell response and skeletal muscle hypertrophy following resistance training. *PloS one*. 2014;9(10):e109739.
80. Murach KA, Walton RG, Fry CS, et al. Cycle training modulates satellite cell and transcriptional responses to a bout of resistance exercise. *Physiological Reports*. 2016;4(18):e12973.
81. Snow MH. Satellite cell response in rat soleus muscle undergoing hypertrophy due to surgical ablation of synergists. *The Anatomical record*. 1990;227(4):437-446.
82. Hyldahl RD, Olson T, Welling T, Groscost L, Parcell AC. Satellite cell activity is differentially affected by contraction mode in human muscle following a work-matched bout of exercise. *Frontiers in physiology*. 2014;5.
83. Crameri R, Aagaard P, Qvortrup K, Langberg H, Olesen J, Kjær M. Myofibre damage in human skeletal muscle: effects of electrical stimulation versus voluntary contraction. *The Journal of physiology*. 2007;583(1):365-380.
84. Moss FP, Leblond CP. Satellite cells as the source of nuclei in muscles of growing rats. *The Anatomical record*. 1971;170(4):421-435.
85. Farup J, Rahbek SK, Riis S, Vendelbo MH, Paoli F, Vissing K. Influence of exercise contraction mode and protein supplementation on human skeletal muscle satellite cell content and muscle fiber growth. *J Appl Physiol (1985)*. 2014;117(8):898-909.
86. Seale P, Sabourin LA, Girgis-Gabardo A, Mansouri A, Gruss P, Rudnicki MA. Pax7 is required for the specification of myogenic satellite cells. *Cell*. 2000;102(6):777-786.
87. McCarthy JJ, Mula J, Miyazaki M, et al. Effective fiber hypertrophy in satellite cell-depleted skeletal muscle. *Development*. 2011;138(17):3657-3666.
88. Relaix F, Zammit PS. Satellite cells are essential for skeletal muscle regeneration: the cell on the edge returns centre stage. *Development*. 2012;139(16):2845-2856.
89. Murach KA, Englund DA, Dupont-Versteegden EE, McCarthy JJ, Peterson CA. Myonuclear Domain Flexibility Challenges Rigid Assumptions on Satellite Cell Contribution to Skeletal Muscle Fiber Hypertrophy. *Front Physiol* 2018;9.
90. Fry CS, Lee JD, Jackson JR, et al. Regulation of the muscle fiber microenvironment by activated satellite cells during hypertrophy. *FASEB journal : official publication of the Federation of American Societies for Experimental Biology*. 2014;28(4):1654-1665.

91. Murach KA, White SH, Wen Y, et al. Differential requirement for satellite cells during overload-induced muscle hypertrophy in growing versus mature mice. *Skeletal muscle*. 2017;7(1):14.
92. Moriya N, Miyazaki M. Akt1 deficiency diminishes skeletal muscle hypertrophy by reducing satellite cell proliferation. *The Journal of clinical endocrinology and metabolism*. 2018.
93. Sinha-Hikim I, Roth SM, Lee MI, Bhasin S. Testosterone-induced muscle hypertrophy is associated with an increase in satellite cell number in healthy, young men. *Am J Physio Endocrinol and Metab*. 2003.
94. Sinha-Hikim I, Cornford M, Gaytan H, Lee ML, Bhasin S. Effects of testosterone supplementation on skeletal muscle fiber hypertrophy and satellite cells in community-dwelling older men. *The Journal of clinical endocrinology and metabolism*. 2006;91(8):3024-3033.
95. Egner IM, Bruusgaard JC, Eftestøl E, Gundersen K. A cellular memory mechanism aids overload hypertrophy in muscle long after an episodic exposure to anabolic steroids. *J Physiol* 2013;591(24):6221-6230.
96. Rossetti ML, Fukuda DH, Gordon BS. Androgens induce growth of the limb skeletal muscles in a rapamycin-insensitive manner. *American journal of physiology. Regulatory, integrative and comparative physiology*. 2018;315(4):R721-r729.
97. Chambon C, Duteil D, Vignaud A, et al. Myocytic androgen receptor controls the strength but not the mass of limb muscles. *Proceedings of the National Academy of Sciences of the United States of America*. 2010;107(32):14327-14332.
98. Rossetti ML, Steiner JL, Gordon BS. Androgen-mediated regulation of skeletal muscle protein balance. *Molecular and cellular endocrinology*. 2017;447:35-44.
99. Morton RW, Sato K, Gallagher MPB, et al. Muscle Androgen Receptor Content but Not Systemic Hormones Is Associated With Resistance Training-Induced Skeletal Muscle Hypertrophy in Healthy, Young Men. *Front Physiol*. 2018;9:1373.
100. Basualto-Alarcon C, Jorquera G, Altamirano F, Jaimovich E, Estrada M. Testosterone signals through mTOR and androgen receptor to induce muscle hypertrophy. *Medicine and science in sports and exercise*. 2013;45(9):1712-1720.
101. Zeng F, Zhao H, Liao J. Androgen interacts with exercise through the mTOR pathway to induce skeletal muscle hypertrophy. *Biol Sport*. 2017;34(4):313-321.
102. Wu Y, Zhao W, Zhao J, et al. Identification of androgen response elements in the insulin-like growth factor I upstream promoter. *Endocrinology*. 2007;148(6):2984-2993.
103. Sinha-Hikim I, Taylor WE, Gonzalez-Cadavid NF, Zheng W, Bhasin S. Androgen receptor in human skeletal muscle and cultured muscle satellite cells: up-regulation by androgen treatment. *The Journal of clinical endocrinology and metabolism*. 2004;89(10):5245-5255.
104. Powers ML, Florini JR. A direct effect of testosterone on muscle cells in tissue culture. *Endocrinology*. 1975;97(4):1043-1047.
105. MacLean HE, Chiu WS, Notini AJ, et al. Impaired skeletal muscle development and function in male, but not female, genomic androgen receptor knockout mice.

- FASEB journal : official publication of the Federation of American Societies for Experimental Biology.* 2008;22(8):2676-2689.
106. Wen Y, Murach KA, Vechetti Jr IJ, et al. MyoVision: Software for Automated High-Content Analysis of Skeletal Muscle Immunohistochemistry. *J Appl Physiol (1985)*. 2018;124:40-51.
  107. Blaauw B, Canato M, Agatea L, et al. Inducible activation of Akt increases skeletal muscle mass and force without satellite cell activation. *The FASEB journal*. 2009;23(11):3896-3905.
  108. Iwata M, Englund DA, Wen Y, et al. A novel tetracycline-responsive transgenic mouse strain for skeletal muscle-specific gene expression. *Skeletal muscle*. 2018;8(1):33.
  109. Jackson JR, Kirby TJ, Fry CS, et al. Reduced voluntary running performance is associated with impaired coordination as a result of muscle satellite cell depletion in adult mice. *Skeletal muscle*. 2015;5(1):41.
  110. Kitzman DW, Nicklas B, Kraus WE, et al. Skeletal muscle abnormalities and exercise intolerance in older patients with heart failure and preserved ejection fraction. *American Journal of Physiology-Heart and Circulatory Physiology*. 2014;306(9):H1364-H1370.
  111. Albers PH, Pedersen AJ, Birk JB, et al. Human muscle fiber type-specific insulin signaling: impact of obesity and type 2 diabetes. *Diabetes*. 2015;64(2):485-497.
  112. Fry CS, Noehren B, Mula J, et al. Fibre type-specific satellite cell response to aerobic training in sedentary adults. *The Journal of physiology*. 2014;592(12):2625-2635.
  113. von Maltzahn J, Bentzinger CF, Rudnicki MA. Wnt7a-Fzd7 signalling directly activates the Akt/mTOR anabolic growth pathway in skeletal muscle. *Nature cell biology*. 2011;14(2):186-191.
  114. Minetti G, Rosenstiel A, Werner A, et al. Gai2 signaling promotes skeletal muscle hypertrophy, myoblast differentiation, and muscle regeneration. *Science Signaling*. 2011;4(201):ra8.
  115. Minetti GC, Feige JN, Bombard F, et al. Gai2 signaling is required for skeletal muscle growth, regeneration, and satellite cell proliferation and differentiation. *Molecular and cellular biology*. 2014;34(4):619-630.
  116. White JP, Wrann CD, Rao RR, et al. G protein-coupled receptor 56 regulates mechanical overload-induced muscle hypertrophy. *Proceedings of the National Academy of Sciences*. 2014;111(44):15756-15761.
  117. Winje I, Bengtson M, Eftestøl E, Juvkam I, Bruusgaard J, Gundersen K. Specific labelling of myonuclei by an antibody against pericentriolar material 1 on skeletal muscle tissue sections. *Acta Physiologica*. 2018:e13034.
  118. Zvaritch E, MacLennan DH. Muscle spindles exhibit core lesions and extensive degeneration of intrafusal fibers in the Ryr1I4895T/wt mouse model of core myopathy. *Biochemical and biophysical research communications*. 2015;460(1):34-39.
  119. Tourtellotte WG, Milbrandt J. Sensory ataxia and muscle spindle agenesis in mice lacking the transcription factor Egr3. *Nature genetics*. 1998;20(1):87.

120. Ruijter J, Ramakers C, Hoogaars W, et al. Amplification efficiency: linking baseline and bias in the analysis of quantitative PCR data. *Nucleic acids research*. 2009;37(6):e45-e45.
121. Livak KJ, Schmittgen TD. Analysis of relative gene expression data using real-time quantitative PCR and the 2<sup>-</sup>ΔΔCT method. *methods*. 2001;25(4):402-408.
122. Kendzioriski CM, Zhang Y, Lan H, Attie AD. The efficiency of pooling mRNA in microarray experiments. *Biostatistics (Oxford, England)*. 2003;4(3):465-477.
123. Herwig R, Hardt C, Lienhard M, Kamburov A. Analyzing and interpreting genome data at the network level with ConsensusPathDB. *Nature protocols*. 2016;11(10):1889.
124. Carlson-Kuhta P, Trank TV, Smith JL. Forms of forward quadrupedal locomotion. II. A comparison of posture, hindlimb kinematics, and motor patterns for upslope and level walking. *J Neurophysiol*. 1998;79(4):1687-1701.
125. Lieber RL, Ward SR. Skeletal muscle design to meet functional demands. *Philosophical transactions of the Royal Society of London. Series B, Biological sciences*. 2011;366(1570):1466-1476.
126. Allen DL, Harrison BC, Maass A, Bell ML, Byrnes WC, Leinwand LA. Cardiac and skeletal muscle adaptations to voluntary wheel running in the mouse. *Journal of applied physiology*. 2001;90(5):1900-1908.
127. Brooks MJ, Hajira A, Mohamed JS, Alway SE. Voluntary wheel running increases satellite cell abundance and improves recovery from disuse in gastrocnemius muscles from mice. *Journal of Applied Physiology*. 2018.
128. Li P, Akimoto T, Zhang M, Williams RS, Yan Z. Resident stem cells are not required for exercise-induced fiber-type switching and angiogenesis but are necessary for activity-dependent muscle growth. *American Journal of Physiology-Cell Physiology*. 2006;290(6):C1461-C1468.
129. Muller FL, Song W, Liu Y, et al. Absence of CuZn superoxide dismutase leads to elevated oxidative stress and acceleration of age-dependent skeletal muscle atrophy. *Free Radical Biology and Medicine*. 2006;40(11):1993-2004.
130. Larkin LM, Davis CS, Sims-Robinson C, et al. Skeletal muscle weakness due to deficiency of CuZn-superoxide dismutase is associated with loss of functional innervation. *American Journal of Physiology-Regulatory, Integrative and Comparative Physiology*. 2011;301(5):R1400-R1407.
131. Mijnders DM, Koster A, Schols JM, et al. Physical activity and incidence of sarcopenia: the population-based AGES—Reykjavik Study. *Age and ageing*. 2016;45(5):614-620.
132. Verdijk LB, Snijders T, Drost M, Delhaas T, Kadi F, van Loon LJ. Satellite cells in human skeletal muscle; from birth to old age. *Age (Dordrecht, Netherlands)*. 2014;36(2):545-547.
133. Berry SD, Miller RR. Falls: epidemiology, pathophysiology, and relationship to fracture. *Current osteoporosis reports*. 2008;6(4):149-154.
134. Krasovsky T, Baniña MC, Hacmon R, Feldman AG, Lamontagne A, Levin MF. Stability of gait and interlimb coordination in older adults. *Journal of Neurophysiology*. 2012;107(9):2560-2569.



135. James EG, Leveille SG, Hausdorff JM, et al. Coordination Impairments Are Associated With Falling Among Older Adults. *Experimental aging research*. 2017;43(5):430-439.
136. Newman AB, Simonsick EM, Naydeck BL, et al. Association of long-distance corridor walk performance with mortality, cardiovascular disease, mobility limitation, and disability. *Jama*. 2006;295(17):2018-2026.
137. Kirby TJ, McCarthy JJ, Peterson CA, Fry CS. Synergist ablation as a rodent model to study satellite cell dynamics in adult skeletal muscle. *Skeletal Muscle Regeneration in the Mouse*: Springer; 2016:43-52.
138. Murach KA, Confides AL, Ho A, et al. Depletion of Pax7<sup>+</sup> satellite cells does not affect diaphragm adaptations to running in young or aged mice. *The Journal of physiology*. 2017;595(19):6299-6311.
139. Lee JD, Fry CS, Mula J, et al. Aged muscle demonstrates fiber-type adaptations in response to mechanical overload, in the absence of myofiber hypertrophy, independent of satellite cell abundance. *Journals of Gerontology Series A: Biomedical Sciences and Medical Sciences*. 2015;71(4):461-467.
140. Kelly FJ, Lewis SE, Anderson P, Goldspink DF. Pre- and postnatal growth and protein turnover in four muscles of the rat. *Muscle & Nerve*. 1984;7(3):235-242.
141. Goodman CA, Kotecki JA, Jacobs BL, Hornberger TA. Muscle fiber type-dependent differences in the regulation of protein synthesis. *PloS one*. 2012;7(5):e37890.
142. van Velthoven CTJ, de Morree A, Egner IM, Brett JO, Rando TA. Transcriptional Profiling of Quiescent Muscle Stem Cells In Vivo. *Cell reports*. 2017;21(7):1994-2004.
143. Machado L, Esteves de Lima J, Fabre O, et al. In Situ Fixation Redefines Quiescence and Early Activation of Skeletal Muscle Stem Cells. *Cell reports*. 2017;21(7):1982-1993.
144. Cui D, Drake JC, Wilson RJ, et al. A novel voluntary weightlifting model in mice promotes muscle adaptation and insulin sensitivity with simultaneous enhancement of autophagy and mTOR pathway. *The FASEB Journal*. 2020.
145. Graber TG, Fandrey KR, Thompson LV. Novel individualized power training protocol preserves physical function in adult and older mice. *GeroScience*. 2019;41(2):165-183.
146. Krüger K, Gessner DK, Seimetz M, et al. Functional and muscular adaptations in an experimental model for isometric strength training in mice. *PloS one*. 2013;8(11).
147. Kirkeby S, Mandel U, Vedtofte P. Identification of capillaries in sections from skeletal muscle by use of lectins and monoclonal antibodies reacting with histo-blood group ABH antigens. *Glycoconjugate journal*. 1993;10(2):181-188.
148. Mortazavi A, Williams BA, McCue K, Schaeffer L, Wold B. Mapping and quantifying mammalian transcriptomes by RNA-Seq. *Nature methods*. 2008;5(7):621.
149. Cutler AA, Corbett AH, Pavlath GK. Biochemical isolation of myonuclei from mouse skeletal muscle tissue. *Bio-protocol*. 2017;7(24).

150. Amthor H, Macharia R, Navarrete R, et al. Lack of myostatin results in excessive muscle growth but impaired force generation. *Proceedings of the National Academy of Sciences*. 2007;104(6):1835-1840.
151. Amthor H, Otto A, Vulin A, et al. Muscle hypertrophy driven by myostatin blockade does not require stem/precursor-cell activity. *Proceedings of the National Academy of Sciences*. 2009;106(18):7479-7484.
152. Omairi S, Matsakas A, Degens H, et al. Enhanced exercise and regenerative capacity in a mouse model that violates size constraints of oxidative muscle fibres. *Elife*. 2016;5:e16940.
153. Raffaello A, Milan G, Masiero E, et al. JunB transcription factor maintains skeletal muscle mass and promotes hypertrophy. *Journal of Cell Biology*. 2010;191(1):101-113.
154. Huijing P, Baan GC, Rebel GT. Non-myotendinous force transmission in rat extensor digitorum longus muscle. *Journal of Experimental Biology*. 1998;201(5):683-691.
155. Mendias CL, Schwartz AJ, Grekin JA, Gumucio JP, Sugg KB. Changes in muscle fiber contractility and extracellular matrix production during skeletal muscle hypertrophy. *Journal of Applied Physiology*. 2017;122(3):571-579.
156. Wood LK, Kayupov E, Gumucio JP, Mendias CL, Claflin DR, Brooks SV. Intrinsic stiffness of extracellular matrix increases with age in skeletal muscles of mice. *Journal of applied physiology*. 2014;117(4):363-369.
157. Ramaswamy KS, Palmer ML, Van Der Meulen JH, et al. Lateral transmission of force is impaired in skeletal muscles of dystrophic mice and very old rats. *The Journal of physiology*. 2011;589(5):1195-1208.
158. Phillips BE, Atherton PJ, Varadhan K, et al. The effects of resistance exercise training on macro-and micro-circulatory responses to feeding and skeletal muscle protein anabolism in older men. *The Journal of physiology*. 2015;593(12):2721-2734.
159. Moro T, Brightwell CR, Phalen DE, et al. Low skeletal muscle capillarization limits muscle adaptation to resistance exercise training in older adults. *Experimental gerontology*. 2019;127:110723.
160. Snijders T, Nederveen JP, Joannisse S, et al. Muscle fibre capillarization is a critical factor in muscle fibre hypertrophy during resistance exercise training in older men. *Journal of cachexia, sarcopenia and muscle*. 2017;8(2):267-276.
161. Christov C, Chrétien F, Abou-Khalil R, et al. Muscle satellite cells and endothelial cells: close neighbors and privileged partners. *Molecular biology of the cell*. 2007;18(4):1397-1409.
162. Verma M, Asakura Y, Murakonda BSR, et al. Muscle satellite cell cross-talk with a vascular niche maintains quiescence via VEGF and notch signaling. *Cell Stem Cell*. 2018;23(4):530-543. e539.
163. Rhoads RP, Johnson RM, Rathbone CR, et al. Satellite cell-mediated angiogenesis in vitro coincides with a functional hypoxia-inducible factor pathway. *American Journal of Physiology-Cell Physiology*. 2009;296(6):C1321-C1328.
164. Phillips BE, Williams JP, Gustafsson T, et al. Molecular networks of human muscle adaptation to exercise and age. *PLoS genetics*. 2013;9(3).

165. Machado L, Dos Santos M, Camps J, et al. Skeletal Muscle Tissue Damage Leads to a Conserved Stress Response and Stem Cell-Specific Adaptive Transitions. *CELL-STEM-CELL-D-20-00065*.

## VITA

Davis A. Englund

### Education

- 2010 – 2013 B.S. in Exercise Science with honors, 2013, University of Massachusetts Boston
- 2013 – 2015 M.S. in Exercise Physiology, 2015, Iowa State University  
Thesis: *Effects of high and low velocity muscle contraction on myosin heavy chain mRNA and protein expression in conjunction with muscle performance in the elderly*
- 2017 - Doctoral Fellow, College of Health Sciences, University of Kentucky. Advisor: Charlotte A Peterson

### Professional Experience

- 2011 – 2013 Physiology Tutor, Center for Clinical Education and Research, UMass Boston
- 2011 – 2012 Undergraduate Research Assistant, Go-Kids Boston, College of Nursing and Health Sciences, UMass Boston
- 2012 – 2013 Undergraduate Research Assistant, Exercise Science Laboratory, Bouve College of Health Sciences, Northeastern University
- 2013 – 2015 Graduate Research Assistant, Department of Kinesiology, Iowa State University
- 2015 – 2017 Senior Research Technician, the Nutrition, Exercise Physiology and Sarcopenia Lab, Jean Mayer USDA Human Nutrition Research Center on Aging, Tufts University
- 2017 – Research Doctoral Fellow, College of Health Sciences, University of Kentucky

### Honors and Awards

- 2013 Awarded, Corcoran/Rody Scholarship, College of Nursing and Health Sciences, UMass Boston
- 2016 Awarded, Alumnus of the Year, College of Nursing and Health Sciences, UMass Boston
- 2017 Awarded, Doctoral Fellowship, Rehabilitation Sciences Doctoral Program, University of Kentucky
- 2018 Awarded, Rehabilitation Sciences Pilot Study Funding, College of Health Sciences, University of Kentucky
- 2018 Awarded, Rehabilitation Sciences Travel Funding, College of Health Sciences, University of Kentucky
- 2018 Awarded, the Donovan Scholarship in Gerontology, Office of Lifelong Learning, University of Kentucky

- 2018                    Awarded, Research Enhancement Award, College of Health Sciences, University of Kentucky
- 2019                    Awarded, Graduate Student Congress Travel Award, University of Kentucky
- 2019                    Awarded, Nathan Shock Center Travel Award, University of Oklahoma
- 2019                    Awarded, Rehabilitation Sciences Travel Funding, College of Health Sciences, University of Kentucky
- 2019                    Awarded, Student Investigator Research Grant, College of Health Sciences, University of Kentucky
- 2020                    Awarded, Supplemental Stipend - Graduate Student Incentive Program, The Graduate School, University of Kentucky
- 2020                    Awarded, Robinson Graduate Award for Research Creativity, College of Health Sciences, University of Kentucky

#### Peer-Reviewed Publications

Englund, D.A., Sharp, R.L., Selsby, J.T., Ganesan, S.S. and Franke, W.D., 2017. Resistance training performed at distinct angular velocities elicits velocity-specific alterations in muscle strength and mobility status in older adults. *Experimental gerontology*, 91, pp.51-56.

<https://www.ncbi.nlm.nih.gov/pubmed/28237604>

Englund, D.A., Kirn, D.R., Koochek, A., Zhu, H., Travison, T.G., Reid, K.F., von Berens, Å., Melin, M., Cederholm, T., Gustafsson, T. and Fielding, R.A., 2017. Nutritional supplementation with physical activity improves muscle composition in mobility-limited older adults, the VIVE2 study: a randomized, double-blind, placebo-controlled trial. *The Journals of Gerontology: Series A*, 73(1), pp.95-101.

<https://www.ncbi.nlm.nih.gov/pubmed/28977347>

Murach, K.A., Englund, D.A., Dupont-Versteegden, E.E., McCarthy, J.J. and Peterson, C.A., 2018. Myonuclear domain flexibility challenges rigid assumptions on satellite cell contribution to skeletal muscle fiber hypertrophy. *Frontiers in physiology*, 9.

<https://www.ncbi.nlm.nih.gov/pubmed/29896117>

Reid, K.F., Laussen, J., Bhatia, K., Englund, D.A., Kirn, D.R., Price, L.L., Manini, T.M., Liu, C.K., Kowaleski, C. and Fielding, R.A., 2018. Translating the lifestyle interventions and independence for elders clinical trial to older adults in a real-world community-based setting. *The Journals of Gerontology: Series A*, 74(6), pp.924-928. NOTE: Selected for Editor's Choice.

<https://www.ncbi.nlm.nih.gov/pubmed/30010808>.

Englund, D.A., Price, L.L., Grosicki, G.J., Iwai, M., Kashiwa, M., Liu, C., Reid, K.F. and Fielding, R.A., 2018. Progressive resistance training improves torque capacity and strength in mobility-limited older adults. *The Journals of Gerontology: Series A*.

<https://www.ncbi.nlm.nih.gov/pubmed/30165595>

Iwata, M., Englund, D.A\*, Wen, Y., Dungan, C.M., Murach, K.A., Vechetti, I.J., Mobley, C.B., Peterson, C.A. and McCarthy, J.J., 2018. A novel tetracycline-responsive transgenic mouse strain for skeletal muscle-specific gene expression. *Skeletal muscle*, 8(1), p.33. \*Shared first authorship.

<https://www.ncbi.nlm.nih.gov/pubmed/30368256>

Dungan, C.M., Murach, K.A., Frick, K.K., Jones, S.R., Crow, S.E., Englund, D.A., Vechetti Jr, I.J., Figueiredo, V.C., Levitan, B.M., Satin, J. and McCarthy, J.J., 2019. Elevated myonuclear density during skeletal muscle hypertrophy in response to training is reversed during detraining. *American Journal of Physiology-Cell Physiology*, 316(5), pp.C649-C654.

<https://www.ncbi.nlm.nih.gov/pubmed/30840493>

Grosicki, G.J., Englund, D.A., Price, L., Iwai, M., Kashiwa, M., Reid, K.F. and Fielding, R.A., 2019. Lower-Extremity Torque Capacity and Physical Function in Mobility-Limited Older Adults. *The journal of nutrition, health & aging*, 23(8), pp.703 709.

<https://link.springer.com/article/10.1007/s12603-019-1232-8>

Englund, D.A., Peck, B.D., Murach, K.A., Neal, A.C., Caldwell, H.A., McCarthy, J.J., Peterson, C.A. and Dupont-Versteegden, E.E., 2019. Resident muscle stem cells are not required for testosterone-induced skeletal muscle hypertrophy. *American Journal of Physiology-Cell Physiology*, 317(4), pp.C719-C724. NOTE: Selected for APSselect.

<https://www.ncbi.nlm.nih.gov/pubmed/31314585>

Figueiredo, V.C., Englund, D.A., Ivan Jr, J., Alimov, A., Peterson, C.A. and McCarthy, J.J., 2019. Phosphorylation of eIF4E is dispensable for skeletal muscle hypertrophy. *American Journal of Physiology-Cell Physiology*.

<https://www.physiology.org/doi/abs/10.1152/ajpcell.00380.2019>

Grosicki, G.J., Barrett, B.B., Englund, D.A., Liu, C., Travison, T.G., Cederholm, T., Koochek, A., Von Berens, Å., Gustafsson, T., Benard, T., Reid, K.F., and Fielding R.A., 2020. Circulating Interleukin-6 is Associated with Skeletal Muscle Strength, Quality, and Functional Adaptation with Exercise Training in Mobility-Limited Older Adults. *The Journal of Frailty & Aging*, pp.1-7.

<https://link.springer.com/article/10.14283/jfa.2019.30>

Englund, D.A., Murach, K.A., Dungan, C.M., Figueiredo, V.C., Vechetti Jr, I.J., Dupont-Versteegden, E.E., McCarthy, J.J. and Peterson, C.A., 2020. Depletion of resident muscle stem cells negatively impacts running volume, physical function and muscle hypertrophy in response to lifelong physical activity. *American Journal of Physiology-Cell Physiology*. NOTE: Selected for *AJPCell* image of the week.

<https://journals.physiology.org/doi/abs/10.1152/ajpcell.00090.2020>